UCL Université catholique de Louvain

École polytechnique de Louvain (EPL)

POLITECNICO DI MILANO

Dynamic analysis of a steel footbridge under running pedestrians

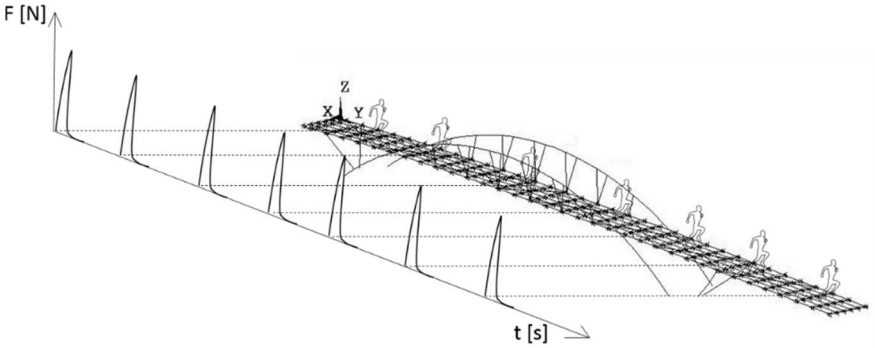

Dissertation presented by
Michele Pisani

for obtaining the master's degree in
Civil Engineering,
Structures

Supervisors
Prof. Maria Gabriella Mulas (PoliMi), Prof. Pierre Latteur (EPL)

Readers
Prof. Catherine Doneux (EPL), Ing. François Beeckmans (McCarré), Ing. Sebastien Goessens (EPL)

Academic year 2016-2017

ACKNOWLEDGMENTS

I would first like to thank most sincerely Professor Maria Gabriella Mulas. From the begin made her available to follow this project under conditions that few others would have accepted. Thanks to her precious advice, to her professionalism and her huge willingness, I learnt a lot, even having worked at a thousand miles away.

Then, I would like to thank Professor Pierre Latteur to have me shown the way toward this footbridge in an environment where I did not have any professional contact and indulging my wish to work in the field of structural dynamics.

But this work would not have been realized if I had not the pedestrian load time history provided by Professor Vitomir Racic. Although there it was few time, since I was in Milan for a while, He made him immediately available to talk about the project and provide me the necessary material to work.

Heartfelt thanks are addressed to Doctor Engineer Eleonora Lai. An expert knower of Ansys Mechanical APDL to which I never hesitated to ask questions. The determination of the method to apply pretension on "my footbridge" has been a true challenge.

Moreover, I must thank the Engineering office McCarré and, in particular, Architect Gaëtan Cordi and Engineer François Beeckmans that provided me all information related to the studied structure.

Great thanks go as well to my Belgian family, my friends and all people that I cannot quote for reasons of space but that, in one way or another, helped me to accomplish this work.

In addition, I must express my very profound gratitude to my parents and to my girlfriend for providing me with unfailing support and continuous encouragement throughout my years of study and through the process of writing this thesis. This accomplishment would not have been possible without them. Thank you!

And last, but not least, great acknowledgments to Politecnico di Milano and Université Catholique de Louvain La Neuve that, being part of the T.I.M.E Universities network, allowed me to go through this very important personal and professional experience that I will never forget.

RINGRAZIAMENTI

Prima di tutto, desidererei ringraziare nel modo più sincero la Professoressa Maria Gabriella Mulas. Fin da subito ha raccolto la sfida di questo progetto in condizioni che pochissimi altri avrebbero accettato. Grazie ai suoi preziosi consigli, alla sua professionalità e immensa disponibilità ho imparato moltissimo, anche avendo lavorato a mille chilometri di distanza.

Dopodiché, vorrei ringraziare il Professor Pierre Latteur per avermi indicato la via quando, in un ambiente in cui non avevo contatti professionali, mi ha diretto verso questa passerella assecondando il mio desiderio di lavorare nell'ambito della dinamica delle strutture.

Ma questo lavoro non sarebbe potuto realizzarsi se non avessi avuto a disposizione la storia temporale di carico fornitami dal Professor Vitomir Racic. Sebbene ci fosse stato poco tempo, visto che mi trovavo a Milano solo di passaggio, si è subito reso disponibile per discutere del progetto e fornirmi il necessario per lavorare.

Un grazie sentito non può mancare anche alla Dottoressa Ingegner Eleonora Lai. Una esperta conoscitrice di Ansys Mechanical APDL a cui, per via della sua disponibilità, non ho mai esitato a porre domande. La determinazione del metodo per l'applicazione delle pretensioni alla "mia passerella" è stata una vera sfida.

Inoltre, non posso fare a meno di ringraziare lo studio di ingegneria McCarré, nelle persone dell'Architetto Gaëtan Cordi e dell'Ingegnere François Beeckmans, che hanno fornito tutto il materiale relativo alla struttura studiata.

Ma un grazie anche a quella che posso dire sia diventata la mia famiglia belga. Passare a trovarvi di tanto in tanto mi ha aiutato in momenti difficili. Uscire ogni tanto a Bruxelles, fare due sane chiacchiere e "faire le tour du monde en parlant" sono cose che, insieme alla 20 km, non dimenticherò mai.

Questa tesi poi è il risultato di un percorso durato sei anni che, senza il supporto e la compagnia dei miei più cari amici, sarebbe stato ancora più difficile. Un grazie va a loro e a tutti coloro che, per mancanza di spazio, non riesco a citare.

Ma chi ha supportato tutto il carico delle mie scelte sei stata proprio tu. Non dimenticherò mai il giorno in cui ci siamo lasciati perché io avevo scelto di andare via. Tu mi hai sempre appoggiato e sostenuto, anche soffrendo questo distacco. Grazie per avermi capito e non esserti messa di traverso. Non posso che dedicarti questo lavoro.

E un grazie incommensurabile va alla mia famiglia. Fin dalla prima volta in cui ho parlato ai miei genitori dell'idea di partire non hanno mai avuto alcun dubbio sul fatto che avrei potuto farcela, sostenendomi fino alla fine da ogni punto di vista. Molto spesso ho dubitato, ma loro mi hanno aiutato a non mollare. Devo a loro, a mio fratello e a mia sorella, il carattere, la forza di volontà e la determinazione che hanno accompagnato il mio percorso fino ad oggi e che, spero, continueranno ad illuminare il mio futuro.

Infine, ma non per importanza, un grazie va al Politecnico di Milano e alla Université Catholique de Louvain La Neuve che, facendo entrambi parte del network delle università T.I.M.E., mi hanno permesso di vivere questa esperienza molto importante per la formazione personale e professionale acquisite. Questi due anni passati lontano hanno sicuramente cambiato me e il mio modo di pensare e, per questo, ne sarò riconoscente per tutta la vita.

ABSTRACT

After the widely known cases of human induced vibrations that affected the Millenium Bridge, London and the Passerelle Solférino, Paris, several and important studies were conducted on this kind of dynamic load. This is still today the cause of discomfort problems, sometimes not negligible, because of the increased slenderness of footbridges required to reach some standards of beauty.

Although many steps further in the field of walking pedestrian induced loads have been done, today's engineers are starting to ask themselves how structures may react when subjected to the action of running pedestrians. In fact, because of the increasing number of running competitions in urban environment, they would know if the current dynamic load models, barely and superficially provided by literature or by the most used design guidelines, are adequate to realize structures where expected comfort levels are satisfied.

So, after the description of fundamental elements concerning the nature of human induced loads and the possible human-structure interaction, a case study is developed. Three numerical models are developed, using the software Ansys Mechanical APDL, for a steel footbridge at the design stage in the engineering office McCarré (Belgium) and that will be built in few months in Louvain-La-Neuve (Belgium). The models differ in the arch geometry, whose effect on the modal properties is investigated. The results of two different dynamic analyses on the footbridge under a running pedestrian are then compared. The first is a harmonic analysis exploiting the running pedestrian load model provided by a well-known European guideline for footbridges design (HiVoSS guidelines, Human induced Vibrations on Steel Structures guidelines). The second is a transient analysis under a moving and time varying load based on the running pedestrian load model proposed by *Racic and Morin* [47]. The load time history produced by their numerical generator and made available for this thesis has been at the base of the work. Since in general the pedestrian will not move only on the nodes of the finite element mesh, a Matlab code named RealRun1 was developed during this thesis to solve the problem. This post-processes the time-history to provide the

equivalent nodal loads on the structure as a function of time and position of the runner on the footbridge.

Finally, clear differences of results are obtained from the two analyses. Being the footbridge still at the design stage, the need of some structural adjustment of the footbridge to ensure expected comfort levels was pointed out. The results also showed that more research is necessary to develop a robust load model for running pedestrians, improving the one provided in HiVoSS.

SINTESI

A partire dai ben noti casi di vibrazioni indotte da pedoni che hanno interessato il Millennium Bridge di Londra e la Passerelle Solférino di Parigi, molti e importanti studi sono stati condotti per comprendere questo carico dinamico. Infatti, ancora oggi, esso è causa di problemi di comfort, a volte non trascurabili, legati alla sempre maggiore snellezza con cui i ponti pedonali vengono costruiti per soddisfare necessità di tipo estetico.

Sebbene siano stati fatti molti passi in avanti nell'ambito della ricerca relativa a pedoni che camminano, al giorno d'oggi, gli ingegneri stanno iniziando a chiedersi come le strutture potrebbero rispondere quando sottoposte all'azione di pedoni che corrono. Infatti, dato il sempre maggior numero di competizioni podistiche in ambito urbano, ci si chiede se gli attuali modelli di carico dinamico, raramente e superficialmente proposti in letteratura o nelle più usate linee guida di progettazione, siano adeguati per la realizzazione di opere in cui i livelli di comfort attesi siano soddisfatti.

Quindi, in seguito alla descrizione degli elementi fondamentali per comprendere la natura dei carichi indotti da pedone e della possibile interazione uomo-struttura, si è sviluppato un particolare cso di studio. Sono stati sviluppati tre modelli numerici, usando il software Ansys Mechanical APDL, di una passerella in acciaio in fase di progetto presso lo studio di ingegneria McCarré (Belgio) e che sarà costruita fra qualche mese a Lovain La Neuve (Belgio). I modelli differiscono nella geometria degli archi, il cui effetto sulle proprietà modali della struttura è analizzato. Quindi, si sono comparati i risultati di due differenti analisi dinamiche del ponte pedonale sotto il carico generato da un pedone che corre. La prima è un'analisi armonica eseguita applicando il modello di carico del pedone che corre proposto dalle linee guida oggi più usate in Europa per il progetto di passerelle pedonali (HiVoSS guidelines, Human induced Vibrations on Steel Structures guidelines). La seconda è un'analisi transiente eseguita applicando un carico in movimento e variante nel tempo basato sul modello di carico indotto da pedone proposto da *Racic et Morin* [47].

La storia temporale di carico prodotta dal loro generatore numerico e gentilmente trasmessaci è stata alla base del lavoro. Dal momento che il pedone non corre necessariamente sui nodi della mesh del modello ad elementi finiti, un codice Matlab, chiamato RealRun1, è stato sviluppato durante la realizzazione della tesi per risolvere il problema. Esso, infatti, tratta ulteriormente la storia temporale in modo da generare i carichi nodali sulla struttura in funzione del tempo e della posizione del pedone sulla passerella.

Infine, si è riscontrata una netta differenza di risultati tra le due analisi. Da un lato, avendo analizzato una passerella ancora in fase di progetto, si è tentato di fornire alcuni suggerimenti di adattamenti strutturali per assicurare i livelli di comfort attesi. Dall'altro, i risultati hanno nettamente mostrato che una ricerca più approfondita è necessaria per sviluppare un più solido modello per pedoni che corrono, migliore rispetto a quello proposto dalle linee guida HiVoSS.

Index of contents

Index of figures

Index of tables

INTRODUCTION

All along the second half of the last century, the search for new architectural solutions in the civil engineering field brought to the construction of increasingly slender structures. Skyscrapers, bridges and footbridges, due to their important visibility and environmental impact, have been the object of this evolution. Since the well-known case of the Takoma Narrow Bridge' collapse on 7 November 1940, several studies linked to the effects of wind allowed to recognize the necessity to take into account this dynamic load already during the design phase. The first who recognized the reason of that collapse was the Italian engineer Giulio Krall. But, for footbridges, until two decades ago, there were no reasons to imagine the possibility for another dynamic load to cause troubles: *human induced loads*.

Human induced loads brought to the structure collapse only in very rare cases, documented in history (*Tilly et al.* [15]), but they are very important for the determination of the serviceability limit state. In fact, users perceive vibrations induced by this kind of loads as a possible sign of unsafety even if they are not dangerous from the structural point of view.
It is not easy to imagine that a walking or running person may induce vibrations that are so large to be annoying. However, the improvement of material properties of the last years contributed to the possibility of designing footbridges with low values of mass, longer spans and, in general, footbridges that are very "light" from the aesthetic point of view. This had the main consequence to make footbridges more sensible to human induced loads.
But, even if someone would had considered the problem, no code or regulations were available to do a right design to face the vibrations problem until the 2000s.

Only after the well-known cases of Millennium Bridge in London and Passerelle Solférino in Paris, the scientific community started to raise questions about the problem, pushed by the necessity to avoid or predict the need of vibrations control measures that could represent an important part of the total construction budget.

The first and very important studies have been conducted on the Millennium Bridge by *Dallard et al.* ([34], [35] and [36]) and by *Fitzpatrick et al.* ([41] and [42]) with the purpose to start to understand the human-structures interactions. Thanks to several crowd tests, they analyzed by different points of view the so-called lock-in phenomenon, coincident with the moment where the pedestrian "synchronizes his footfall rate to the frequency of the swaying platform" [34]. This particular case of resonance phenomenon generates a significant increasing of the oscillations amplitude of the structure due to a natural accumulation of energy inside the system. Furthermore, *Dallard et al* [34] established a direct link between degree of synchronization and crowd density.
On the other hand, studies on the Passerelle Solférino made by *Cremona* [4],through the execution of crowd tests under different situations, for example walking or running people, rectilinear trajectory or round trajectory, allowed for the determination of the critical number of people to initiate large levels of lateral uncomfortable accelerations and showed how the installation of Tuned Mass Damper systems (TMDs) affected positively the structure response.

Then, the civil engineering academic community started do discover the world of biomechanics to create models suited to describe the human induced loads. Works like the ones of *Vaughan et al.[5]*, *Perry* [28] and *Inman et al.*[48], represent milestones in the gait analysis, the branch of biomechanics studying the human locomotion from the mechanical point of view, while accurate shapes of loads time histories are given in *Andriacchi et al.* [44] and in *Keller et al.*[45].
Thanks to these studies, several mathematical models of Ground Reaction Forces (GRFs), have been proposed for the application in the civil engineering field. Deterministic and stochastic proposed models had the objective to reproduce in the more accurate possible way the inter- and intra-subjects' variability, linked to several variables such as stiffness of the walking surface, the speed of movement or the crowd density. In addition, the perception of vibrations has been discovered to be dependent on the same variables and it has been difficult to determine that acceleration of vibrations is the parameter that must be checked during the design phase to assess the serviceability limit state of a footbridge.
Moreover, the problem consisted also in the precise determination of the structures features. Mass, stiffness and, above all, damping characteristics are properties that highly affect the structure response. More specifically, they play a role in the determination of natural frequencies of the structure that, in case of footbridges designed and built in the last years, fall more and more often in the interval of frequencies that characterize loads induced by walking, running or jumping pedestrians.

For all these reasons, the objective of this Master thesis, is to enter the flow of studies on the topic and evaluate two available models for a running pedestrian load case. At the same time, a first judgment about the serviceability state of the footbridge will be given. In fact, a steel footbridge at the design phase will be considered.

First of all, three different finite elements models of the footbridge will be studied to observe how possible variations in the geometry can affect the structure response and understand which are their most sensitive zones. In particular, we will consider the real designed geometry of the footbridge and two other models where the arches geometry will be modified to evaluate how these modifications will affect its static behavior and its dynamic properties.

For the computation of the latter, it is necessary to determine the amount of pretension to which tendons supporting the deck will be subjected once the structure will be realized. Then, the response of the structure when excited by human induced loads can be evaluated.

Exploiting results coming from the modal analysis done at the previous point, the model of the designed structure is subjected to two different dynamic analysis in the case of a running pedestrian load. In effect, models to represent loads induced by running pedestrians are only barely present in literature and design methods given in codes and guidelines taking into account this load are not really used and verified. Until now, in effect, this kind of load has never been considered as critical given the low probability of running crowds to cross footbridges. But today, because of the increasing number of urban run competitions, a new concern is raised around the topic.

The load model elaborated by *Racic and Morin* [47] is adopted to generate the load time history for a running pedestrian crossing the bridge at study accounting for its natural variability. An innovative approach is here adopted to apply this time history to the footbridge FE model.

To this aim, some challenges have been overpassed. In particular, the load time history provided by Professor Vitomir Racic, is post-processed to take into account the position of the pedestrian moving over the footbridge as a second time-dependent variable of the load. Each load cycle, in fact, represents a load applied at a different contact point between the runner and the structure. Moreover, the need to consider that contact points do not necessarily coincides with mesh nodes, pushed us to find a method for the determination of nodal vertical forces and bending moments applicable on nodes surrounding the load application point.

The numerical results are compared with the ones obtained applying the design method proposed by one of the guidelines used in Europe for the design of footbridges (Human induced Vibrations on Steel Structures guidelines, HiVoSS [22]).

The software Ansys Mechanical APDL is used to create the Finite Elements models and to perform static, modal, harmonic and transient analysis of the structure. To let Ansys make the transient analysis with the proposed load model, the text file to use as input will be

generated through a Matlab code specifically created, that transforms the time history previously mentioned in nodal loads.

Thus, this Master thesis is subdivided according to the following scheme:

- CHAPTER 1 describes the physics behind the problem of human induced vibrations. After the description of the Millennium Bridge and Passerelle Solférino cases study, the fundamental works in the field of gait analysis is introduced. Then, all components and phenomena contributing to the creation of the vibrations problem is discussed referring to the most recent literature. In the order, the reader can meet: the description of the features of human-induced loads and their mathematical modeling, the description of the structure most important parameters affecting the dynamic response to this kind of loads and the description of the human induced load models and the possible human-structure interaction effects.

- CHAPTER 2 presents the footbridge that is analyzed in next chapters. Key aspects like the geometry and materials properties are provided. Some information about the process that lead to its conception and the place where it will be built are presented as well.

- Using information presented in CHAPTER 2, the procedure for the creation of the FE model using the Ansys Mechanical APDL software and all the assumptions at the base of the modeling method are described in CHAPTER 3. Details about commands used to create the model are reported in APPENDIX C to avoid an unnecessary burden of the dissertation.
  Then, the geometric differences among the three proposed models are presented to the aim of evaluating the influence of the arches geometry on the structure behavior. Aspects such as the static response of the structures and their natural frequencies are analyzed.
  Finally, a method to validate the modeling procedure will be presented.

- CHAPTER 4 is addressed to the presentation of HiVoSS guidelines for design and check of footbridges during the design phase.

- In CHAPTER 5, after a first introduction to the paper of *Racic and Morin* [47] the approach is based on, it follows the description of challenges related to the

treatment of the load and a brief description of the Matlab code written to create a text file readable by Ansys. Then, results obtained applying the HiVoSS prescriptions and results obtained using the innovative approach presented above are discussed.

- Finally, CHAPTER 6 presents the main conclusions drawn from the work as well as recommendations for possible developments in the field of running pedestrians induced loads.

CHAPTER 1
DESCRIPTION OF THE PROBLEM

Chapter 1 is devoted to the description of the state of the art in the world of human induced vibrations. Before presenting analysis of the structure object of the work, the physics behind the problem of human induced vibration is described. Thus, in this chapter, after the description of a case study, all the components and phenomena that contribute to create the vibration problem are presented: human-induced loads, structure characteristics and human-structure interaction effects.

1.1 A case study: the Solferino Footbridge, Paris

A wide literature describing effects of human induced dynamic loading on footbridges exists. Failure of footbridges under marching regiment moving across them (for example [15]) are reported also. Anyway, since human sensitivity to vibrations is very high and no oscillations capable to damage the structure are usually reached, it is well accepted that vibration produced by human induced loads is a serviceability rather than a safety problem.
In the civil society, the vibration of footbridges is a phenomenon attracting attention only in correspondence of well-known vibrations problems. Among the most important, it is possible to find the cases of the London Millennium Bridge (Figure 1.1.1) and of the Paris Solferino Footbridge (Figure 1.1.2).
The opening of the Millennium Bridge can be considered as the moment in which the scientific community started to approach in a systematic way the problem of human induced vibration. A large literature exists about the dynamic behavior of this structure. Images of lateral oscillations caused by the crowd crossing the structure during the public opening (10th June 2000) went all around the world. Some important works analyzing reasons and causes of the structure behavior were done by *Dallard et al.* ([34], [35] and [36]) and by Fitzpatrick et al ([41], [42]).

Figure 1.1.1 Views of the Millennium Bridge, London [36].

In this study, more emphasis is given to the other case. Literature about the Solferino Footbridge, today named Passerelle Léopold-Sédar-Senghor, is less wide with respect to the previous case. Nevertheless, the problem was less important. In fact, the construction cost was 14 *M*€ [30] and the installation of tuned mass dampers (TMDs) increased the bill of 1*M*€ [III].

Figure 1.1.2 The Solferino Footbridge, today Passerelle Léopold-Sédar-Senghor, Paris.

The Solferino Footbridge links the left and right side of the Seine river in Paris in correspondence of Jardin des Tuileries and Orsay's Museum. The bridge was designed by the architect Marc Mimram and built by the Eiffel company between 1995 to 1999. The structure is composed of two couples of welded steel arches that support timber decks through coupled steel struts forming a V-shape in the bridge cross-section (Figure 1.1.3 and Figure 1.1.4). The cross section of the struts is semielliptical, with thickness equal to 30 mm. The length of the struts changes along the structure as well as their inclination.

a)

b)

Figure 1.1.3 Two detail pictures of the Solferino footbridge steel structure: a) Struts have semi-elliptical section and are coupled forming a V-shape (*Ph. Nicolas Janberg [II]*); b) Arches and deck are linked through struts(*Ph. Philip Bourret [I]*).

The two arch substructures are linked through one more deck, at a different level than the other two (Figure 1.1.4).

Figure 1.1.4 Solferino Footbridge cross section [32].

The main structural components are the arches. At their highest point, they meet the upper deck and merge into it. At their bases, arches have a section depth of 1,25 m while they taper toward midspan, where their depth is only 0,55 m.

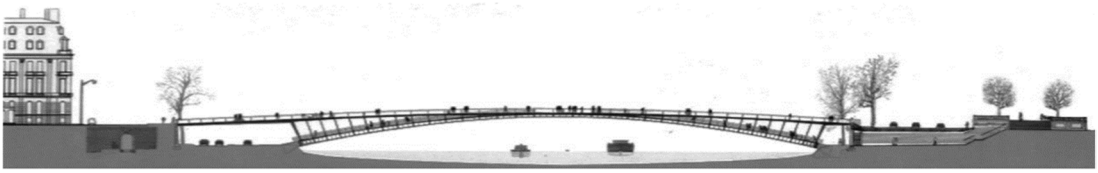

Figure 1.1.5 Solferino Footbridge elevation[32].

The total length of the footbridge is 140 m and the main span is 106m long. An architectural elevation view is given in Figure 1.1.5. The cross-section width varies between 11 and 15 m. For more details, readers can refer to [18].

As in the case of the Millennium Bridge, during the day of public opening of the Solferino Footbridge on 14th December 1999, people crossing the structure caused and felt unforeseen oscillations. Few days later the bridge was closed to public traffic and subjected to studies with the aim to find a solution to decrease the amount of vibration of the structure. The objective was to obtain a good solution without the modification of the stiffness or of the mass of the bridge to maintain aesthetic principles. Only after almost one year, and the application of a TMD system the footbridge returned to service, on November 2000.

After the first campaign of studies, recalled in [12], it was confirmed that the cause of oscillations was a resonance phenomenon on the first lateral mode of vibration of the bridge, at a frequency around 0.8 Hz.

As an example, Figure 1.1.6 shows time histories of accelerations reached by deck displacements during two crowd tests at slow speed and high speed with the same number of people. Larger accelerations are reached for lower speeds, with step frequencies nearer to the fundamental lateral frequency of the bridge.

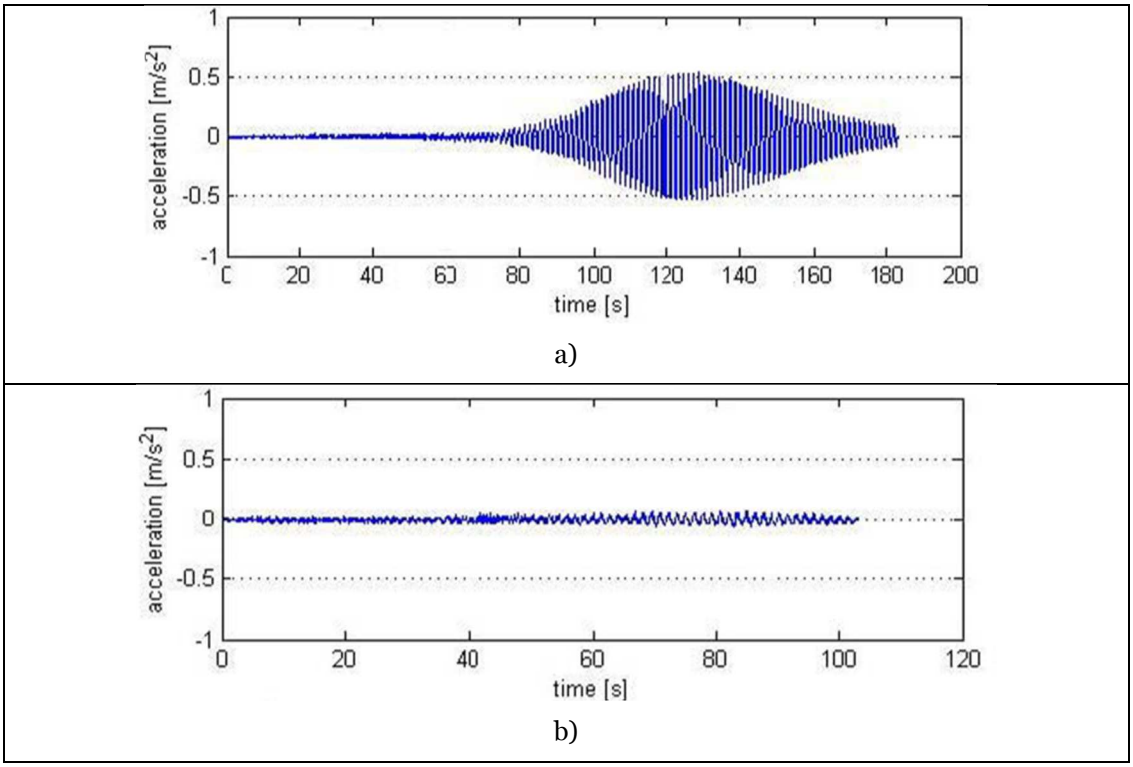

Figure 1.1.6 Acceleration response of the Solferino Footbridge during testing: a) low walk speed; b) quick walk speed. Values of speeds are not specified [4].

After [4], with a series of crowd test, "it was noticed that 140-160 pedestrians can initiate large levels of lateral accelerations making the footbridge uncomfortable". In the same paper, the effect of the installation of a TMDs system on the natural frequencies of the structure is described. Table 1.1.1 presents the comparison between the situations before and after the installation of the system.

Table 1.1.1 Comparison between calculated and identified frequencies in different conditions (specified in apexes) [4].

Mode	Experimental (Hz)	Numerical (Hz)	Characteristics
1	0.71	$0.811^{(0)}$ - $0.70^{(1)}$	Symmetrical lateral bending (with torsion)
2	1.09	-	Non symmetrical torsion, 1 node, 2 lobes
3	$1.12^{(2)}$	$1.123^{(0)}$	Non symmetrical bending, central node, 2 lobes
4	1.55	$1.386^{(0)}$	Non symmetrical torsion, central node (with lateral bending)
5	1.56	$1.787^{(0)}$	Symmetrical bending, 1 lobe
6	1.70	$1.527^{(0)}$ - $1.680^{(1)}$	Non symmetrical torsion, central node, 2 lobes (with lateral bending)
7	1.95	$1.971^{(0)}$	Non symmetrical torsion, 2 nodes, 3 lobes (with lateral bending)
8	2.01	$2.076^{(0)}$ - $2.31^{(1)}$	Symmetrical torsion, 2 nodes, 3 lobes (with lateral bending)
9	$2.36^{(x)}$		Vertical bending of the access bridge, 1 lobe Torsion of the main footbridge
10	$2.51^{(x)}$-$2.60^{(x)}$	$2.386^{(0)}$	Vertical bending of the access bridge, 1 lobe
11	-	$2.722^{(0)}$	Non symmetrical lateral, 2 nodes, 3 lobes (with torsion of the access bridge)
12	2.88	$2.784^{(0)}$	Symmetrical bending, 2 nodes, 3 lobes
13	3.02 – $2.92^{(x)}$	$2.928^{(0)}$	Torsion of the access bridge, 1 node
14	3.09	$3.024^{(0)}$	Non symmetrical bending, 3 nodes, 4 lobes
15	-	$3.204^{(0)}$	Symmetrical torsion, 3 nodes, 4 lobes
16	3.32	$3.42^{(0)}$	Non symmetrical vertical bending, 1 node, 2 lobes (with movement of the side arches)
17	3.52	$3.506^{(0)}$	Symmetrical bending, 2 nodes, 3 lobes (with lateral)
18	$3.64^{(x)}$	$3.958^{(0)}$	Symmetrical bending, 1 lobe (with movement of the lateral arches)
19	3.74	$3.385^{(0)}$	Symmetrical bending, 1 lobe (with movement of the side arches)
20	4.22	-	Symmetrical bending, 1 node, 2 lobes (with movement of the side arches)

(0) calculation without TMDs - (1) calculation with TMDs – (2) with crowds
(x) identified modes when actuator of the access bridge

In general, the structural response depends on several variables that are still object of a research effort. First, the human behavior presents a great inter- and intra- variability, such that both the human induced load and the perception of vibrations are very complex matters. They are influenced, for example, by the stiffness of the walking surface, the speed of movement, the conditions of movement (for instance, being alone or within a sparse or a dense crowd). Moreover, the structure behaviour is also important. Damping phenomena are not fully predictable and, even more, not precisely replicable on analytical or FE models.

Finally, a kind of human structure interaction may appear and change completely the behaviour of the structure because of the coupling between the bridge and the human body in terms of vibration. In the following paragraphs a brief overview on these aspects will be given.

1.2 Gait analysis and study of movement

When a pedestrian is in movement, during its normal walking produces dynamic forces. In [24], a design standard substituted by more recent guidelines but fundamental for definitions, dynamic forces are defined as “forces varying so quickly that they give rise to vibrations”. As for the vibration source, in the same work, a distinction is made. The vibration source can be inside or outside the building and human excitations are classified as part of the former group.

Gait analysis is the branch of biomechanics studying the human locomotion from the mechanical point of view, as defined in the introduction of [33]. In this paper, the human motion is analyzed in terms of mechanical principles. Minimization of the loss of mechanical energy in the motion of the center of body mass explains why all humans walk in the same way: pelvic rotation, pelvic tilt, knee flexion and plantarflexion and dorsiflexion of the supporting foot have the objective, working all together, to reduce the vertical displacement of the center of mass of the human body. Hereafter, only a brief introduction to human movement analysis is given.

To fully understand the human gait process, it is necessary to introduce a definition: “The gait cycle is the period of time between any two nominally identical events in the walking process” [8]. One important distinction must be done between the term gait and walking. They have two different meanings. Gait is more general then walking, that only refers to the particular gait used at low speeds. The speed for normal walking is equal to 80m/min [28]. According to a series of textbooks that formalize the base notions of sports science and biomechanics [48], [28], [5], we refer to gait as a cycle, because it is the sum of a number of processes that repeat at each step during human movement. Even if the assumption that all cycles are equal is not always and completely true, it is accepted to make possible analysis of the phenomenon: a huge intra - other than inter-subject - diversity exists among humans when producing loads on structures. Moreover, a gait cycle refers to only one side of the body and the assumption of symmetrical behavior holds true, too. The beginning of the cycle is conventionally chosen as the moment in which one of the two feet hits the ground. A walking gait cycle is divided in two main phases:

- *Stance phase*: known as the support or contact phase, it is the moment when the foot is on the ground. It begins when the heel hits the ground and finishes when the toe leaves the ground. It lasts 62% of the entire gait cycle;
- *Swing phase*: it represents the interval of time between the end of a stance phase and the beginning of the following, i.e. the 38% of the gait cycle. It denotes the time interval in which the foot does not touch the ground.

Both are better fractionated in sub-phases: 5 for the stance and 3 for the swing phase. The nomenclature defined by *Perry et al.* [28] will be used here to identify the sub-phases. Their names give an idea of what happens, while percentage refers to their normalized duration with respect to the gait duration:

1. Stance
   1.1. *Initial contact (IC 0%)*;
   1.2. *Loading response (LR 0-10%);*
   1.3. *Mid-stance (MSt 10-30%);*
   1.4. *Terminal stance (TSt 30-50%);*
   1.5. *Pre-swing (PSw 50-62%);*
2. Swing
   2.1. *Initial swing (ISw 62-70%);*
   2.2. *Mid-swing (MSw 70-85%);*
   2.3. *Terminal swing (TSw 85-100%);*

In Figure 1.2.1, it is possible to appreciate schematically the evolution of the gait cycle.

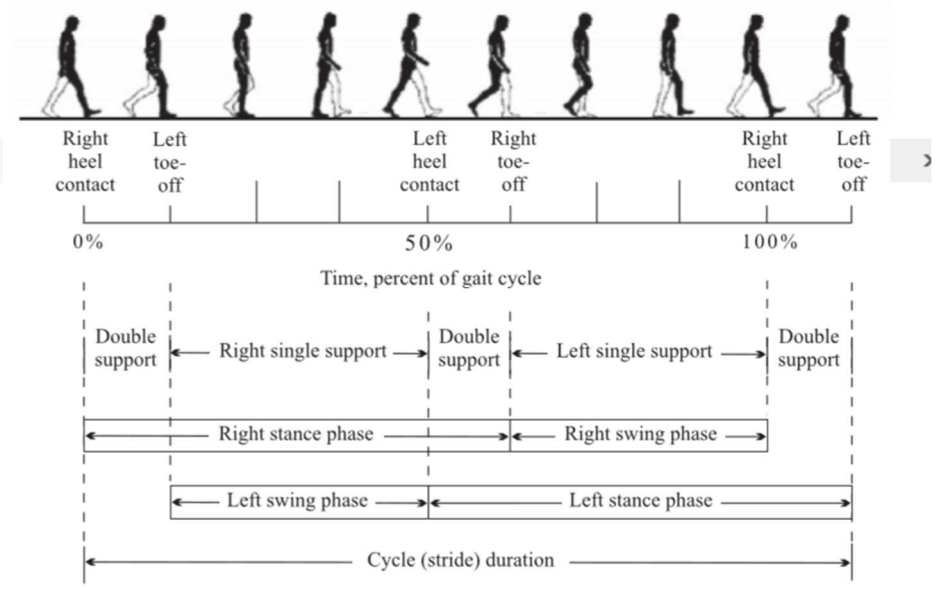

a)

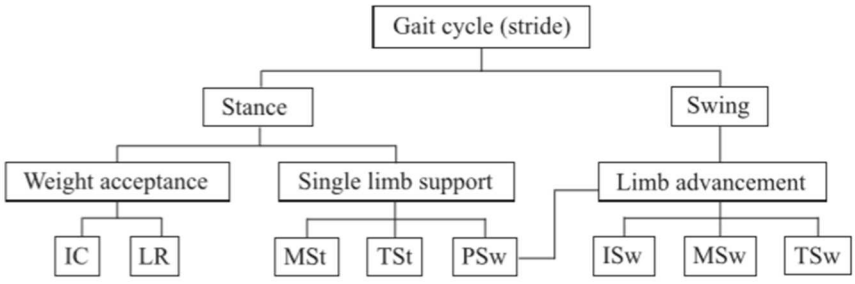

b)

Figure 1.2.1 The gait cycle in two different representations: a) Inman et al. [48]; b) Perry et al.[28].

Figure 1.2.2 shows graphically the gait cycle in a quite clear way, even though the terms adopted are not presented in the text.

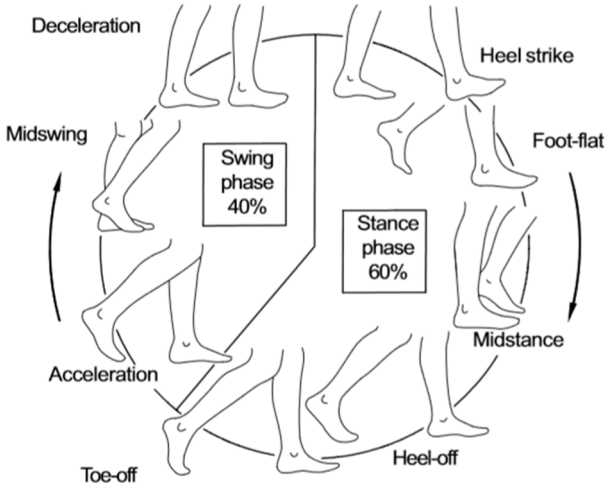

Figure 1.2.2 The gait cycle according to a nomenclature different from the one of *Perry et al.* [5].

Different parameters exist, related to time and space, characterizing the human gait allowing to make definitions of walking, jogging or running, for example.
Time parameters are widely described in [48]. If the time duration is the interval over which the gait is realized, the stride, or cycle frequency, also known as cadence, is its reciprocal. The walking speed is the distance covered during the time to make a cycle, obtained also as the product of a given stride frequency times the distance. Thus, the walking speed can be modified in two ways: varying the stride frequency or the distance.
Space parameters are:

- *stride length*, the distance measured between a heel strike and the successive in the direction of advancement;
- *step width*, is the distance between the two parallel lines passing through the mid-points of heels in the direction of progression.

These last concepts are clarified in Figure 1.2.3.

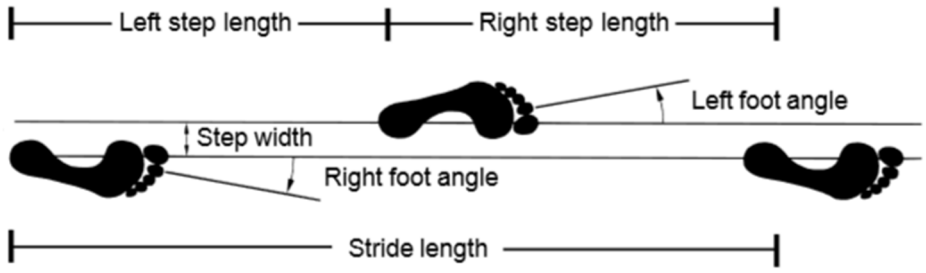

Figure 1.2.3 Spatial parameters of the gait cycle [5].

Finally, it is important to report terminology about description of motion of the human body in the space. This will be useful to locate GRFs components in the 3D space with respect to the human body.

Figure 1.2.4 describes the standard anatomical position. As defined in the Dictionary of Medical Terms [7], this is "the standard position of the body from which all directions and positions are derived. The body is assumed to be standing, with the feet together, the arms to the side, and the head, eyes and palms facing forward". Three fundamental planes are defined:

- *mid-sagittal plane*, corresponding to a side view, divides the body in two equal halves;
- *coronal (or frontal) plane* divides the body in back and front portions;
- *transverse plane,* passing through the navel, separates the body into head and tail portions.

Directions of movements are defined with respect to these planes. An anterior-posterior movement is done in the sagittal plane parallel to the transverse plane. The right-left direction is defined in the frontal plane, for a movement parallel to the transverse plane and, finally, the superior and inferior direction are defined in the frontal plane but are perpendicular to the transverse plane. The three directions are also defined as *antero-posterior, medial-lateral and vertical*.

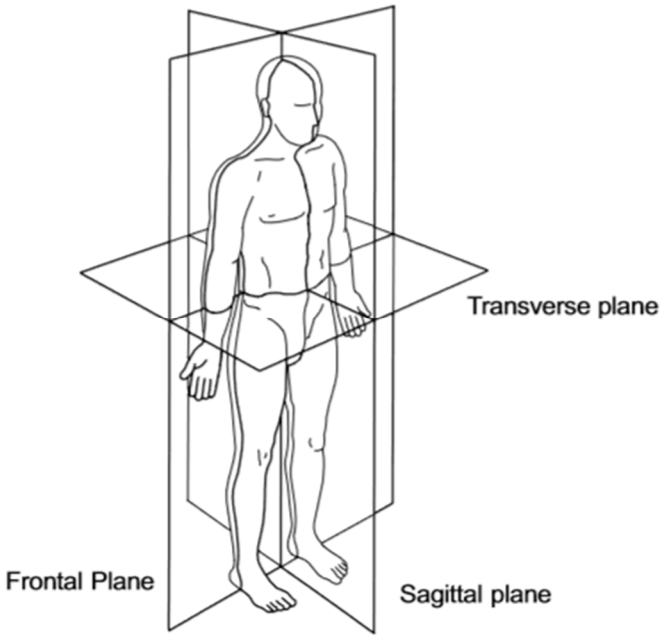

Figure 1.2.4 Standard anatomical postion [48].

1.3 The human-induced load

Ground reaction forces (GRFs) represent the response of the ground to the loading induced by the movement of humans over a surface. As every kind of forces in space, they have three components: vertical, medial lateral and anterior posterior components. Obviously, the forces are generated when the foot is in contact with the ground, i.e. during the stance phase. Stance phase has already been subdivided in five sub-phases. The subdivision is not merely important from the gait analysis point of view, but to each of these phases corresponds a different stage of the loading transfer process.

Using a very simple idealization, human load transfer to the ground could be seen like an impulse. The stance phase, in effect, has a duration of less than 1 s. However, even though it may seem counterintuitive, during each sub-phase of the stance the load has a particular way to be transferred. For example, going more in detail in the analysis of the vertical component, right after the heel strike, when “foot and leg act like shock absorbers” [28], the body weight is suddenly transferred to the ground. After this first moment, because of the movement of the other leg, and the consequent variation of the body’s center of mass position, a decrease in the reaction force can be appreciated. Finally, in the heel off phase, at the instant in which the foot start to detach from the ground, a new increase of the reaction appears that reaches its maximum when the heel of the other foot touches the ground. Then, the force decreases until the entire foot lifts off reporting the reaction to zero.

Each of these instants has been characterized by distinct points, also known as force parameters, $(F_i - T_i)$ in force vs. time diagrams. Considering the three components of the force, there are nine points characterizing ground reaction forces, varying as a function of individuals, speed and other boundary conditions. A precise representation of GRFs components is presented in [46].

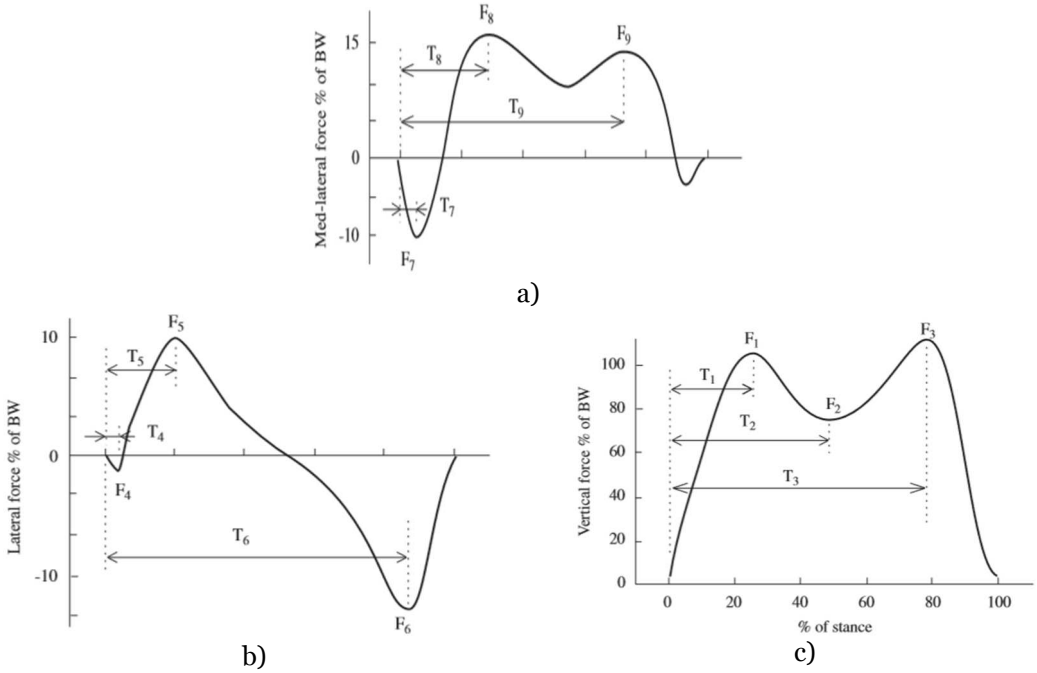

Figure 1.3.1 Representation of Ground Reaction Forces: a) Medial-Lateral, b) Anterior-Posterior and c) Vertical components [46].

In Figure 1.3.1, the axes of the diagrams represent normalized values of forces with respect to body weight and time with respect to stance duration.

These results have been obtained through measurements. One important work was done by *Andriacchi et al.* [44]. They were the first to measure all the three components of GRFs through a force plate for a single footstep. Looking for indicators of limb diseases in the gait analysis, they analyzed 17 normal subjects in two different occasions and 16 subjects with knee pathologies 3 and 6 months after operation. The method of the experiment is rigorously described in the paper. Without considering patients affected by pathologies, the fundamental results they found are related to the range of variation of the above defined 9 force parameters $(F_i - T_i)$ as a function of the walking speed with simple relationships ($F_1, F_2, F_3, F_4, F_5, F_6, F_7$ vary linearly with velocity). In Figure 1.3.2 a change of notation with respect to the above definition is noticed.

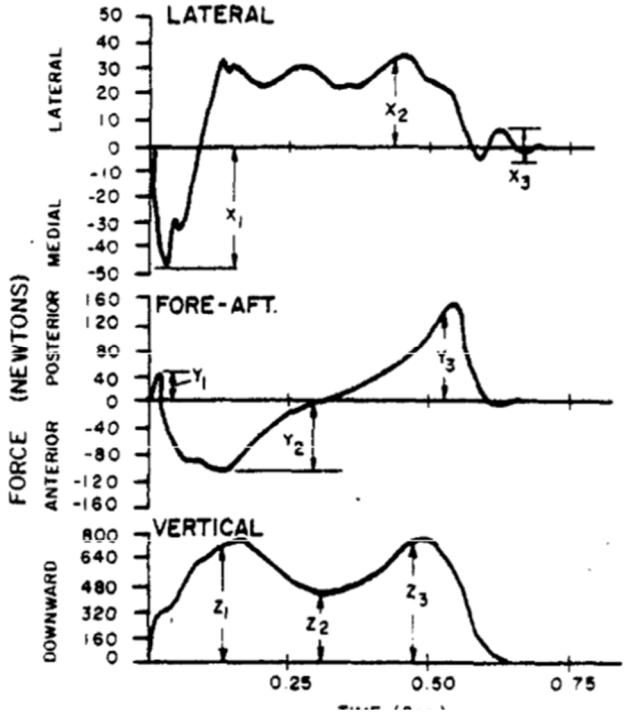

Figure 1.3.2 Plate measurements of GRFs after *Andriacchi et al.*[44]

In addition, they proved that “time of swing and time of support were found to be inversely proportional to walking speeds… As a subject increased his walking speed, a decrease in both time of swing and time of support was observed” (Figure 1.3.3).

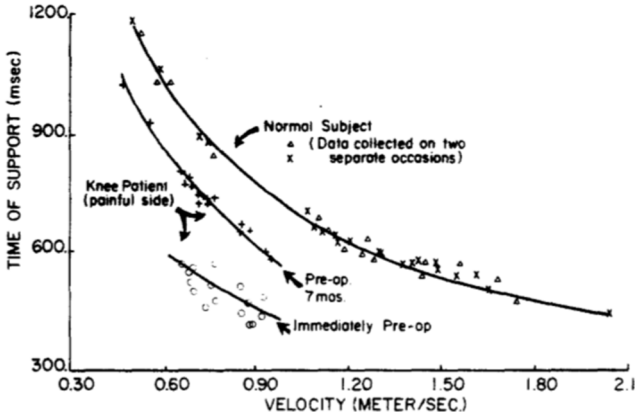

a)

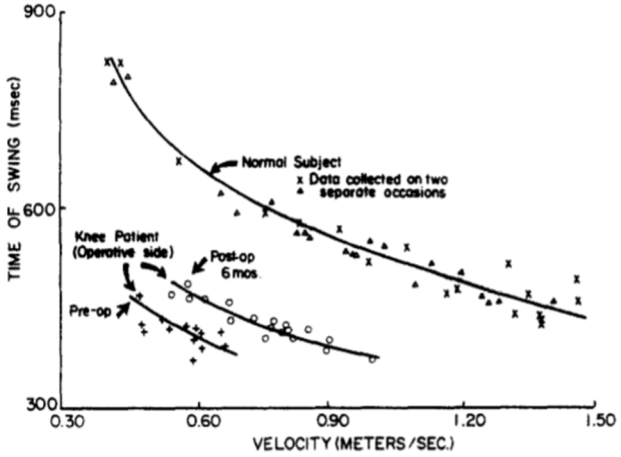

b)

Figure 1.3.3 Relationship of a) time of support and b) time of swing with walking velocity [44].

Unfortunately, the disadvantage of this study was that it was limited to a small statistic sample. A larger significant work was done by *Keller et al.* [45]. Their idea was to study the variation of GRFs amplitude as a function of speed, to answer the questions about the possibility to cause injuries when passing from fast walking to slow jogging and running. They found that, even if small, there is a difference in the vertical component of the GRFs between males and females. They reported their time histories separately for males and females (Figure 1.3.4).

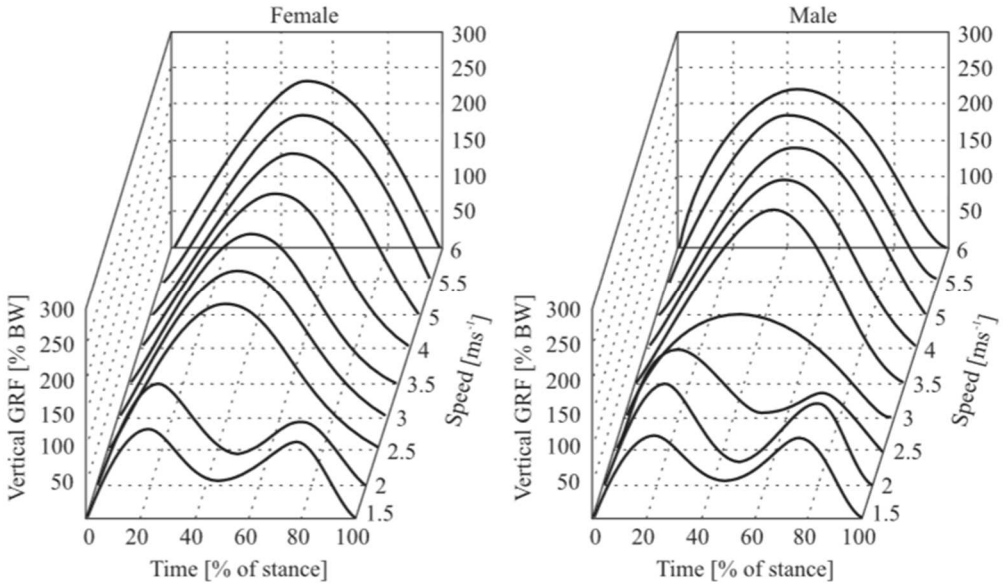

Figure 1.3.4 Vertical component of GRF for males and females as a function of velocity and normalized with respect to body weight [45].

They derived, through a linear regression, expressions to compute amplitude of peaks as a function of speed in the interval $1.5 < v < 3.5\ {}^{m}/_{s}$:

Males $F_z = 0.598v + 0.249$ Eq. 1.3.1

Females $F_z = 0.634v + 0.159$ Eq. 1.3.2

And, due to a limited variation between the two groups, they proposed an averaged expression for both groups:

$F_z = 0.614v + 0.208$ Eq. 1.3.3

For speeds above $3{,}5\ m/s$, F_z is approximately constant and equal to 2.5 times the body weight (Figure 1.3.4). Being $v = 3.5\ {}^{m}/_{s}$ the 60% of the maximum speed for every of the tested subjects, no differences appeared in fast walking and running. But for slow jogging, being a non-natural movement and amplifying oscillations of the center of mass, they found that "produced vertical forces as much as 1.6 times larger than normal walking at the same speed or running at higher speeds".

Up to now, the analysis was carried out on GRFs produced during the gait cycle for only one foot. For normal walking speed, it has been already mentioned the fact that the presence and movement of the other limb as well as its interaction with the ground influence the GRFs. Moreover, there is a period of time, called double support phase, in which both feet are in contact with the ground. It appears at the beginning and at the end of each foot gait cycle,

taking up to 20% of the entire gait duration. To evaluate the relationship between the double support phase duration and the gait speed, *Galbraith and Barton* [14] reported some important test results for three subjects "moving at rates ranging from very slow (sneak) to very fast (run) over three types of surface in footwear varying from oxfords (high heels) to stocking feet". They concluded that no substantial influence was recorded as a consequence of the different ground and footwear types. In addition, they drawn two more important conclusions. First, as in the work by *Keller et al.* [45], they obtained that moving from low speeds to higher values, the vertical component of the GRFs has only one peak instead of two. Second, they measured duration of double support phases and plotted results for one normal walking speed and one running speed, proving that the double support phase has a duration linked to the speed and it does not exist anymore for running speed (Figure 1.3.5Figure 1.3.5 Vertical components of GRFs for both feet and two different velocities [45].).

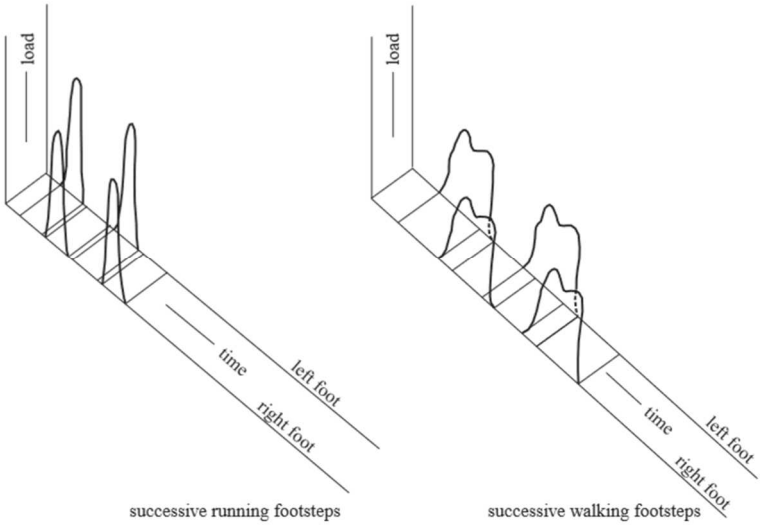

Figure 1.3.5 Vertical components of GRFs for both feet and two different velocities [45].

A relevant effort to give a harmonic view of human induced load with the perspective to present a useful procedure for footbridges design, has been done by *Wheeler* [25]. He organized the work done by previous researchers and presented the dependence of a series of gait parameters as a function of the pacing frequency (stride length, speed, step frequency, static weight and contact time) in an engineering format (Figure 1.3.6).

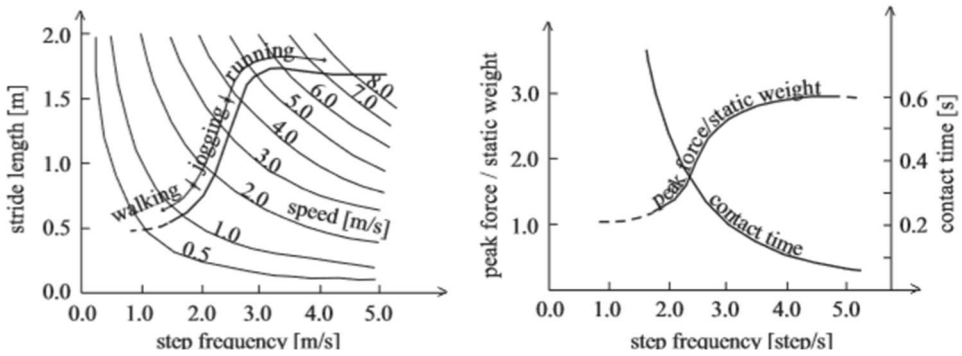

Figure 1.3.6 Gait parameters as function of pacing frequency [28].

From a different point of view, *Matsumoto et al.* [49], according to what reported by *Živanović et al.* [40], made a relevant statistical work. They collected information about normal walking frequencies of 505 persons. Using a typical statistical approach, considering the step frequency as a random variable, they derived a distribution curve that is well represented by a Gaussian probability function with a mean value of 2.0 Hz and standard deviation of 0.173 Hz (Figure 1.3.7).

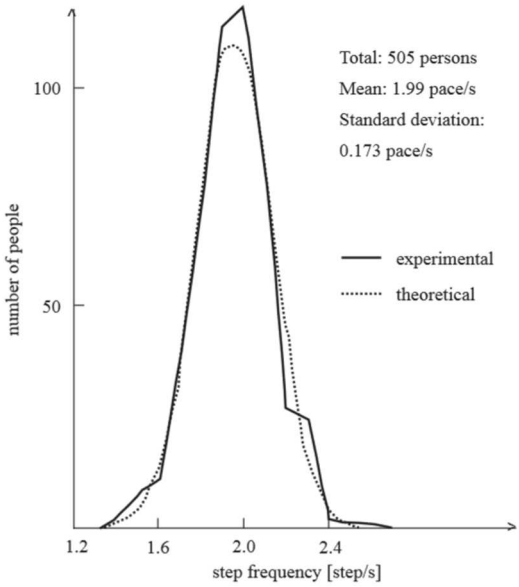

Figure 1.3.7 Gaussian distribution of human step frequencies [49].

Human induced loads have also been analyzed regarding their energy content. In his Phd thesis, *Eriksson* [37], as reported by *Živanović et al.* [40], concluded that the continuous walking human force is a narrow band process, i.e. a random stationary process that can be well represented by its auto spectral density function (ASD) (Figure 1.3.8).

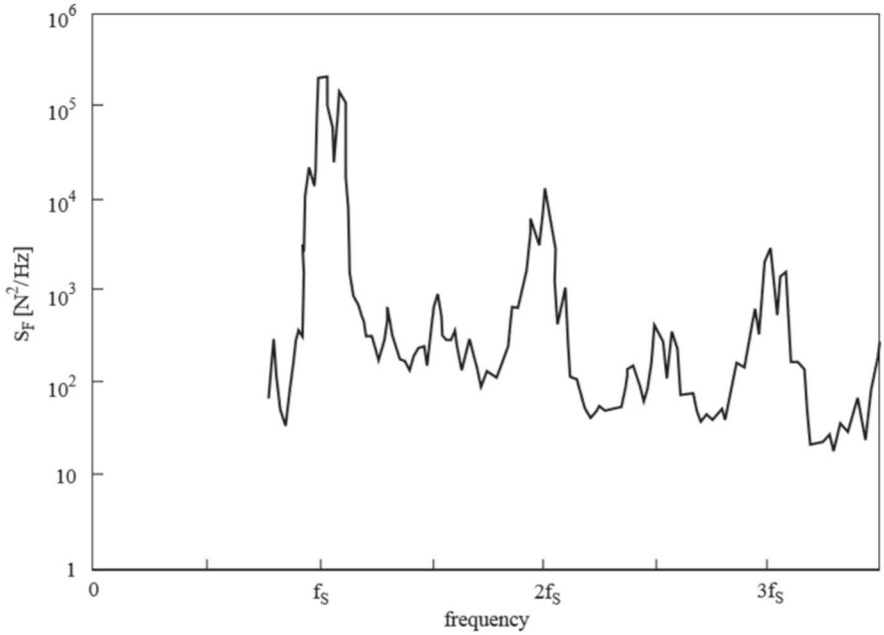

Figure 1.3.8 Auto Spectral Density function of the human gait [37].

Finally, in the last two decades, technology developments allowed a better observation of the human gait. However, results of these measurements are still not used in civil engineering and several studies are in progress to improve the knowledge about evaluation and modeling of human-induced loads with these techniques.
A literature review about this topic is provided in *Racic et al* [46]. The basic idea is to use the Newton's Second Law to compute GRFs F_{GR}:

$$\boldsymbol{F_{GR}} = m(\boldsymbol{a_{BCM}} + \boldsymbol{g}) \qquad \text{Eq. 1.3.4}$$

In the above equation $\boldsymbol{a_{BCM}}$ and $\boldsymbol{g}$ are vectors of the human body center of mass (BCM) and gravity accelerations respectively. The determination of the $\boldsymbol{a_{BCM}}$ vector is not straightforward, being difficult the determination of the center of gravity of the human body and, then, of its kinematic quantities. Considering results typical of anthropometry, i.e. of the science doing statistical studies of measurable quantities of the human body, the problem is made easier by the body discretization in smaller segments. Based on cadaver studies, the first scientists of this discipline tried to estimate the position of the human body center of mass identifying smaller parts and determining their centers of gravity. If the term *proximal* indicates the point of a segment nearer to the body center and *distal* its opposite, in Table 1.3.1 results by three different authors are given on the position of centers of gravity for each of the segments in which the body has been discretized.

Table 1.3.1 Locations of segmental center of mass after various authors. If the length of each segment is equal to one, the positions of their center of mass are given through the *proximal* and *distal* notation [46].

Source	Dempster [235]		Clauser et al. [237]		de Leva [252]	
	Proximal	Distal	Proximal	Distal	Proximal	Distal
Hand	0.506	0.494	0.1802	0.8198	0.7900	0.2100
Forearm	0.430	0.570	0.3896	0.6104	0.4574	0.5426
Upper arm	0.436	0.564	0.5130	0.4870	0.5772	0.4228
Foot	0.500	0.500	0.4485	0.5515	0.4415	0.5585
Shank	0.433	0.567	0.3705	0.6295	0.4459	0.5541
Thigh	0.433	0.547	0.3719	0.6281	0.405	0.5905
Trunk	0.495	0.505	0.3803	0.6197	0.5514	0.4486
Head	1.00	0.000	0.4642	0.5358	0.4024	0.5976

Today, the method to estimate BSIP (body segment inertial parameters) of human body is to develop a mathematical model capable to approximate segments even with geometric complex solids. To implement these complex models (Figure 1.3.9), several measurements are needed but the results are satisfactory.

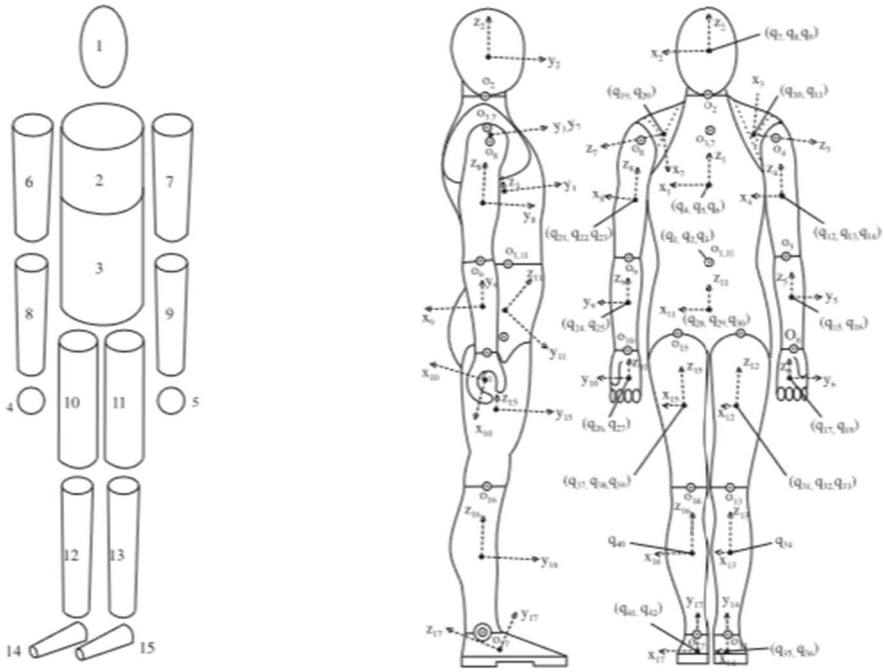

a) b)

Figure 1.3.9 Mathematical model for human body segments, after a) *Hanavan* [11] and b) *Hatze* [17].

The second issue is the determination of accelerations to be given to the mathematical model in order to well reproduce the human movement and, then, to allow the computation of human induced loads. Skin markers, nothing but optical sources attached to the skin of the subject, can be retro-reflective (passive) or light emitting (active). They are placed on special points on the body called *anatomical landmarks* and their movement is detected through

different technologies. Time histories of accelerations are used to compute the center of gravity acceleration and finally the total GRFs. Anyway, the whole process, from the positioning of markers to the acquisition of acceleration time histories and determination of complex solids properties with reference to a given subject, presents a lot of advantages as well as disadvantages. It has been proven that the method could work to well represent GRFs but there are still a lot of imperfections. The method presents enormous potential but a research effort is still necessary before it is possible to use these results in civil engineering.

1.4 Force modeling

Because of the great variability of GRFs, depending on the very particular nature of this type of forces it is, still today, very difficult to model human induced loads. It is not simple to determine a way to take into account their variation in time but also in space, the inter- and intra-subject variability, the influence of external situations like the presence of other people and the possibility of a certain degree of correlation, the possibility that humans adapt their way of walking in case they perceive or not vibrations produced by themselves.
Different models have been proposed:

- *Time-domain force models:* they are based on the assumptions that both feet produce the same effects and repeat periodically. They are classified in:
  - *Deterministic force models*, whose aim is to try to model each type of human activity in every situation;
  - *Probabilistic force models*, that consider the great randomness of the whole process and want to model probability distribution functions of random variables influencing it.
- *Frequency-domain force models*, assume that human walking is a narrow-band process.

Time-domain force models are largely the most commonly used.

1.4.1 Deterministic force models

According to the assumption that human induced loads are periodic forces, they can be represented in the time domain by a Fourier series:

$$F_p(t) = G + \sum_{i=1}^{n} G\alpha_i \sin(2\pi i f_p t - \phi_i) \qquad \text{Eq. 1.4.1}$$

Where:

- G is the person's weight $[N]$, usually assumed equal to 700 N;

- α_i are the Fourier's coefficients of the i-th harmonic, usually identified as dynamic load factors (DLFs);
- f_p is the step frequency $[Hz]$;
- ϕ_i is the phase shift with respect to the i-th harmonic;
- n is the total number of the contributing harmonics.

Given that activity rates are measurable and phase shifts can be determined randomly, the most important parameters are DLFs. Starting from the seventies, many trials and full-scale experiments have been conducted. It has been found that DLFs depends on the rate activity as well as on the person's velocity and contributing harmonics. *Živanović et al.* [40] reported results of different authors (Table 1.4.1).

Table 1.4.1 DLFs for single person force models after different authors [40].

Author(s)	DLFs for considered harmonics	Comment	Type of activity and its direction
Blanchard et al. [34]	$\alpha_1 = 0.257$	DLF is lessen for frequencies from 4 to 5 Hz	Walking—vertical
Bachmann and Ammann [14]	$\alpha_1 = 0.4 - 0.5$ $\alpha_2 = \alpha_3 = 0.1$	Between 2.0 and 2.4 Hz At approximately 2.0 Hz	Walking—vertical
Schulze (after Bachmann and Ammann [14])	$\alpha_1 = 0.37$, $\alpha_2 = 0.10$, $\alpha_3 = 0.12$, $\alpha_4 = 0.04$, $\alpha_5 = 0.08$	At 2.0 Hz	Walking—vertical
	$\alpha_1 = 0.039$, $\alpha_2 = 0.01$, $\alpha_3 = 0.043$, $\alpha_4 = 0.012$, $\alpha_5 = 0.015$	At 2.0 Hz	Walking—lateral
	$\alpha_{1/2} = 0.037$, $\alpha_1 = 0.204$, $\alpha_{3/2} = 0.026$, $\alpha_2 = 0.083$, $\alpha_{5/2} = 0.024$	At 2.0 Hz	Walking—longitudinal
Rainer et al. [42]	α_1, α_2, α_3 and α_4	DLFs are frequency dependent (Fig. 10)	Walking, running, jumping—vertical
Bachmann et al. [48]	$\alpha_1 = 0.4/0.5$, $\alpha_2 = \alpha_3 = 0.1/-$	At 2.0/2.4 Hz	Walking—vertical
	$\alpha_1 = \alpha_3 = 0.1$	At 2.0 Hz	Walking—lateral
	$\alpha_{1/2} = 0.1$, $\alpha_1 = 0.2$ $\alpha_2 = 0.1$	At 2.0 Hz	Walking—longitudinal
	$\alpha_1 = 1.6, \alpha_2 = 0.7$, $\alpha_3 = 0.2$	At 2.0–3.0 Hz	Running—vertical
Kerr [36]	α_1, $\alpha_2 = 0.07$, $\alpha_3 \approx 0.06$	α_1 is frequency dependent (Fig. 11)	Walking—vertical
Young [56]	$\alpha_1 = 0.37(f - 0.95) \leqslant 0.5$ $\alpha_2 = 0.054 + 0.0044f$ $\alpha_3 = 0.026 + 0.0050f$ $\alpha_4 = 0.010 + 0.0051f$	These are mean values for DLFs	Walking—vertical
Bachmann et al. [48]	$\alpha_1 = 1.8/1.7$, $\alpha_2 = 1.3/1.1$, $\alpha_3 = 0.7/0.5$	Normal jump at 2.0/3.0 Hz	Jumping—vertical
	$\alpha_1 = 1.9/1.8$, $\alpha_2 = 1.6/1.3$, $\alpha_3 = 1.1/0.8$	High jump at 2.0/3.0 Hz	Jumping—vertical
	$\alpha_1 = 0.17/0.38$, $\alpha_2 = 0.10/0.12$, $\alpha_3 = 0.04/0.02$	At 1.6/2.4 Hz	Bouncing—vertical
	$\alpha_1 = 0.5$	At 0.6 Hz	Body swaying while standing—lateral
Yao et al. [52]	$\alpha_1 = 0.7$, $\alpha_2 = 0.25$	Free bouncing on a flexible platform with natural frequency of 2.0 Hz	Bouncing—vertical

1.4.2 Probabilistic force models

The probabilistic force models are still based on the idea that human induced loads are periodic. The difference is that they are built with the aim to reproduce the large randomness of the human gait.

One important example of force modeling with a probabilistic approach is provided by *Živanović et al.* [39]. The innovation of this work is to consider DLFs as random variables and represent them through their normalized distribution (Figure 1.4.1). DLFs are computed for the main harmonics but, looking at the spectrum of GRFs, it is possible to identify the presence of sub-harmonics with their own DLFs.

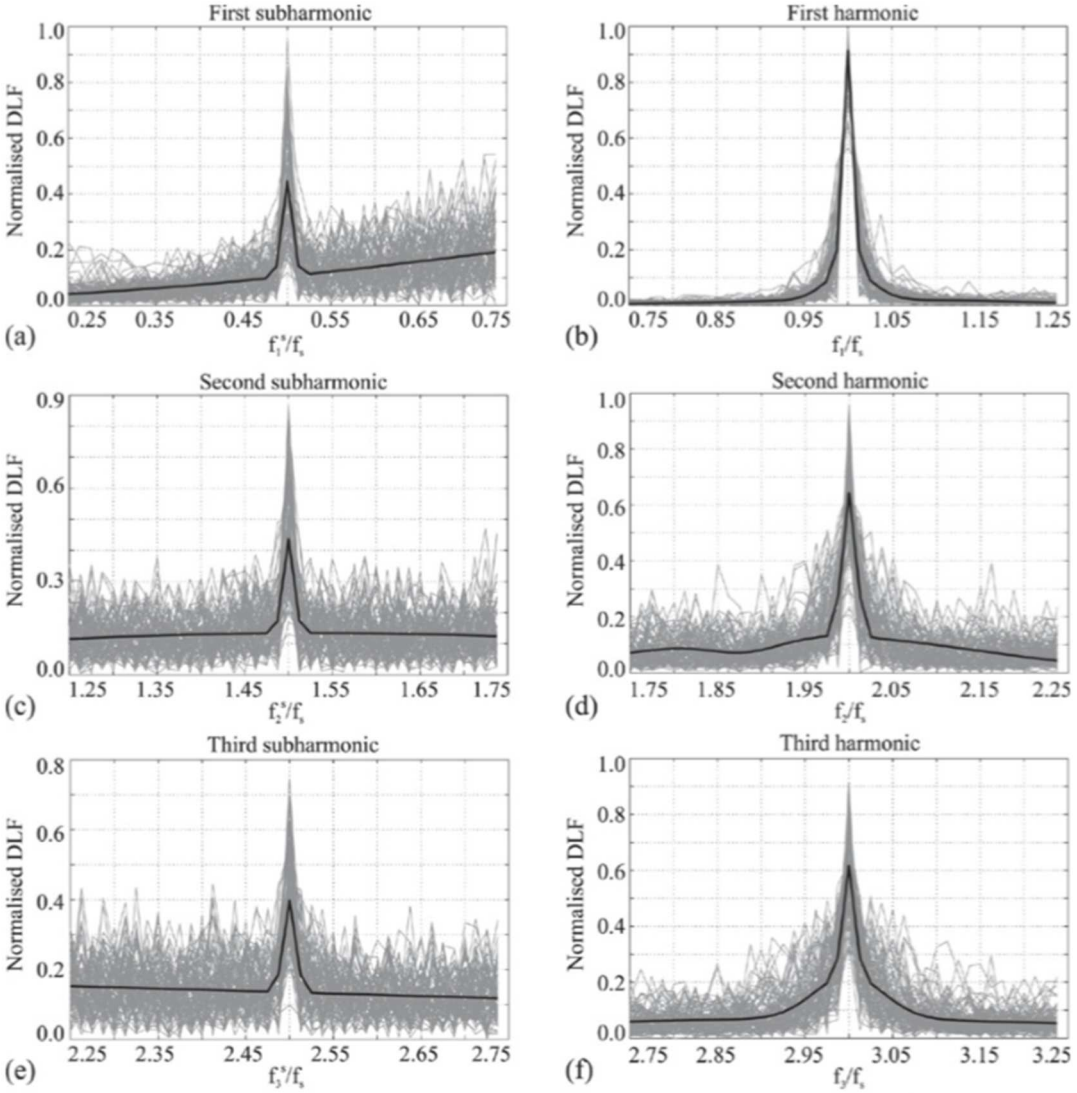

Figure 1.4.1 Normalized distributions of DLFs up to the third harmonic [39].

Instead of applying discrete values in Eq. 1.4.1, DLFs are inserted in form of normalized distribution, to obtain normalized distribution of forces in time domain. Applying this kind of forces with the procedure described in [39], the response of the structure can be given in terms of probability of overcoming a given threshold of vibrations.
The method presents a great potential and its simplicity could be, as stated in the conclusions of the paper, the determinant for future applications in vibration assessment due to a single person walking.

1.4.3 Frequency-domain force models

The force model described in the previous paragraph has been developed from the results obtained in the frequency-domain analysis by *Brownjohn et al.* [27], reached after several studies done in this field opened by Eriksson [37]. He first produced the ASD of a walking force (Figure 1.3.8). *Brownjohn et al.* established a frequency-domain force model to represent a group of imperfect pedestrians with a varying degree of correlation or synchronization.
Based on the assumption that the spatial distribution of this load can be similar to the wind action, using a coherence function, they proposed to estimate the ASD of the structure response as follows:

$$S_X(f) = \psi_z^2 |H(f)|^2 S_{P,1}(f) \int_0^L \int_0^L \psi_{z_1} \psi_{z_2} coh(f, z_1, z_2) dz_1 dz_2 \qquad \text{Eq. 1.4.2}$$

Where

- $S_{P,1}(f) = \left({}^{NW}/_{L}\right)^2 \phi(f) \frac{G_1^2(f)}{2}$ is the ASD of walking loads per unit length for the fundamental harmonic;
- N, W and L are the number and weight of pedestrians and the span length;
- $\phi(f) = \frac{1}{\sqrt{2\pi}\sigma_f} exp\left(-\frac{(f-\mu_f)^2}{2\sigma_f^2}\right)$ is the probability density function of pedestrians' distribution with a mean μ_f and variance σ_f^2;
- $G_1(f)$ is the normalized distribution of DLF for the first harmonic (Figure 1.4.2);
- $H(f) = \frac{1}{m_r} \frac{-f^2}{f_r^2\left(1-\frac{f^2}{f_r^2}+2i\xi_r\frac{f}{f_r}\right)}$ is the frequency response function for acceleration response;
- f_r, m_r and ξ_r are the r-th natural frequency, modal mass and modal damping ratio respectively;
- ψ_{z_i} are mode shape ordinates related to the location of two pedestrians on the bridge at distances z_i;

- $0 < coh(f, z_1, z_2) < 1$ is the function expressing the degree of correlation between pedestrians;

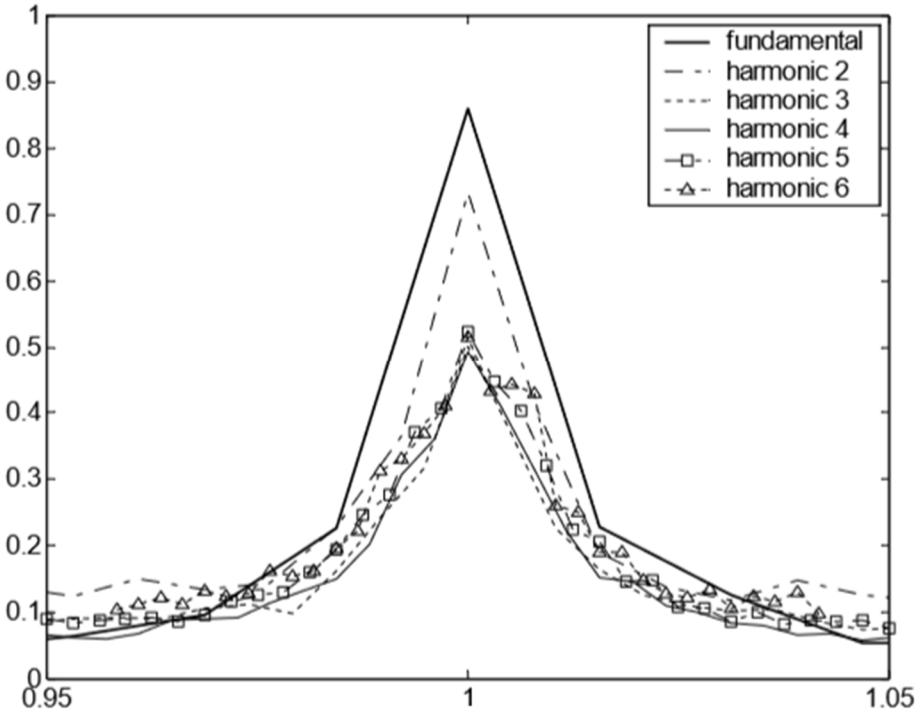

Figure 1.4.2 Normalized DLFs distributions [27].

The complexity of method makes it not easily usable. That is the reason why time-domain force models are more applied in serviceability assessment of footbridges.

1.5 The vibration path: features

The transmission path is the way through which vibrations coming from the source arrive to the receiver. ISO10137 [24] states that "the transmission path has the effect of modifying the vibrations from the source to the receiver due to discontinuities, attenuation due to geometric spreading and material damping, and possible amplification or attenuation in certain frequency ranges".
To obtain the dynamic response of a multi degrees of freedom system, as in the case of a FE model, the software will compute the solution of the following equations of motion:

$$\boldsymbol{M}\ddot{\boldsymbol{x}}(t) + \boldsymbol{C}\dot{\boldsymbol{x}}(t) + \boldsymbol{K}\boldsymbol{x}(t) = \boldsymbol{f}(t) \qquad \text{Eq. 1.5.1}$$

where $\boldsymbol{M}$, $\boldsymbol{C}$, and $\boldsymbol{K}$ are the structural matrices of mass, damping and stiffness respectively, while $\boldsymbol{x}(t)$, $\dot{\boldsymbol{x}}(t)$, $\ddot{\boldsymbol{x}}(t)$ are displacements, velocities and accelerations vectors. On the right-hand side, $\boldsymbol{f}(t)$ is the forces vector.

The mass and stiffness matrices are determined as a function of geometry and material properties. Obviously, in geometry, the choice about the degree of discretization plays a role. The finest the discretization, the more precise will be the determination of the structure stiffness. Anyway, even knowing all details of the structure, a certain level of error in the computation of eigenmodes is always there, as proved by different papers, quoted in *Živanović et al.* [40]. There are, however, procedures to improve final element models so that they provide results in agreement with experimental data. However, at the design stage, they are not applicable since there are not available experimental data. The most common criteria are the MAC (Modal Assurance Criterion) and COMAC (Coordinate Modal Assurance Criterion). Through a sensitivity analysis, making small variations of material properties and/or geometry, it is possible to evaluate MAC and COMAC such that these parameters tend to be equal to one, showing a high degree of correlation between experimental and analytical data. Procedure and principle of these criteria are described in *Brownjohn et al.* [29] and *Gardner-Morse et al.* [31] applied to cases of given structures.
The damping matrix represents the energy dissipation in the equation of motion, and its derivation can be the most complex aspect to play with when doing a dynamic analysis. Damping phenomena can be due to the following reasons:

- Hysteretic behavior of structural elements;
- Behavior of joints and connections between structural elements
- Motion of foundation elements
- Introduction in the structural system of damping devices for vibration mitigation;
- Effects of relative movement between structure and surrounding fluid (air or water for example).

From a mathematical point of view, these phenomena are so complex that their modeling is a challenge. They are generally seen as a source of damping forces, almost one order of magnitude smaller than inertia or elastic forces. The most efficient and practical way to model them is to use a viscous model. This leads to add the velocity dependent term in the equation of motion. The coefficients C_{ij} of damping matrix must be determined. Being not easy to derive $n \times n$ coefficients of the damping matrix, where n is the number of degree of freedom for the discretized structure, one possible solution is to follow a modal approach. Assuming that the damping matrix is uncoupled by the same coordinate transformation that uncouples mass and stiffness matrix, a system of decoupled equations is obtained, each associated to a value of modal damping ratio. In this case, the number of equations to solve is much smaller since the structure response depends on a limited number of modes. Higher modes effect can be neglected.
To decouple equations, the diagonalization of the damping matrix is necessary. Following developments of [38] and [26], the modal expansion of displacements is adopted:

$$\boldsymbol{x}(t) = \boldsymbol{\Phi}\, \boldsymbol{y}(t) \qquad \text{Eq. 1.5.2}$$

where $\boldsymbol{\Phi}$ is the matrix of eigenvectors $\boldsymbol{\varphi}_n$ and $\boldsymbol{y}(t)$ the vector of modal coordinates. If the orthogonality condition is guaranteed for the damping matrix too, uncoupled modal equations will have the following shape:

$$\ddot{y}_n(t) + 2\xi_n\omega_n\dot{y}_n(t) + \omega_n^2 y_n(t) = \frac{F_n(t)}{M_n} \qquad \text{Eq. 1.5.3}$$

In which:

- $M_n = \boldsymbol{\varphi}_n{}^T \boldsymbol{M} \boldsymbol{\varphi}_n$
- $2\xi_n\omega_n = \frac{\boldsymbol{\varphi}_n{}^T \boldsymbol{C} \boldsymbol{\varphi}_n}{M_n}$
- $\omega_n^2 = \frac{\boldsymbol{\varphi}_n{}^T \boldsymbol{K} \boldsymbol{\varphi}_n}{M_n}$
- $F_n(t) = \boldsymbol{\varphi}_n{}^T \boldsymbol{f}(t)$

One possible way to ensure uncoupling can be achieved through the well-known proportional damping model, introduced by Rayleigh, for which the damping matrix, in case of homogeneous systems, results from a linear combination of mass and stiffness matrices:

$$\boldsymbol{C} = \boldsymbol{\alpha M} + \boldsymbol{\beta K}$$

In this equation $\boldsymbol{\alpha}$ and $\boldsymbol{\beta}$ are two arbitrary proportionality factors. Otherwise, for non-homogeneous systems, it is necessary to determine the two parameters independently for each subsystem (Figure 1.5.1).

For any two modes *i* and *j*, we can specify damping ratios ξ using the following expressions, where ω_i is equal to $f_i/2\pi$:

$$\begin{aligned} \boldsymbol{\varphi}_i{}^T \boldsymbol{C} \boldsymbol{\varphi}_i &= \boldsymbol{\varphi}_i{}^T (\boldsymbol{\alpha M} + \boldsymbol{\beta K}) \boldsymbol{\varphi}_i = 2\xi_i\omega_i = \boldsymbol{\alpha} + \boldsymbol{\beta}\omega_i{}^2 \\ \boldsymbol{\varphi}_j{}^T \boldsymbol{C} \boldsymbol{\varphi}_j &= \boldsymbol{\varphi}_j{}^T (\boldsymbol{\alpha M} + \boldsymbol{\beta K}) \boldsymbol{\varphi}_j = 2\xi_j\omega_j = \boldsymbol{\alpha} + \boldsymbol{\beta}\omega_j{}^2 \end{aligned} \qquad \text{Eq. 1.5.4}$$

Or, in a different way:

$$\xi_n = \frac{1}{2}\left(\frac{\boldsymbol{\alpha}}{\omega_i} + \boldsymbol{\beta}\omega_i\right) \qquad \text{Eq. 1.5.5}$$

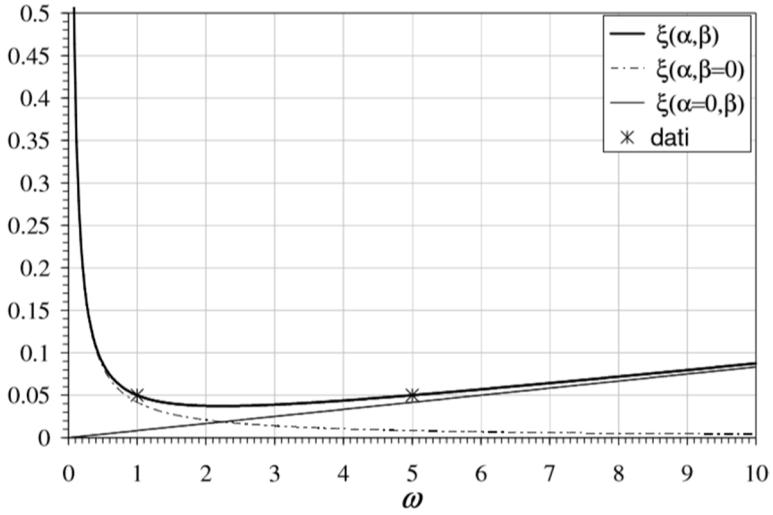

Figure 1.5.1 Graphical visualization of Rayleigh Damping as function of circular frequency after *Perotti* [13].

Through experimental data, it is possible to determine $\boldsymbol{\alpha}$ and $\boldsymbol{\beta}$ parameters knowing one or two, at least, damping ratios values. They can be determined from the response logarithmic decay. In the case of free vibration response of an under-damped structure ($\xi < 1$) for a SDOF system, the response has the shape illustrated in Figure 1.5.2.

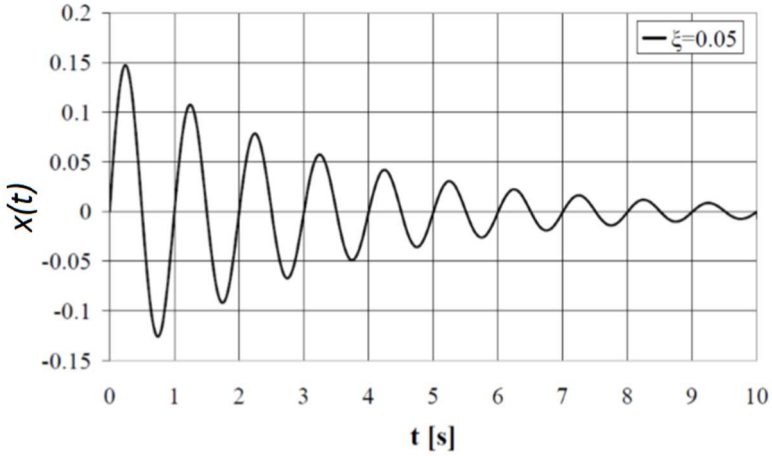

Figure 1.5.2 Free vibration oscillations for a damped SDOF [13].

Free vibration is a periodic response with period T_D. If we denote the displacement as $x(t)$, it is represented by the analytical solution of the equation of motion for a free vibration damped problem:

$$x(t) = \bar{x}e^{-\xi\omega_1 t}\sin(\omega_D t + \varphi) \qquad \text{Eq. 1.5.6}$$

Considering peaks of displacements at times $\bar{t}$ and $\bar{t} + T_D$, the logarithmic decrement is defined as the natural logarithm of the ratio between the two peaks and is equal to:

$$\delta = \ln\left(\frac{x(\bar{t})}{x(\bar{t}+T_D)}\right) = \xi\omega_1 T_D = 2\pi\xi \qquad \text{Eq. 1.5.7}$$

From Eq. 1.5.7 the damping ratio ξ is determined. Several test procedures to determine damping ratios have been developed starting from 1970s. This thesis refers to the work of *Živanović et al.* that, in the literature review at [40], collected results of over ten years of studies between 1990s and 2000s for damping ratios for different bridge types, span length, material and mode of vibrations (Table 1.5.1).

Table 1.5.1 Measured damping ratios (h=horizontal, v=vertical, t=torsional) for some footbridges [40].

Author(s)	Bridge type	Main Span (m)	Girders	Deck	ζ_v (%)	ζ_h (%)	ζ_t 9(%)	Estimation method
Gardner-Morse and Huston [86]	Cable-stayed	54.9	Steel	Laminated wood	0.53/0.22	–	0.46/0.36	Curve fitting
Brownjohn et al. [87]	Suspended	50	Steel	Concrete panels	2.68/0.50	1.00/0.70	0.84[a]/0.50	Curve fitting
Brownjohn [91]	Suspended	35	Steel	Timber	1.0/1.0	High[b]	2.4[b]/1.4[b]	Free-decay after jumping
Cantieni and Pietrzko [111]	Continuous space truss	54	Wood	—	1.4/1.3	2.9/2.1[c]	1.4	Curve fitting
Pimentel [58]	Pre-cambered beam	19.9	Steel	Concrete	0.73 & (0.40) [0.53]/0.65	—	—	Curve fitting & free-decay after (walking) [jumping]
Pimentel [58]	Stressed ribbon	34	—	Prestressed concrete	0.56 (0.65)/ 0.64 (1.02)	—	–	Free-decay after walking (jumping)
Pimentel [58]	Cable-stayed	63	—	Glass-reinforced plastic	0.84/0.94	—	—	Free-decay after bouncing
Pavic and Reynolds [112]	Stressed ribbon	34	—	Pre-stressed concrete	0.53/0.65	—	0.50/0.60	Curve fitting
Pavic et al. [113]	Suspended	144	Steel	Aluminium	—	0.76/1.30	—	Curve fitting
Hamm [114]	Framework	68	Wood and steel	—	1.2 (0.8-1.35)	—	—	Half-power bandwidth (free decay)
Caetano and Cunha [115]	Stressed ribbon	30	—	Concrete	1.7/3.6[d]	—	—	Free-decay after skipping
Fletcher and Parker [116]	Multi-cable-stayed	53	—	Reinforced concrete	0.40 (0.51)/ 0.21 (0.41)	0.44[b]	—	Free decay (curve fitting)

Note: In case of more than one damping value measured, the average value is given.
[a]Half power bandwidth.
[b]Estimated methods are not stated.
[c]Coupled with vertical movement.
[d]Not clear the way of identification having in mind that two closely spaced modes appeared.

Underlining that damping ratio values varies as a function of span length, structural system and many other parameters, very interesting data that can be extracted from Table 1.5.1 are those coming from *Brownjohn et al.,* because they concern the same structural materials and almost the same bridge type of the one at study in this thesis.

To determine $\boldsymbol{\alpha}$ and $\boldsymbol{\beta}$ parameters for the Rayleigh during the design phase of a given structure, damping measures on existing structures or assumptions based on literature can provide the value of the damping ratios. The parameters are then obtained by solving the system in Eq. 1.5.4:

$$\boldsymbol{\alpha} = 2\omega_i\omega_j \frac{\xi_j\omega_i - \xi_i\omega_j}{\omega_i^2 - \omega_j^2} \qquad \text{Eq. 1.5.8}$$

$$\boldsymbol{\beta} = 2\frac{\xi_i\omega_i - \xi_j\omega_j}{\omega_i^2 - \omega_j^2} \qquad \text{Eq. 1.5.9}$$

1.6 Human-structure interaction

The phenomenon originating the excessive level of vibration in both Solferino and Millennium footbridge is named *lock-in*. This phenomenon can be defined as the one in which the pedestrian "synchronizes his footfall rate to the frequency of the swaying platform" [34]. Today, after the large number of studies done on Solferino and Millennium Footbridges, it is generally accepted that during footbridge vibrations there is a kind of human-structure interaction. Its effects cannot be neglected throughout the design phase.

There are two important aspects that deserve to be examined. First, the presence of pedestrians and their movement change the damping properties and natural frequencies of the footbridge. Second, the degree of synchronization among pedestrians or between pedestrians and structure is directly linked to the crowd density.

As for damping properties, it is well demonstrated but even intuitive that before lock-in appears, humans behave like extra dampers on the structure: damping is more efficient in the joint human-structure system with respect to the case of the empty structure. For example, to account for this issue other than for the change in the structure stiffness, *Lai and Mulas* [9], modeled the pedestrian as a MSD (Mass-Spring-Damper) system to obtain the bridge numerical response considering the mutual influence between human and structure (Figure 1.6.1).

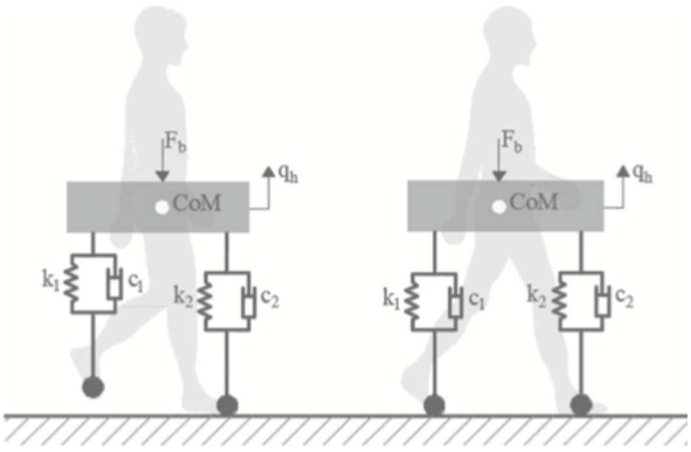

Figure 1.6.1 Mass-Spring-Damper model to model human structure interaction [9].

As for the influence of crowd density on human behavior, several studies confirmed that crowd density influences the walking speed, the degree of synchronization and the intensity

of human induced load. This phenomenon, that may be also subconscious, can be understood considering the road traffic: drivers adapt their velocity to that of cars in front and behind them. As the traffic density increases, the probability that all cars have the same speed increases too.

The lock-in phenomenon could be caused by lateral or vertical synchronization. After video evaluations, during the opening of Millennium Bridge, *Dallard et al.* [34] estimated that lateral acceleration was $0.20 - 0.25\ g$ while displacements had an amplitude of up to 7 cm in the lateral direction. They proposed that, after synchronization, the dynamic force produced by pedestrians $F(t)$ was proportional to the deck lateral velocity $v(t)$:

$$F(t) = kv(t) \qquad \text{Eq. 1.6.1}$$

Where k is a proportionality constant estimated to be equal to 300 $^{Ns}/_{m}$ for the Millennium Bridge. This shows that human induced loads should be modeled differently before and after the lock-in occurrence.

Another parameter to estimate the possibility for the lateral lock-in to occur is the critical number of people crossing the bridge:

$$N_L = \frac{8\pi cfM}{k} \qquad \text{Eq. 1.6.2}$$

In this equation c is the modal damping ratio, f is the lateral frequency of the bridge, M is the corresponding modal mass and k was already defined [34]. The problem is that a collection of k values to determine the proper value for a given bridge does not exist yet.

As for the vertical synchronization issue, two attempts to deal with the problem must be quoted. The first one is based on the idea that the design should be done by prescribing that the response acceleration produced after the synchronization must be below a certain threshold. In [16], as reported by *Živanović et al.* [40], it was proposed that the acceleration response of the structure a_g must be computed as a function of the probability of synchronization $P_S(a_g)$, the number of people on the structure N and the response acceleration for a single pedestrian a_{1rz} in vertical direction:

$$a_g = P_S(a_g)KNa_{1rz} \qquad \text{Eq. 1.6.3}$$

where K is a factor accounting for the fact that the load changes position on the structure. Unfortunately, K is not tabulated for large numbers of configurations. But, on the other hand, the author suggested to consider the multiplication factor:

$$S = P_S(a_g)K \qquad \text{Eq. 1.6.4}$$

This factor is given for groups of people up to 10 as a function of the frequency in Figure 1.6.2.

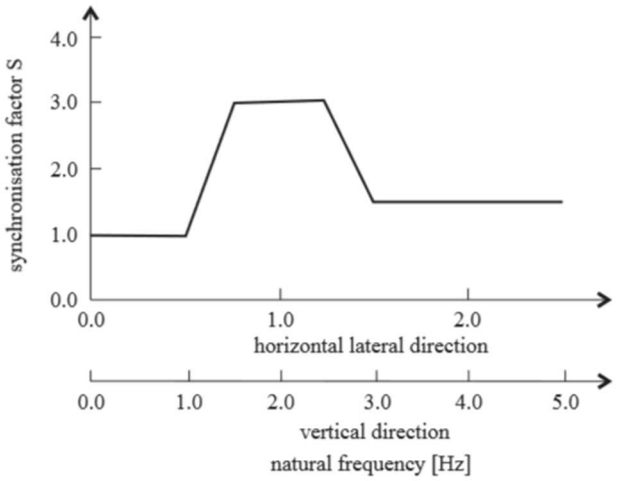

Figure 1.6.2 Multiplication factor values as function of natural bridge frequencies [16].

The second approach is based on principles typical of the wind engineering and was proposed by *McRobie and Morgenthal* [1]. The serviceability of a pedestrian footbridge could be assessed by evaluation of the *vertical Pedestrian Scruton Number*:

$$vPSN = k_1 k_2 m \qquad \text{Eq. 1.6.5}$$

Where $k_1 = {}^{\xi}/_{0.005}$, $k_2 = {}^{0.6}/_{n}$ and m are factors representing the influence of the damping ratio, of the crowd density, that could be different from the typical value of 0,6 ${}^{persons}/_{m^2}$, and of the mass per unit deck area for an equivalent simply supported beam having constant cross section. In wind engineering, in fact, the Scruton number is defined as a dimensionless parameter evaluating the sensitivity of a structure to wind induced vibrations. High values of the Scruton number correspond to a reduced amplitude of oscillations. Depending on the structure at study, there are certain thresholds to ensure to reduce vibrations.

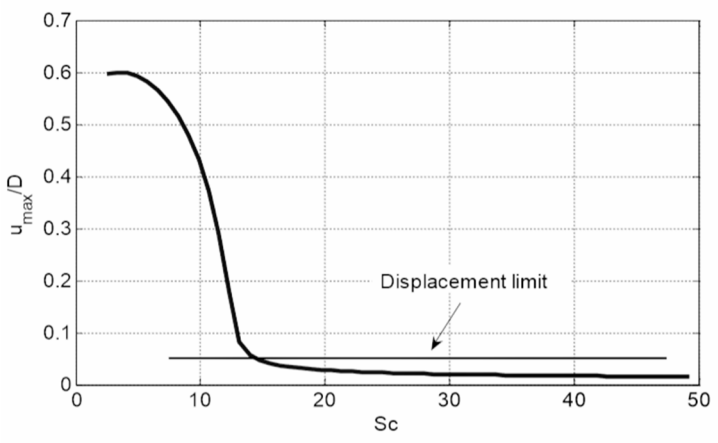

Figure 1.6.3 Displacement of the tip of a chimney as function of the Scruton number [43]

Unfortunately, in footbridges design, values of the Scruton number as a function of frequencies are not available, mainly for two reasons. First, the approach is relatively recent and no database of pedestrian Scruton Number exists. Second, footbridges tend to vibrate in lateral way, so it has not been possible to evaluate on large scale pedestrian Scruton numbers values.

CHAPTER 2
THE STRUCTURE

Chapter 2 describes the structure analyzed in this thesis, a footbridge that should be realized in a few months. It is a steel structures and has a peculiar geometry: two arches with a linearly variable L-shaped section are inclined of 15° and sustain the deck through steel tendons. The plane of walking is made of wood.
First, the structure is inserted in its geographical context. The process that led to its conception is presented, and its characteristics are described.

2.1 Position of the structure

The structure at study is a new footbridge that will be built in the town of Louvain La Neuve (Figure 2.1.1). The preliminary design was carried out by the Engineering office Mc Carré. The design stage is currently in progress.

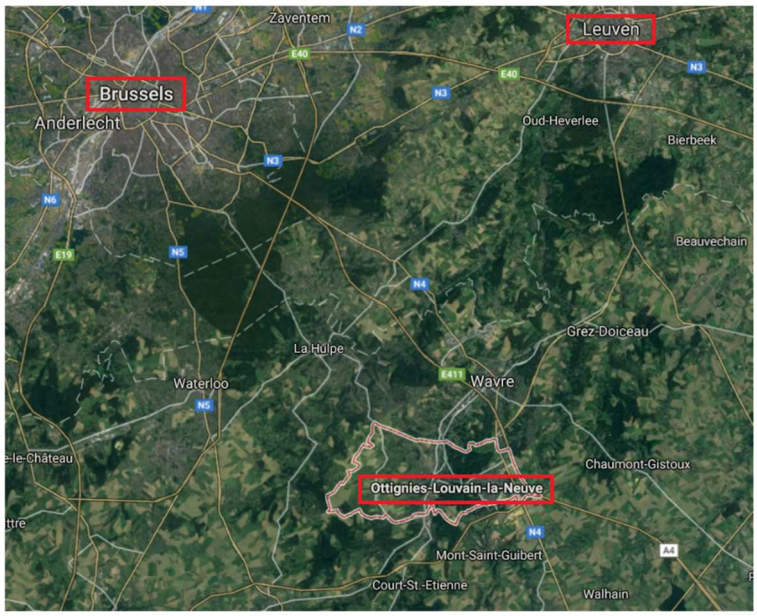

Figure 2.1.1 Position of Louvain La Neuve with respect to Brussels and Leuven (Google maps).

Louvain la Neuve is part of the municipality of Ottignies-Louvain La Neuve. This small town was born in seventies after the will of the Academic French speaking community of KUL (*Katholieke Universiteit Leuven*), the historical University of Leuven in the Flemish region of Belgium, to have a reference university with a French background. In its name, the history of this settlement can be recognized in the term "La Neuve", that just refers to "the new" Leuven. This city is situated in the French speaking region of Belgium, Wallonia, about thirty-five kilometers South with respect to Brussels and Leuven (Figure 2.1.1).

As a very young city, Louvain is still in an expansion phase. A new district (Courbevoie) will be built near an existing one (Lauzelle). Figure 2.1.2 and Figure 2.1.3 illustrate where the footbridge will be placed.

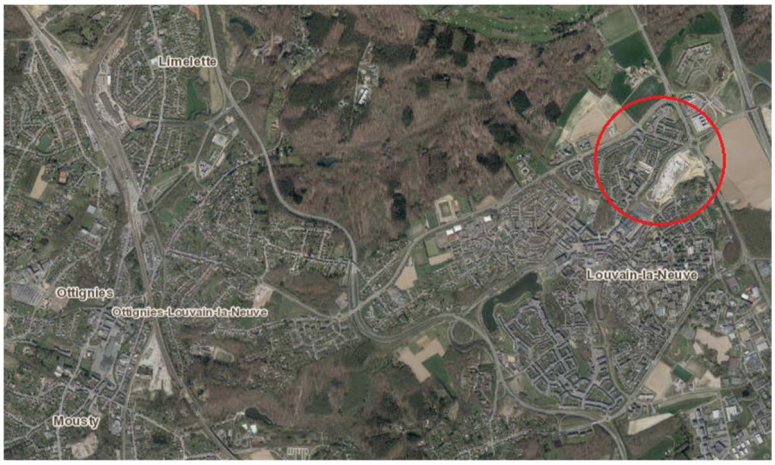

Figure 2.1.2 Location of the future district in the municipality (GeoPortail Wallonia).

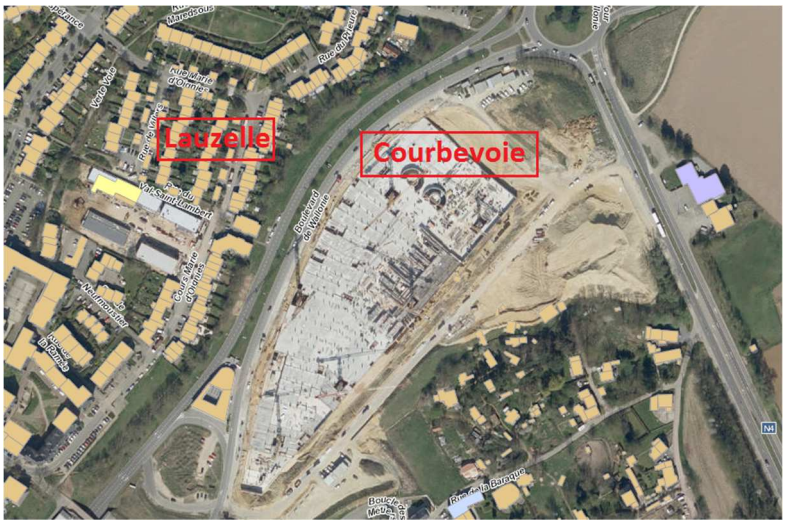

Figure 2.1.3 Works in progress for the construction of the new district (GeoPortailWallonia).

The goal of the footbridge is to connect the old and the new to ensure continuity in the expansion of the city. In effect, Louvain La Neuve can be considered as a particular city, not only for its history extremely linked to the establishment of a university, but, above all, for the fact that it is a completely pedestrian city. No vehicles pass in the center of the town and car parks are underneath the city. So, the footbridge will guarantee the possibility to move from a district to the other without necessarily using a vehicle, either public or private.

2.2 Geometry and material properties

The footbridge, located as in Figure 2.2.1, is a steel structure. Two arches, with a linear

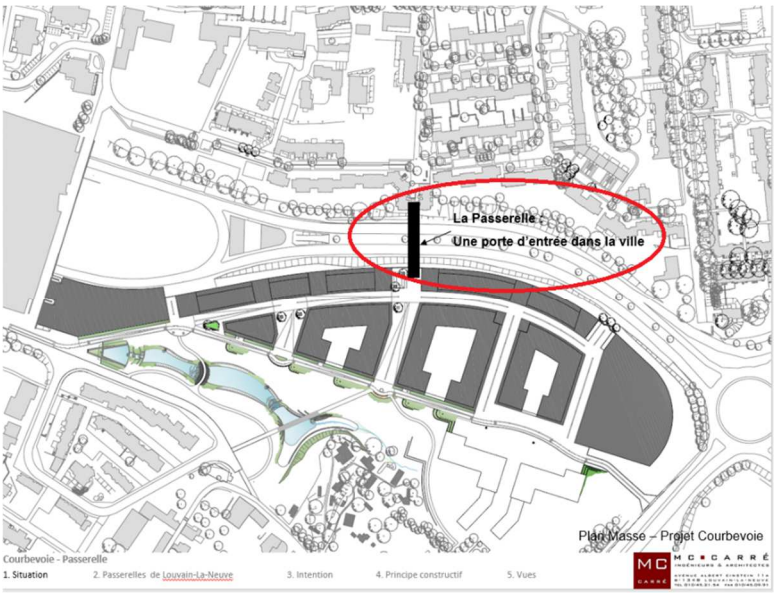

Figure 2.2.1 Position of the footbridge (MC Carré).

variable section, support the deck. They are inclined with an angle of 15° with respect to the vertical line, being nearer each other at their bases. In addition, four struts elements, H tapered section, link the deck with the ground. (Figure 2.2.2)

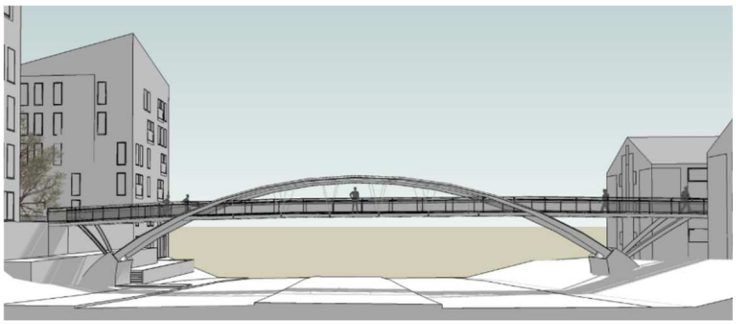

a)

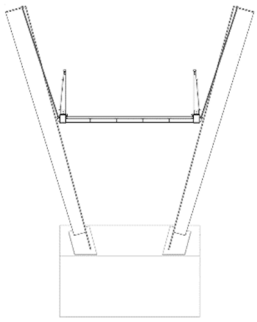

b)

Figure 2.2.2 a) Lateral view of the structure (Mc Carré): the footbridge links the Lauzelle District (on the left) with the Courbevoie District (on the right); b) Footbridge section of the central span.

The latter are positioned, in couple, such that their end sections represent additional supports for the deck in the zone between neoprene supports and arches-deck connection. They start from the ground at the same footings of the arches. In a lateral view, the inclination of the two couple of struts is different. With respect to the vertical direction, they are inclined of an angle of 37° on the left side and of an angle of 52°, on the other side (Figure 2.2.2). This difference reflects the different length of elements (2.75 m for the element at the

left side and 4.35 *m* for the one at the right side) as well as the in-plane angle of inclination. In fact, even if they start and end in points lying on parallel lines, also in this case, angles of inclination are different: with respect to the horizontal, 40° for elements on the left and 22° for those on the right (Figure 2.2.3 b).

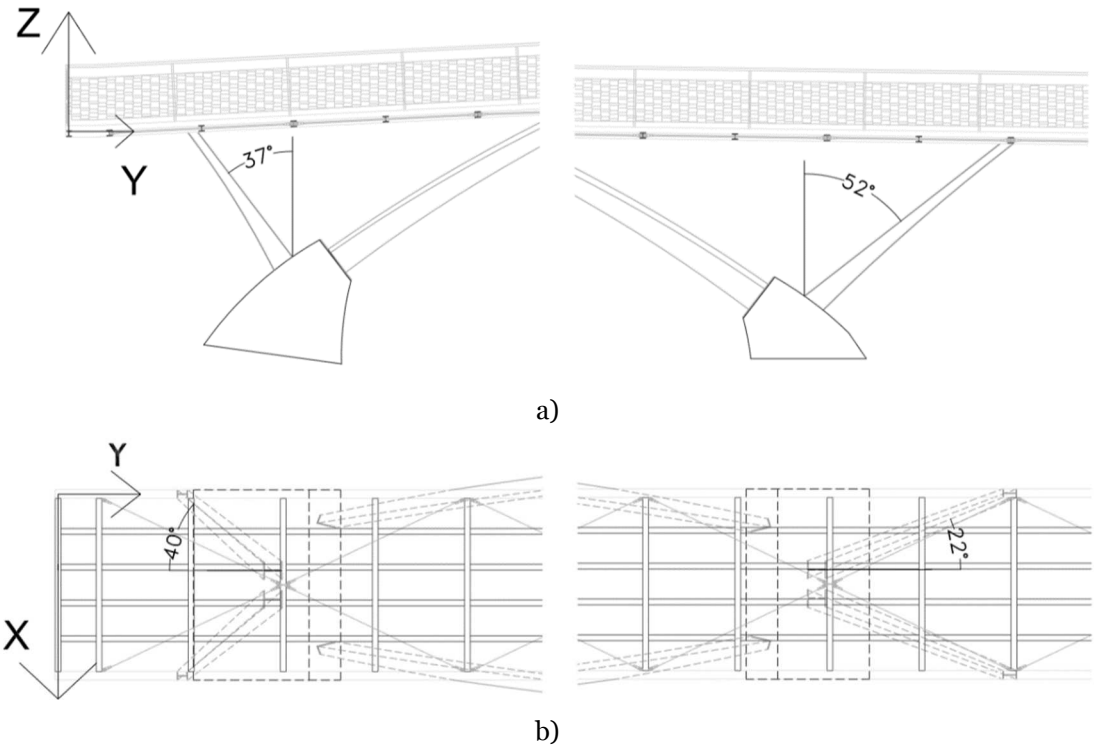

Figure 2.2.3 Details of struts inclinations: a) lateral view; b) in-plane view.

Their lower (bigger) and upper (smaller) sections are compared in Table 2.2.1.

Table 2.2.1 Dimensions of largest and smallest sections of tapered struts.

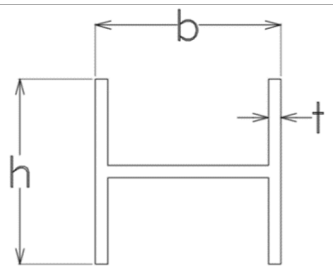

Dimension	Upper section	Lower section
h [*m*]	0.15	0.3
b [*m*]	0.18	0.3
t [*m*]	0.01	0.02

Arches cross-sections are L-shaped and their dimensions vary linearly in a continuous way. At supports, the cross-section depth is larger than its width ($500x200x20\ mm$) while, at top, the contrary holds true ($300x550x20\ mm$). They represent an arch of a circumference with radius of 27 m and the subtended angle is of 75°. As consequence, the arches length is equal to 35.30 m each.

The deck length is equal to 54 m, subdivided in 5 spans by intersection points with arches and struts elements. Slope of deck is not uniform, even within each span, and varies all along the deck. In Table 2.2.2, the length of each span and the related slope are listed and ordered so that the span nearest to Lauzelle District is at the first line and the farthest is at the last.

Table 2.2.2 Span lengths and relative slopes.

Span N°	**Length [m]**	**Slope N°1 [%]**	**% Of length with slope N°1**	**Slope N°2 [%]**	**%Of length with slope N°2**	**Slope N°3 [%]**	**%Of length with slope N°3**
1	2.2	0	22.7	5	77.3	-	-
2	7.0	5	100	-	-	-	-
3	24.4	0	8.6	2.6	24.6	0.5	66.8
4	9.0	1.3	100	-	-	-	-
5	11.4	1.3	100	-	-	-	-

The central span of the structure is linked to the arch, at each side, trough ten suspension cables having diameter $\phi 25\ mm$ (Figure 2.2.4).

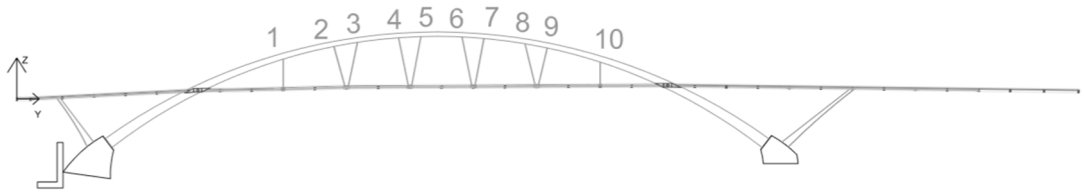

Figure 2.2.4 Numeration of tendons linking arches and deck.

Considering only one side of connections and numbering tendons from 1 to 10 starting from Lauzelle side, in Table 2.2.3 geometrical data of each of them are listed, in terms of length, angle of inclination in longitudinal view with respect to the vertical direction and position of connection point with the deck as percentage of the middle span length.

Table 2.2.3 Geometrical data about tendons linking arches and deck.

Tendon N°	**Length [m]**	**Inclination [°]**	**Starting point [% $Span\ Lenght$]**
1	1.70	0	17.72
2	2.25	16	31.06
3	2.45	12	31.06
4	2.65	11	44.46
5	2.70	11	44.46
6	2.67	11	57.25
7	2.60	11	57.25
8	2.37	14	70.47
9	2.15	14	70.47
10	1.40	0	83.6

Arches and deck are linked through the suspension cables and at the points where the arches meet the deck (Figure 2.2.5 d)). In every point of this span, the height with respect to the ground respects the minimum of 4.80 m to allow the passage of vehicles in the road below.

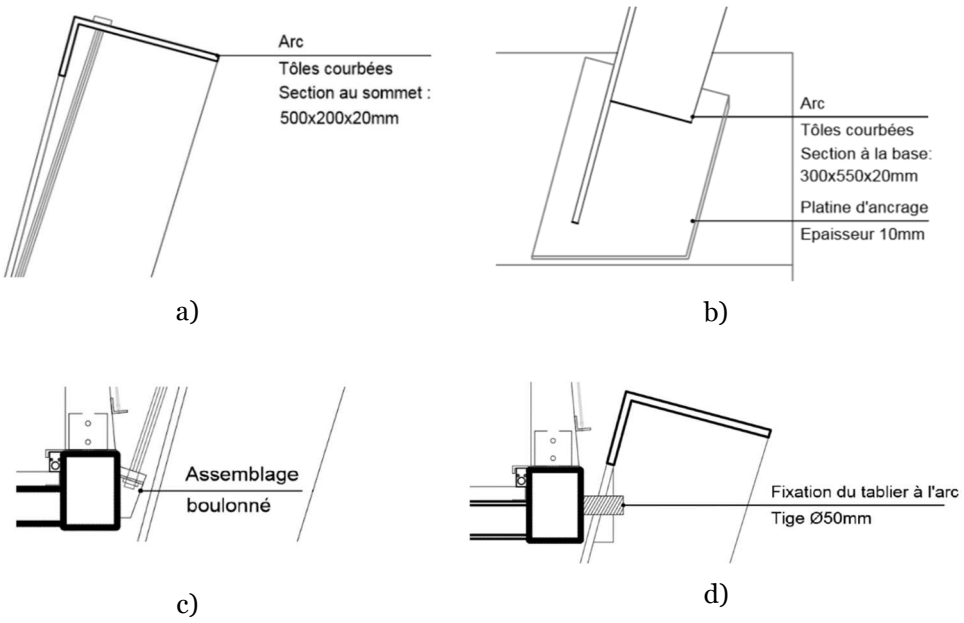

Figure 2.2.5 Some details of the structure: a) arch top section; b) arch base section; c) connection between suspension cables and deck; d) connection between arch and deck.

The structure of the deck is a grid. Two longitudinal beams (hollow rectangular section ($200x150x10\ mm$)) of $53.95\ m$ are on the edges of the deck, spaced $3.15\ m$ apart. They are connected by transversal elements ($HEB\ 100$) every $1.61\ m$, except for the first inter-axis distance in correspondence of the Lauzelle edge of the deck, equal to $0.77\ m$. In total, there are 35 of these elements.

Other longitudinal elements contribute to the rigidity of the deck: T shaped elements ($100x100x9\ mm$), spaced 0,60 m apart, connect longitudinally $HEB\ 100$ beams. Being in the number of 4 for each interval included between two transversal elements, the total number of these elements is equal to 136.

Section geometries of these last two element types are detailed in Table 2.2.4.

Table 2.2.4 T-shaped and HEB100 section dimensions.

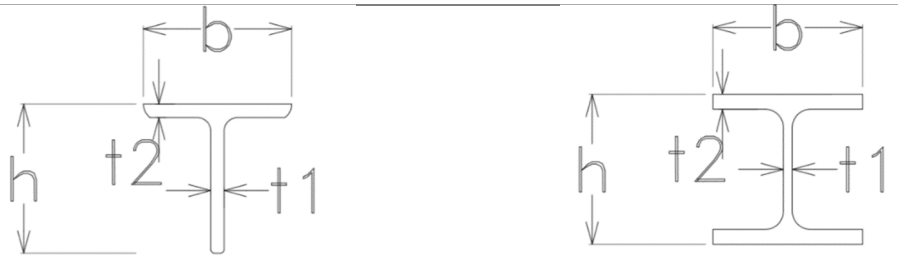

Dimensions	T-shaped	HEB100
h [m]	0.1	0.1
b [m]	0.1	0.1
t1 [m]	0.009	0.006
t2 [m]	0.009	0.01

Connections among the steel elements are all welded. Cables with $\phi 20\ mm$ ensure bracing in the horizontal plane of the structure. Planking level is designed with wood elements, disposed transversally with respect to hollow beams and with rectangular cross-section $40x160\ mm$ (Figure 2.2.6).

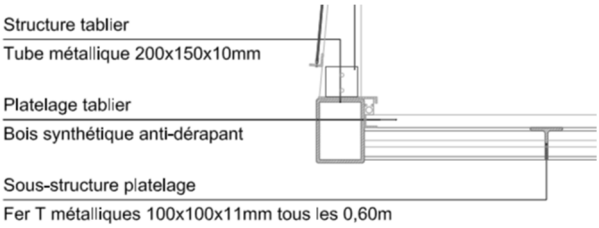

a)

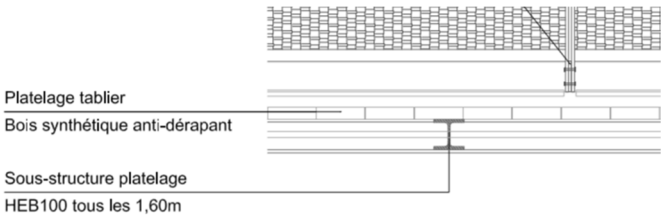

b)

Figure 2.2.6 Details of deck structure: a) transversal view; b) longitudinal view.

The definition of boundary conditions is very important. There are four points of structure-ground contact. The deck rests on neoprene supports at its smaller edges. The two sides of arches are linked to the ground through concrete footings whose features allow to consider them as two clamping conditions. Material properties are listed in Table 2.2.5.

Table 2.2.5 Material properties adopted for the analysis of the model

Material	**Density** $[^{kg}/_{m^3}]$	**Young's Modulus** $[GPa]$	**Poisson's Ratio [-]**	**Yielding Stress** $[MPa]$
Steel (S235)[1]	8000	210	0.3	235
Tendons Steel (S460N)[2]	7850	210	0.3	440
Wood	1050	-	-	-

Finally, it should be noted that handrails, whose details are not described, do not play any structural role. Their presence is considered only in terms of self-weight as well as for the wood planks.

For more details and technical considerations, readers can refer to APPENDIX A.

[1] Minimal class required for structural applications.
[2] Data obtained from data sheet of producer [6].

CHAPTER 3
STRUCTURAL MODELING

Chapter 3 presents the modeling process of the structure described in CHAPTER 2. As stated in the introduction, the software used for this purpose is Ansys Mechanical APDL (Ansys Parametric Design Language).

After a brief description of the software, all the assumptions at the base of the FE modeling are presented referring to the footbridge features. More details about the coding language to create and analyze the model are presented in APPENDIX C

Subsequently, three possible geometries of the footbridge are presented to the aim of evaluating the dependency of their behavior on inclination of arches and their cross section.

Finally, differences among the three proposed models are discussed into a detailed overview. Aspects such as the static behavior of footbridges and their modal analysis are analyzed. Finally, a method to validate the modeling procedure is presented.

3.1 Ansys software

The study of the structure presented above has been conducted using a student license of the commercial software Ansys. A brief description of the software is presented in the following.
Ansys is a Computer aided engineering software based on the application of the finite elements method. It is a powerful software that can be exploited to solve problems of different nature and it is distributed under different interfaces. There are interfaces, also called platforms, for impacts or explosions problems (Ansys Autodyn), fluid dynamics (Ansys Fluent, CFD, CFX), electronics (Ansys HFSS, Maxwell and Slwave) as well as for mechanics (Ansys Mechanical). They can be distributed all together with Ansys Multiphysics or Ansys Workbench. Different releases exist, updated periodically by the developer.
Every physical problem can be solved with this software. The idea is that the user has to model the reality that he wants to analyze through the software, paying attention to all the variables that influence the problem. Materials, boundary conditions, loads and so on can be represented in a very simply way. The quoted versions of Ansys present a very simple and accessible user interface. Modeling is done using buttons and options present on the desktop. However, in order to have a better control on the model, in the initial approach with the software and in case of modeling errors, it is possible to use a more complex version where the user can build the model, make analysis, and obtain results writing directly the source code of the problem. This opportunity is given by the Ansys Mechanical APDL (for this work, release 17.1 is used) version of the software. APDL stands for Ansys Parametric Design Language.
The driving idea of APDL is to model the problem writing a code in a text format file, following the rules given in the Help guide of the product. Once the model is ready, Ansys can read the file and perform analysis following the instructions written in the file. The analyst, when understands the way to use commands and to implement all parameters necessary to complete the FE model, can really appreciate the power of this very compact language that allows for making very difficult operations by simply writing one line of code.

3.2 Modeling assumptions

Since the footbridge is not built yet, it is not possible to compare numerical results with experimental ones and care is necessary to obtain reliable results. The assumptions at the base of the model derivation are presented in the following.
All dimensions, positions and, in general, the complete geometry of the structure have been taken from a CAD file, made available by McCarré. Tables in APPENDIX A have been obtained from data contained in this file.

To practice with the parametrical language of Ansys and to explore slightly different bridge configurations, at the begin of the study a simplified structure was modeled. The inclined arches were replaced with vertical ones and the L-shaped cross-section of the arch was replaced with a hollow rectangular one, even though the variability of section dimensions along the arches was maintained.

The model was improved in a second phase by considering the correct inclination of the arches. Finally, the real shape of the cross-section was assigned to arches (Figure 3.2.1).

At the end of this phase, as it will be showed at the end of this chapter, the behavior of these three configurations of the footbridge was analyzed. The three configurations are compared to verify which parameters affect their behavior in a significant way

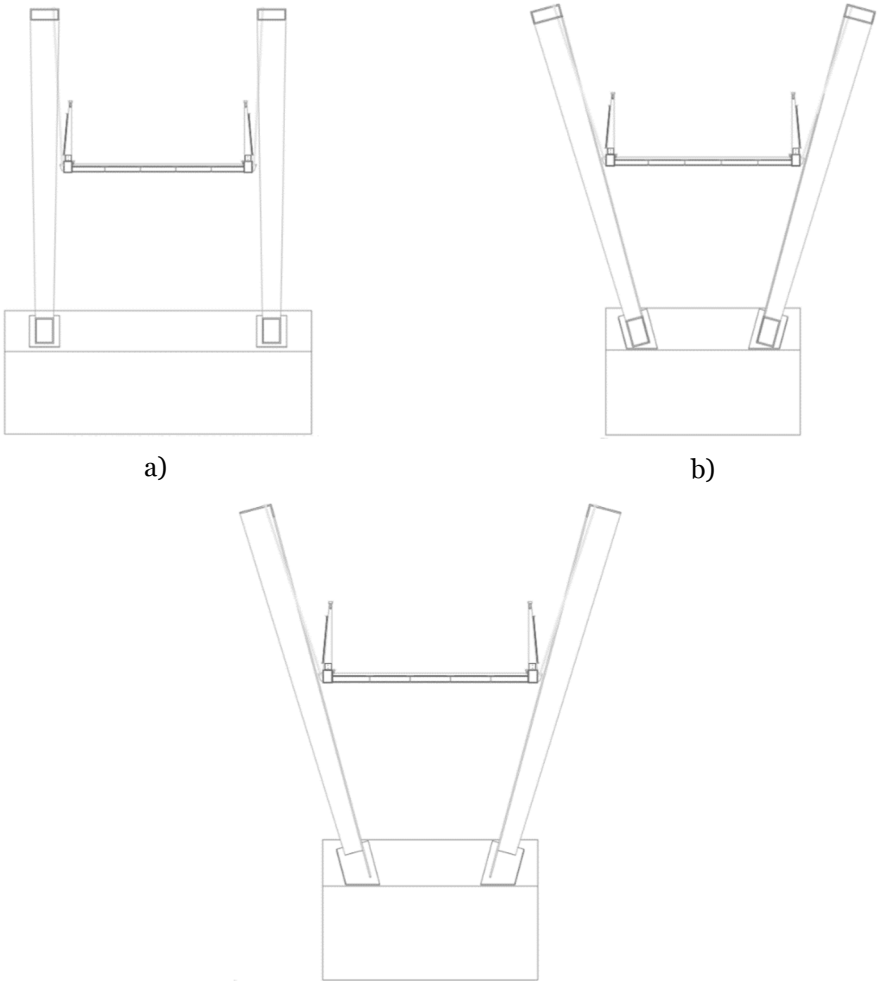

a) b)

c)

Figure 3.2.1 The three different middle sections of the models: a) first, b) second, c) third, and more realistic, model.

In our case, to be consistent with a research code that could be used in subsequent analyses, the choice for setting origin of reference system and its characteristics was imposed. The right-handed reference system has vertical positive z-axis upwards, x and y-axis, in the plane

of the deck, respectively transversal and parallel to the deck. The origin of this system was set on the Lauzelle side of the deck.

In Ansys, it is possible to create a model with two different methods. The first is the *automatic meshing method*, for which nodes and elements are generated starting from lines and surfaces, choosing *a posteriori* the level of refinement for the mesh grid. The second method is known as *direct generation* and prescribes to create a model starting from manual generation of nodes and elements. Even though the latter could seem less useful and time consuming, it presents the advantage that the model can be easily checked by the analyst, that can decide *a priori* whether better refinement is necessary or not and allowing him to know number and position of each node and element, very important to interpret output results directly from computation notes and not only from plots.

In this work, the direct generation method was chosen. To this aim, it was necessary to define a grid of nodes all along the structure. The numbering of nodes is presented in APPENDIX B. In this table, arches and struts nodes have numbers from 236 to 266 and from 336 to 366; orienteering nodes for transversal beams of the deck have numbers from 501 to 536. The usage of this last group of nodes will be presented in the next section. Nodes number 1000, 2000, 3000, …, 8000, represent points of contact of struts and arches with the deck (Figure 3.2.2).

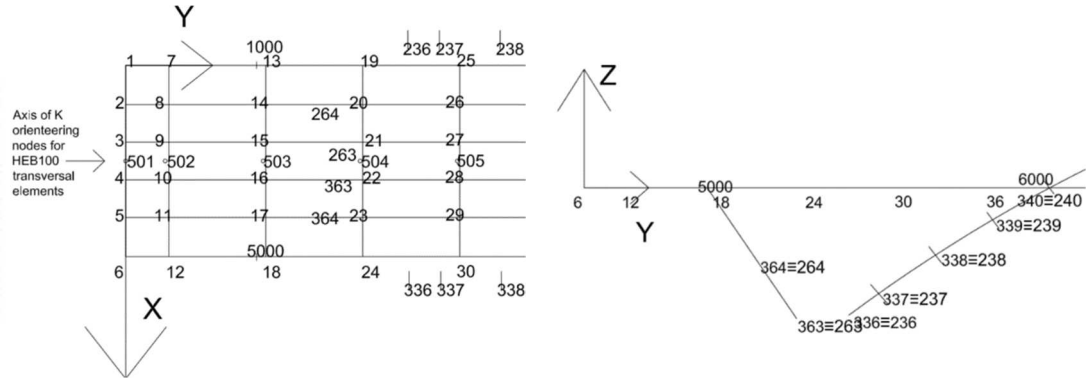

a) b)

Figure 3.2.2 a) Nodes grid in horizontal plan; b) Nodes grid in vertical view.

One important aspect in the modeling process is the transformation of real boundary conditions in numerical ones. Starting from the simplest engineering problem, the capability to well represent boundary condition will affect enormously the results of the problem. Boundary conditions must be assigned on some nodes of the discretized structure. These are the supports of the deck connecting the structure with the ground on the smaller edges of Lauzelle and Courbevoie Districts and the bases of arches and struts. Constraints between different parts of the structure have to be modeled as well. Some degrees of freedom are unconstrained at connecting nodes between arches and deck. Rotations of deck nodes are

independent from the ones of nodes belonging to arches, while only the displacements continuity is ensured. Arches nodes are considered as master, i.e. displacements of deck nodes will be equal to the computed displacements for arches nodes.
Just to have an idea of the static conditions of the footbridge, we can consider a two dimensions representation of the footbridge, where it could be seen as a beam resting on six supports. They are represented by: two points of connection to the ground, at extremities of the deck, and four points of support, that can be modeled as elastic, where the two H shaped struts and the arches connect to the deck (Figure 3.2.3).

Figure 3.2.3 2-D static scheme of the footbridge neglecting the presence of tendons.

The scheme in Figure 3.2.3 cannot be considered complete, since it does not include the representation of tendons, or better, the representation of their influence on the structure as equivalent static conditions. Each tendon adds to the structure a degree of hyperstaticity. Tendons can be modeled as elastic supports with a given stiffness, to be computed as a function of assigned pretensions (δ in Figure 3.2.4).

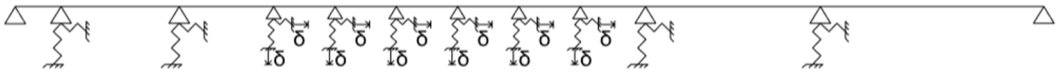

Figure 3.2.4 Correct static scheme of the footbridge accounting for tendons and their pretension.

However, the 3-D nature of the problem cannot be neglected. The in-plane behavior of the structure must be analyzed. In addition, we assume that the wood elements of the walking surface do not contribute to the stiffness of the structure.

3.3 Differences among the models

A view of the three finite elements models, following the order of their creation, is given in Figure 3.3.1. Differences are linked to the shape and orientation of arches.
In Figure 3.3.1 an axonometric view of the three models is given. In a) the model is characterized by vertical arches with a hollow rectangular section. In c) arches are inclined by an angle of 15° but their section is L-shaped. Model b) is a compromise between the two: it presents inclined arches with hollow rectangular section. For the geometrical description

of the three models, the reader could better refer to paragraph 3.2. The three mid sections of the footbridges central span are illustrated in Figure 3.2.1.
In the following of this section, the focus will be on other aspects concerning differences among the models. In particular, static deflection under gravitational loads, with and without pretension, and modal analysis will be presented.

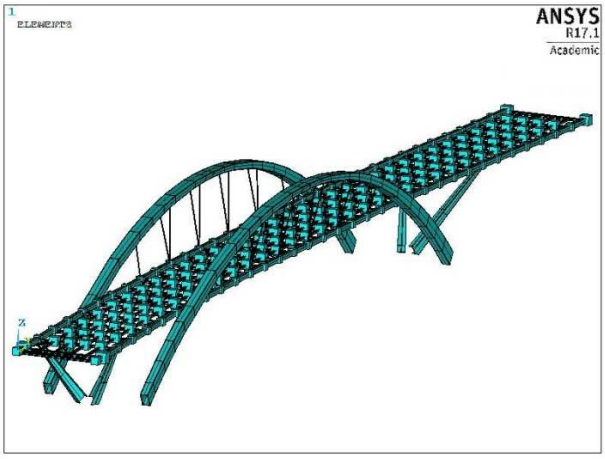

a)

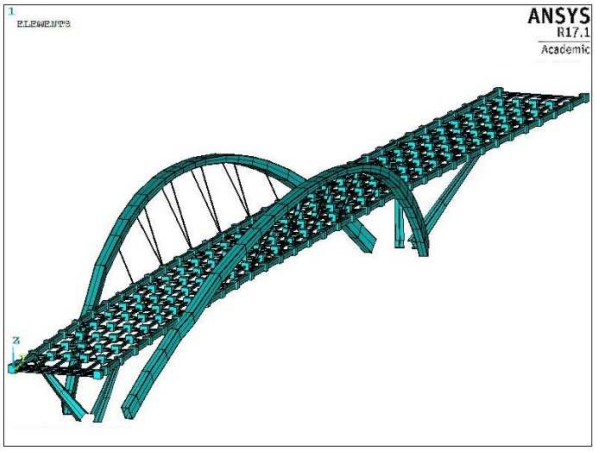

b)

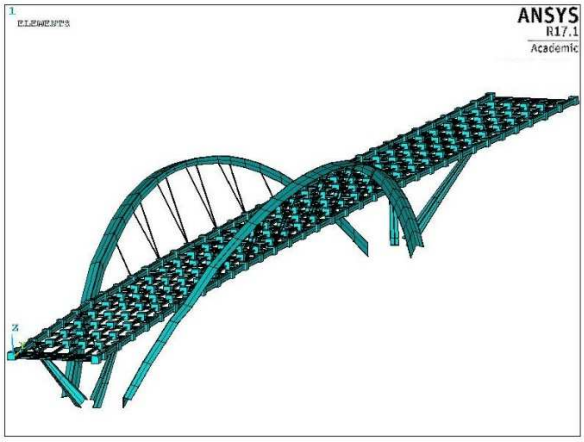

c)

Figure 3.3.1 Elements plot of the three different models: a) vertical arches with rectangular section; b) inclined arches with rectangular section; c) inclined arches with L shaped section.

3.3.1 Effects of gravity loads

The different geometry of the three models reflects in values of displacements of their nodes. Considering the case of gravity loads, values of vertical displacements of the deck are presented in the following tables and figures. These values are related to nodes listed in column 1 of Table 3.3.1, belonging to one of the two longitudinal beams of the structures (Figure 3.3.2).

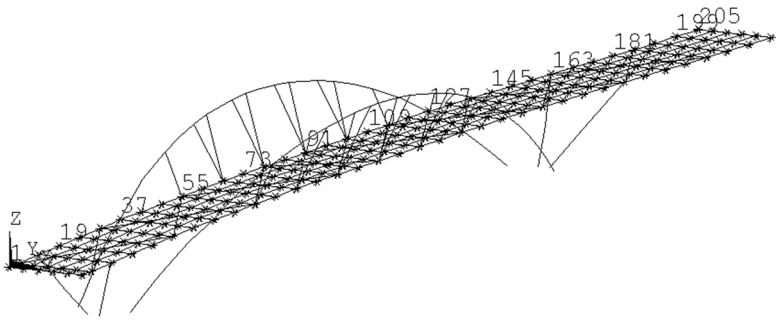

Figure 3.3.2 Position of nodes selected for analysis.

They were chosen for two main reasons. First, given the longitudinal symmetry of the structures, nodes on one side of the footbridge are representative of the behavior of both sides. Second, considering that pretension will be applied at these points, we wanted their vertical displacements in order to make comparisons before and after application of pretension. If we had chosen nodes on transversal elements the comparison would have required one step further: analytical computation of their vertical displacements and subtraction from total Ansys computed vertical displacements of the longitudinal beam. Considering the simplified model in Figure 3.3.3, $\delta_2 = \delta_{tot} - \delta_1$, where δ_2 is the quantity we need to make comparisons.

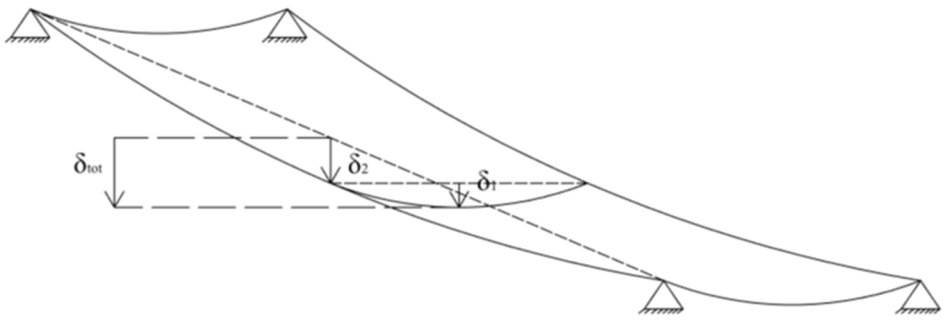

Figure 3.3.3 Simplified model of the deck to explain one of the two reasons for choosing nodes belonging to the longitudinal beams.

Table 3.3.1 Vertical displacements U_z of some nodes of one of the two longitudinal beams due to self-weight.

Node	U_z Model1 [mm]	U_z Model2 [mm]	U_z Model3 [mm]
1	0	0	0
19	-1.11	-1.16	-1.24
37	-0.57	-0.67	-0.94
55	-1.19	-0.57	-0.67
73	-1.80	-1.01	-1.56
91	-1.52	-0.85	-1.04
109	-0.69	-0.14	0.14
127	0.34	0.26	0.46
145	-3.21	-3.45	-3.47
163	-0.68	-0.64	-0.85
181	-19.3	-19.2	-19.5
199	-11.3	-11.3	-11.4
205	0	0	0

As already stated, Table 3.3.1 reports numerical values of displacements of some particular nodes. Figure 3.3.4 is the graphical representation of these values but is also a realistic representation of the complete deformed shape of longitudinal beams.

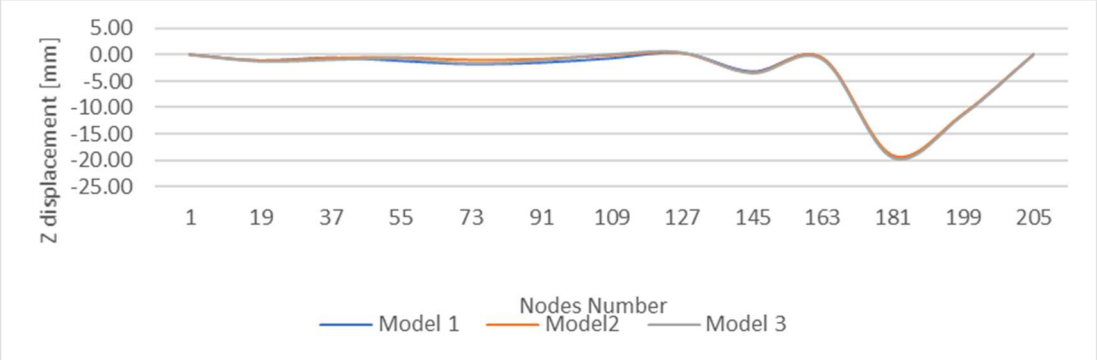

Figure 3.3.4 Graphical representation of displacement values reported in Table 3.3.1.

On the left of node 19, the smallest span does not allow for large deformations and for this reason, in all the models, only four spans are recognized instead of five.
The three models have the same structural scheme and behave essentially in the same way. The span between nodes 37 and 127, even being the longest, has values of vertical displacements comparable to the two smallest spans to its left, between node 1 and 37. This is due to the fact that this span is sustained by tendons. However, the influence of tendons is

not limited to the span to which they are applied. In fact, the action of pulling up nodes of the longest span induces the lowering of nodes of the two nearer spans. For the same reasoning, in absence of tendons, displacements of their nodes would have been smaller while displacements of nodes of the longest span would have been larger.

Nodes of the span between nodes 163 and 205 have the larger values of vertical displacements. In the three cases, due to the span length of 11.4 m, they reach values of around 2 cm, almost equal to the ratio of deflection limit under permanent loads $l/500 = 2.28\ cm$.

The change in the arches geometry affects the bridge response.

For the three models, we are going to compare only spans mid nodes vertical displacements. Since Model2 is a compromise between Model1 and Model3, having inclined arches with hollow rectangular section, we will refer to it to detect the geometry modification that has the greater influence (Table 3.3.2).

The change in the geometry of the arches has the most important influence on the series of nodes in the span to which tendons are applied. For node 73, the verticality of arches has an effect larger than the opening of sections (-77.58% and -54.54% of percentage difference respectively).

As already stated, the presence of tendons affects also the behavior of nearer spans, in the same way as changes in arches geometry do. For node 19 (on the left span), the two variations have almost the same impact, producing percentage differences of displacements of the same order ($+4.46\%$ and -6.07%). On the contrary, for node 145 (at midspan), the opening of section has almost no impact (-0.42%) while the presence of vertical arches is the most important cause in changes of values of displacements ($+6.97\%$). Finally, the two changes of geometry do not have any relevant influence for node 181 (at the right span) and the related span.

Table 3.3.2 Vertical displacements U_z of span central nodes and percentage difference of displacements of Model1 and Model3 with respect to displacements of Model2.

Node	**U_Z Model1 [mm]**	**U_z Model2 [mm]**	**U_z Model3 [mm]**	**M1-2**	**M3-2**
73	-1.80	-1.01	-1.56	-77.58%	-54.54%
19	-1.11	-1.16	-1.24	+4.46%	-6.07%
145	-3.21	-3.45	-3.47	+6.97%	-0.42%
181	-19.3	-1.92	-1.95	-0.67%	-1.75%

As for the arches, vertical displacements of their nodes change as consequence of variations in their geometry.

Five nodes of one arch only will be considered: arch top node (249), constraining nodes between arch and deck (241 and 257), and two nodes at the half curvilinear distance between the latter and the former (245 and 253). Refer to Figure 3.3.5.

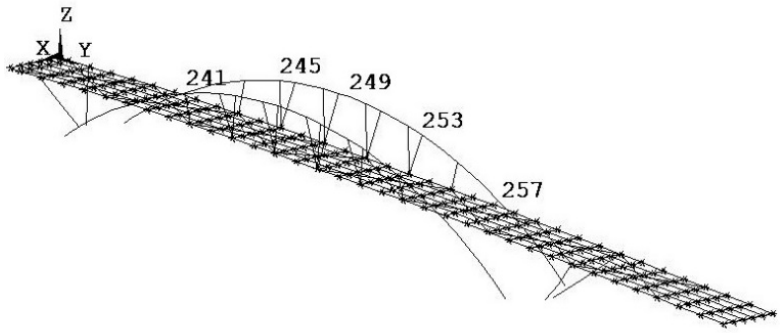

Figure 3.3.5 Position of arch nodes that will be analyzed in the following.

Table 3.3.3 Vertical displacements U_z values of five nodes of one arch for the three models and percentage difference of displacements of Model1 and Model3 with respect to displacements of Model2.

Node	U_z Model1 [mm]	U_z Model2 [mm]	U_z Model3 [mm]	M1-2	M3-2
241	-0.37	-0.43	-0.67	+11.9%	-59.0%
245	-1.22	-2.21	-5.98	+44.9%	-170.1%
249	-1.35	-2.79	-7.32	+51.8%	-162.0%
253	-5.11	-1.36	-3.27	+62.3%	-141.2%
257	0.23	0.12	0.31	+9.8%	+158.0%

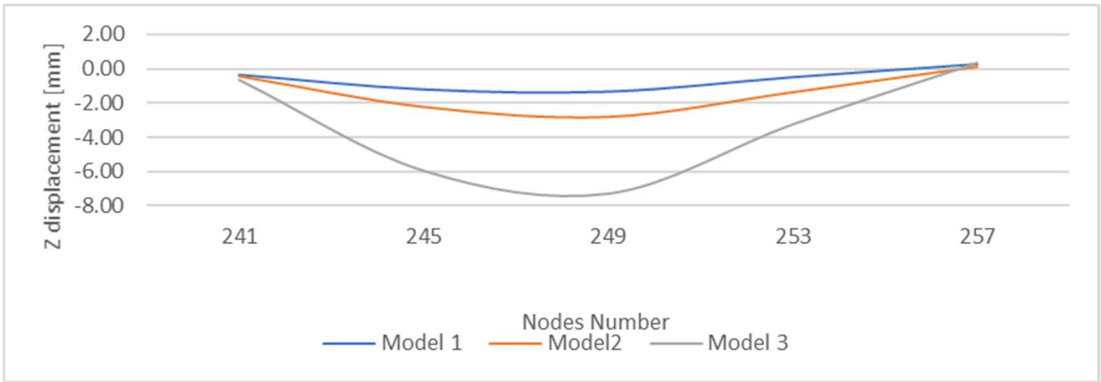

Figure 3.3.6 Graphical representation of displacement values reported in Table 3.3.3.

From Table 3.3.3 and Figure 3.3.6, it is evident how the adoption of an open section induces a large increment of displacements in vertical direction for arch nodes. However, this increment is limited to an amount of 5 *mm* more with respect to the case of the Model2. It is equal to the 0,2 ‰ of the central span length (24,4 *m*).

It is necessary to analyze also horizontal displacements of arches. The presence of inclined tendons in the transversal direction that link them with the deck induces horizontal displacements. The fact that the two arches are not linked to each other does not allows the mutual cancellation of horizontal components of forces transmitted by tendons (Table 3.3.4 and Figure 3.3.7).

Table 3.3.4 Horizontal displacements U_x values of five nodes of one arch for the three models and percentage difference of displacements of Model1 and Model3 with respect to displacements of Model2.

Node	U_x Model1 [mm]	U_x Model2 [mm]	U_x Model2 [mm]	M1-2	M3-2
241	0.06	-0.07	0.03	+188.4%	142.1%
245	1.98	-3.57	-11.1	+155.5%	-212.3%
249	2.58	-4.63	-15.0	+155.8%	-223.9%
253	1.71	-2.89	-7.65	+159.3%	-164.7%
257	0.001	-0.11	-0.003	+102%	+97.7%

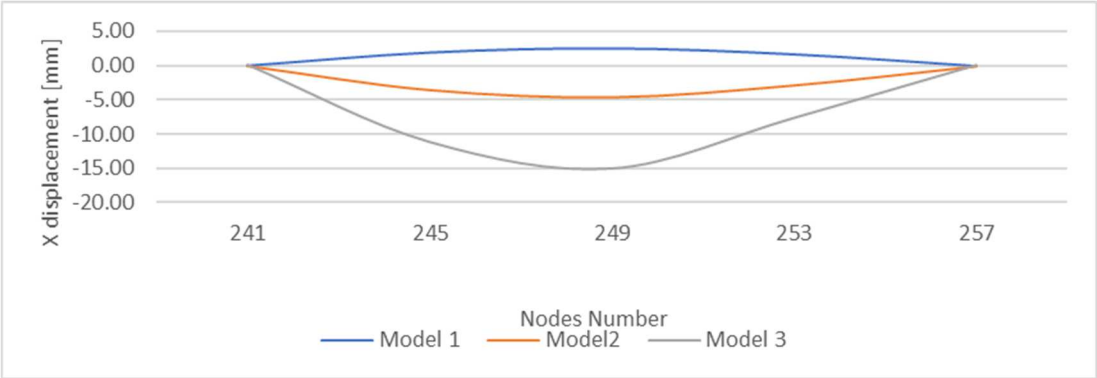

Figure 3.3.7 Graphical representation of displacement values reported in Table 3.3.4.

Also in the study of horizontal displacements, the larger influence of the change in the section geometry is remarked. Values of displacement of node 249 in Model3 is about 3 times the value for Model2, i.e. 1.5 *cm* against 0.47 *cm*.

3.3.2 Pretension: determination and effects

To increase the stiffness of the structure, a certain degree of pretension should be provided to tendons linking arches and deck. This because in case of unsymmetrical loading on the deck, some tendons could be subjected to a certain unload. Then, to avoid reaching negative values of axial force in some tendons, a preventive increase of the initial load could very useful.
Considering the case of only gravity loads, pretension values of load were determined by an iterative procedure. As described in section 2.2, for each arch there are ten tendons: 2 of them do not have inclination with respect to y-axis on the plane y-z and are not coupled to any other tendon, while the remaining 8 are inclined in the same plane and they work in couple with another tendon having in common the contact point with the deck (Figure 2.2.4). As consequence, they have also different lengths.
Thus, since each tendon is attached to an arch at a different point from the others, the pretension value resulted to be different for each tendon.
All these features made an iterative procedure the most suitable to compute values of pretension. For each of the three structures, the starting point was the uniform application of pretension. Couple by couple of tendons, pretension in one of the two elements was modified. The purpose was to obtain the same values of stress in both elements of the couple.
This operation was done to avoid incorrect interpretations. When pre-tension is applied through the INISTATE command, output stresses of Ansys of the pre-tensioned element do no include the pretension contribution. Thus, in cases when the output stress is zero, it is reasonable to think two things:

1) The tendon has pretension while it is unloaded
2) The tendon is unloaded while it is subjected to pretension.

Since in case of uniform pretension applied it was frequent to have large values of tension stress in one of the two tendons and zero, or near zero, tension stress in the other, it was decided to balance values of stresses in the two cables to have a better control on the problem.
The analyzed tendons are the coupled ones. Their identifying number is in column 1 of Table 3.3.5, Table 3.3.6 and Table 3.3.7. The tables report values of net stress σ_0 after application of uniform pretension on all tendons (Column 2). The value of pretension applied was $P_{max} = 150\ kN$.

Table 3.3.5 Results linked to the iterative procedure to determine the pretension force in tendons of Model1. Net tension stresses, pretension stresses and forces, deformations, lengths and imposed displacements are showed.

Tendon n°	σ_0 **[MPa]**	σ_1 **[MPa]**	σ_2 **[MPa]**	σ_3 **[MPa]**	σ_{pret} **[MPa]**	**P [kN]**	**ε [‰]**	**L [m]**	**δ [mm]**
2	5.67	5.96	5.9	6.13	305.6	150	1.49	2.25	3.4
3	6.4	6.11	6.23	5.99	296.1	145	1.44	2.45	3.5
4	8.5	8.4	4.96	5.5	305.6	150	1.49	2.65	4.0
5	2.86	2.98	6.23	5.64	295.6	145	1.44	2.7	3.9
6	7.6	6.92	5.26	5.21	305.6	150	1.49	2.67	4.0
7	3.05	3.78	5.5	5.62	299.6	147	1.46	2.6	3.8
8	7.5	6.49	6.49	6.48	305.6	150	1.49	2.37	3.5
9	5.18	6.32	6.47	6.45	302.1	148	1.47	2.15	3.2

This value of pretension, generating values of stress equal to $\sigma = 305.6\ MPa$, was decided considering typical technical data for tendons. In the consulted data sheet ([6]), tendons with a diameter of 25 mm have a load capacity $N_{R,d} = 158.6\ kN$.

Table 3.3.6 Results linked to the iterative procedure to determine the pretension force in tendons of Model2. Net tension stresses, pretension stresses and forces, deformations, lengths and imposed displacements are showed.

Tendon n°	σ_0 **[MPa]**	σ_1 **[MPa]**	σ_2 **[MPa]**	σ_3 **[MPa]**	σ_{pret} **[MPa]**	**P [KN]**	**ε [‰]**	**L [m]**	**δ [mm]**
2	1.36	4.8	5.9	6.17	305.6	150	1.49	2.25	3.4
3	11.55	7.62	6.44	6.15	290.1	142	1.42	2.45	3.5
4	7.74	8.19	5.53	5.96	305.6	150	1.49	2.65	4.0
5	4.3	4.16	6.7	6.24	299.1	147	1.46	2.7	3.9
6	6.19	6.05	5.77	5.74	305.6	150	1.49	2.67	4.0
7	4.99	5.38	5.96	6.05	304.6	150	1.49	2.6	3.9
8	1.48	4.93	6.36	6.35	305.6	150	1.49	2.37	3.5
9	11.81	7.93	6.27	6.25	291.6	143	1.42	2.15	3.1

In columns 3, 4 and 5 net stresses after 1, 2 and 3 cycles of iterations. A certain balance between stresses of the same couple of tendons has been reached in the third cycle. Final values of pretension stress, pretension value and produced deformation are reported in columns 6, 7 and 8 respectively. Deformation values never reach the critical value of 2 ‰,

caused by the yielding stress $f_y = 460\ MPa$ for steel S460N (*EN 1993-1*), the one tendons are made of.

Table 3.3.7 Results linked to the iterative procedure to determine the pretension force in tendons of Model3. Net tension stresses, pretension stresses and forces, deformations, lengths and imposed displacements are showed.

Tendon n°	σ_0 **[MPa]**	σ_1 **[MPa]**	σ_2 **[MPa]**	σ_3 **[MPa]**	σ_{pret} **[MPa]**	**P [KN]**	**ε [‰]**	**L [m]**	**δ [mm]**
2	5.17	6.13	6.03	6.07	305.5	150	1.49	2.25	3.4
3	7.25	5.96	6.02	5.99	295.0	145	1.44	2.45	3.5
4	3.52	4.72	5.97	5.7	305.5	150	1.49	2.65	4.0
5	8.55	7.17	5.69	5.97	284.5	140	1.39	2.7	3.7
6	6.54	7.01	7.21	6.19	305.5	150	1.49	2.67	4.0
7	4.94	5.45	5.47	6.26	298.5	147	1.46	2.6	3.8
8	4.35	7.12	6.09	6.3	305.5	150	1.49	2.37	3.5
9	8.64	5.04	6.12	6.22	292.5	144	1.43	2.15	3.1

Finally, lengths and elongations to apply to each tendon during the pretension phase are listed in columns 9 and 10.

Elongations are proportional to deformation and length of tendons. Considering the three models, maximum and minimum of imposed displacement to be applied are 3.1 *mm* and 4 *mm* respectively. The difference between elongations of two coupled tendons ranges from 0.1 *mm* and 0.4 *mm*.

We have already reported in Table 3.3.1 and Figure 3.3.4 values of vertical displacements for the deck when subjected to gravity load only. To make a comparison before and after application of pretension, we report vertical displacements values and their plot for the same nodes after application of pretension in Table 3.3.8 and Figure 3.3.8.

Table 3.3.8 Vertical displacements U_z of some nodes of one of the two longitudinal beams after application of pretension and gravity load on the structure.

Node	U_z Model1 [mm]	U_z Model2 [mm]	U_z Model3 [mm]
1	0.00	0.0	0.00
19	-1.28	-1.35	-1.41
37	-0.74	-0.85	-1.10
55	1.23	2.25	1.94
73	1.90	3.32	2.50
91	2.40	3.67	3.46
109	2.25	3.15	3.47
127	0.44	0.36	0.53
145	-3.84	-4.19	-4.20
163	-0.67	-0.61	-0.80
181	-19.1	-19.0	-19.3
199	-11.3	-11.2	-11.3
205	0.00	0.00	0.00

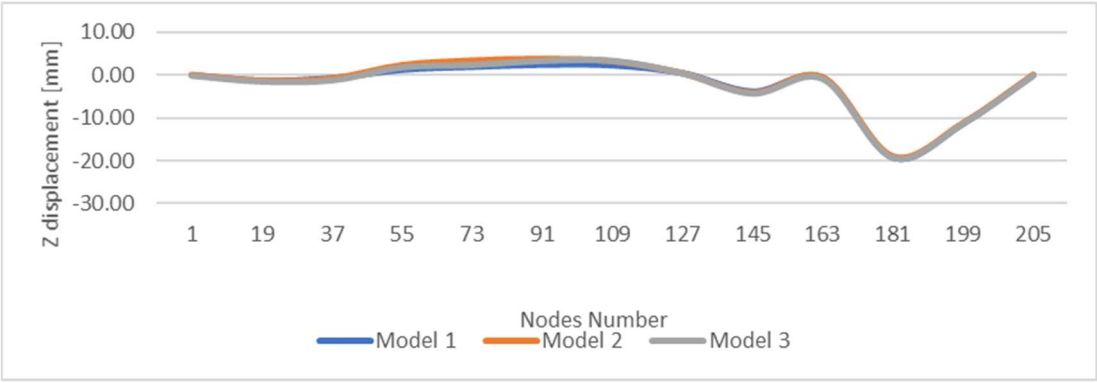

Figure 3.3.8 Graphical representation of displacement values reported in Table 3.3.8

Without considering numerical values, it is sufficient to observe the plot in Figure 3.3.8 to appreciate a completely different behavior of the structure with respect to the case in which no pretension was applied Figure 3.3.4.

After pretension is applied, the span where tendons are present has an opposite deformed shape. As already explained previously, this has an influence on nearer spans. Looking now at numerical values of Table 3.3.8 and Table 3.3.1, the comparison between the two situation

is easier. Nodes 19 and 145 have larger vertical displacements after application of pretension while the span which central node is the 181 is practically not affected.

Finally, to check that pretension was applied correctly, a quantitative verification on displacement values before and after application of pretension on the footbridge was done. Let us consider the case of a simply supported beam. The midspan displacement of a beam subjected to two different loads is given by the sum of those produced by the loads applied individually. Obviously, this can be done due to the superposition principle validity, ensured by the fundamental assumptions of linear elasticity and small displacements (Figure 3.3.9).

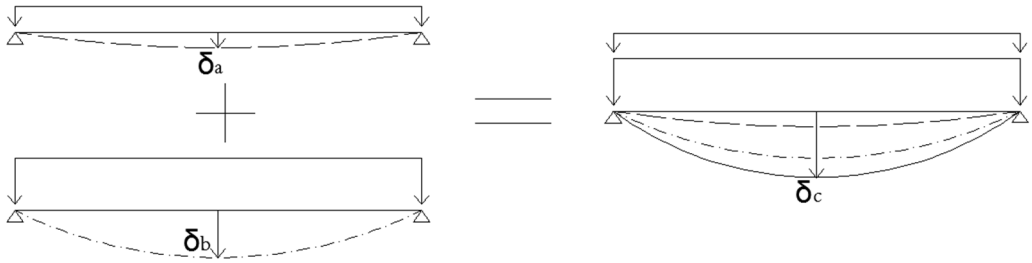

Figure 3.3.9 Superposition principle: midspan displacement of model C is the sum of those of models A and B.

The same situation applies for the footbridge. In this case, load of model A is represented by the self-weight while the one of model B by the system of pretension forces. Model C is the case in which both loads are applied. Then, the purpose of the check was to evaluate if displacements computed by Ansys for the model C were equal to the sum of results obtained for models A and B individually.
Data for the three FE models with respect to the situations A and C of Figure 3.3.9 have already be given in Table 3.3.1 and Table 3.3.8. For data related to displacements in the case of only pretension applied, refer to Table 3.3.9.

Table 3.3.9 Vertical displacements U_Z of some nodes of one of the two longitudinal beams after application on the structure of only pretension forces.

Node	U_Z Model1 [mm]	U_Z Model1 [mm]	U_Z Model1 [mm]
1	0.00	0.00	0.00
19	-0.16	-0.18	-0.17
37	-0.15	-0.17	-0.15
55	2.48	2.86	2.72
73	4.30	4.96	4.74
91	4.42	5.12	4.85
109	2.87	3.34	3.11
127	0.04	0.04	0.02
145	-0.61	-0.70	-0.67
163	0.04	0.05	0.07
181	0.19	0.22	0.24
199	0.07	0.08	0.08
205	0.00	0.00	0.00

Without reporting numerical values of the sum of data coming from Table 3.3.1 and Table 3.3.9, the check is showed only in a graphical way. Moreover, not all the nodes of previous tables have been reported in order to have a better view on what happens in the span where pretension forces are applied (Figure 3.3.10, Figure 3.3.11 and Figure 3.3.12).

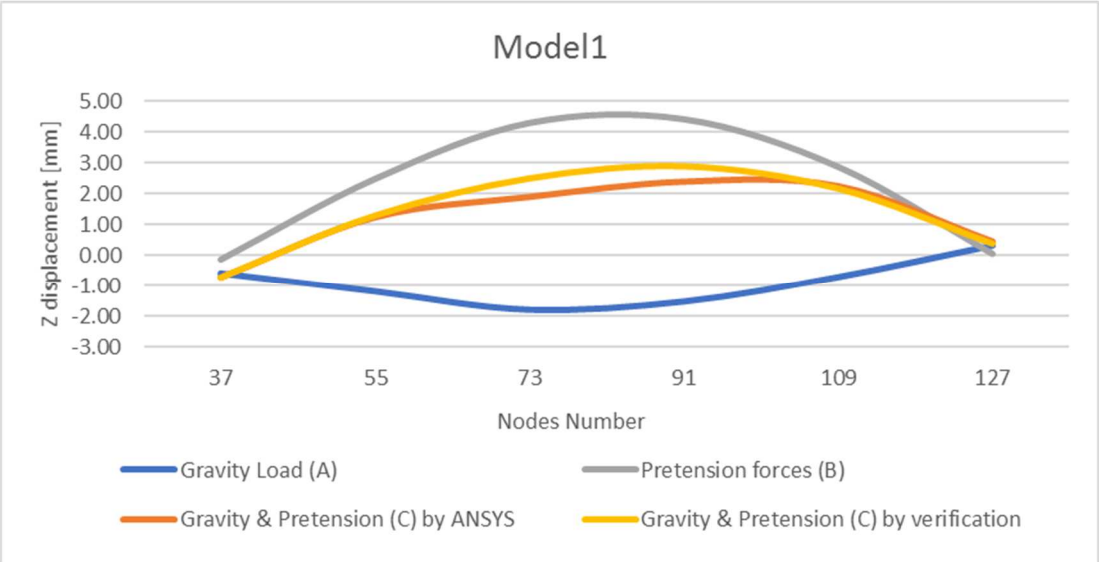

Figure 3.3.10 Verification for Model1.

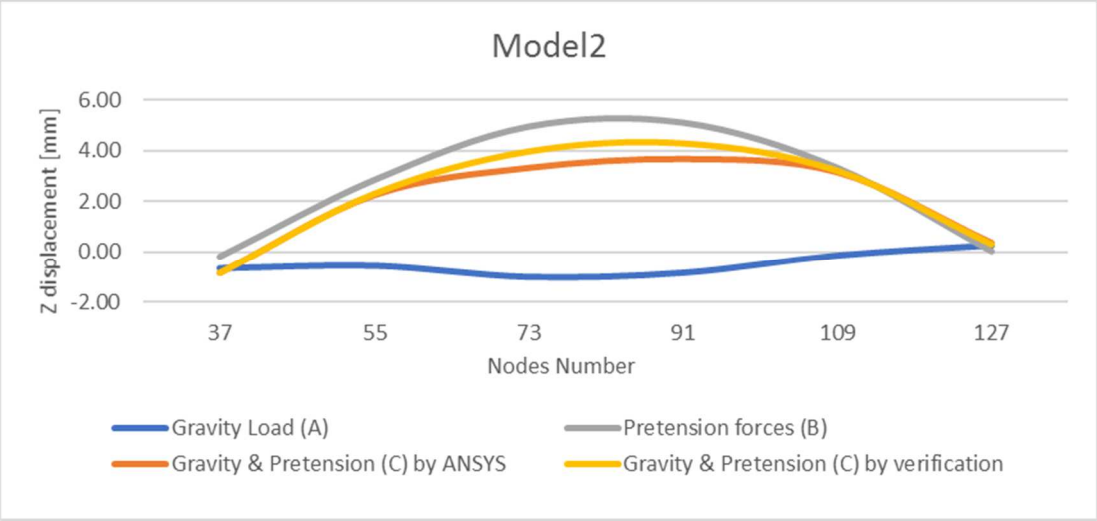

Figure 3.3.11 Verification for Model2.

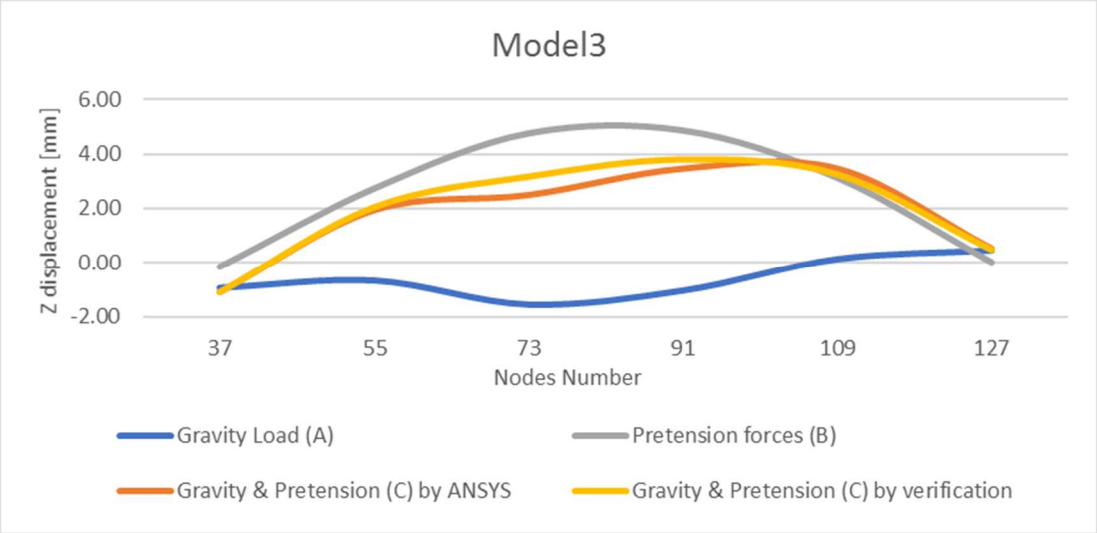

Figure 3.3.12 Verification for Model3.

A small discrepancy among results for situation C obtained by Ansys computations and verifications analysis is visible for all the three models. Such differences, even though negligible and acceptable, is attributable to the kind of computation done. In effect, a non-linear static analysis was done in Ansys to take into account geometrical non-linearities of the models. The analysis was performed by load steps and with a ramped application of loads, meaning that loads were linearly interpolated between different load steps. Thus, each analysis was not performed on the undeformed shape, according to one of the assumptions necessary to apply the superposition principle, but a new configuration of the structure was considered at each load increment. We concluded that the application of pretension forces was done correctly.

3.3.3 Modal analysis

A modal analysis provides the dynamic properties of the structure, in terms of natural modes and frequencies. In the present case, for each one of the three models, eigenfrequencies were computed considering structural masses only. In fact, all that would contribute to the increase of the structure mass, for example a crowd mass, at the same time would contribute to the modification of structure eigenfrequencies.

Indeed, eigenfrequencies depend on the mass and the stiffness matrix of the structure finite element model. As for the stiffness, they are linked to geometry and materials of structure elements other than constraints between different elements and boundary conditions.

Moreover, pretension plays also a role on values of eigenfrequencies, due to the stiffening effect of tendons and since changes the initial geometry of the structure because of the imposed displacements assigned to nodes where it is applied.

The first 10 eigenfrequencies are listed in Table 3.3.10 and Table 3.3.11 for all the three models in both cases of absence and presence of pretension. In "Mode type columns", it is given some information about the eigenmode. When the eigenmode refers to arches vibrations it is specified by the mention *"Arches"*. In that case, if there is a significant deformation also for the deck it is specified by *"+ Deck"*. No clarification is given if the eigenmode refers to the deck only. Through the abbreviations "L", "V" and "T" in brackets we wanted to specify if the eigenmode was lateral, vertical or torsional. *Deformed shapes related to each frequency and model are reported in APPENDIX D.*

Table 3.3.10 Eigenfrequencies for the three models computed in *absence* of pretension.

	without pretension					
n°	**f Model1 [Hz]**	**Mode type**	**f Model2 [Hz]**	**Mode type**	**f Model3 [Hz]**	**Mode type**
1	2.00	Arches (L)	1.91	Arches (L) + Deck (L)	1.10	Arches (L)
2	3.59	Arches (L) + Deck (V)	3.03	(L)	1.56	Arches (L)
3	3.63	(V)	3.53	(V)	2.73	Arches (L)
4	3.96	(L)	3.62	(V)	3.23	(L)+(T)
5	4.49	(T)	4.45	(L)	3.60	(V)
6	5.47	(L)	5.01	(T)	4.27	Arches (L)
7	6.89	(V)	6.47	(T)	4.64	(L)+ (T)
8	6.93	(T)	6.90	(T)	6.07	(L)
9	7.00	(V)	6.90	(V)	6.25	(V)
10	7.12	(V)	7.06	(V)	6.35	(T)

The numerical values in the quoted tables show that show that frequencies depend on the structural geometry. Lateral, vertical, torsional and mixed modes of vibrations appear, having different frequencies. Although variations of frequencies values may be not significant, for a given mode, deformed shapes can be very different among the three models. For instance, between the first and the second model there are more similarities than between the third and the previous two. In particular, there are four eigenfrequencies associated to the vibration of arches among the first ten computed in the third model, while they are only two and one for the first and the second model respectively. The opening of the arches section, then, makes the structure more prone to arches vibrations.

Table 3.3.11 Eigenfrequencies for the three models computed in *presence* of pretension.

	with pretension					
n°	**f Model1 [Hz]**	**Mode type**	**f Model2 [Hz]**	**Mode type**	**f Model3 [Hz]**	**Mode type**
1	2.03	Arches (L)	2.01	Arches (L)	1.12	Arches (L)
2	3.59	Arches (L) + Deck (V)	3.52	(V)	1.56	Arches (L)
3	3.63	(V)	3.53	(V)	2.74	Arches (L)
4	3.96	(L)	3.62	(L)	3.38	(L) +(T)
5	4.51	(T)	4.53	(T)	3.60	(V)
6	5.51	(L)	5.38	(T)	4.27	Arches (L)
7	6.92	(V)	6.90	(V)	4.78	(L) +(T)
8	6.94	(T)	6.91	(T)	6.19	(V)
9	7.13	(V)	7.03	(V)	6.29	(T)
10	7.28	(V)+(T)	7.06	(T)	6.42	(V)

The same situation appears to be considering the presence of pretension. Even in this case, the third model behaves differently from the other two.
To better see differences and similarities between the three models, the reader could refer to Figure 3.3.13, where modes and their frequencies are reported in a graphical way.

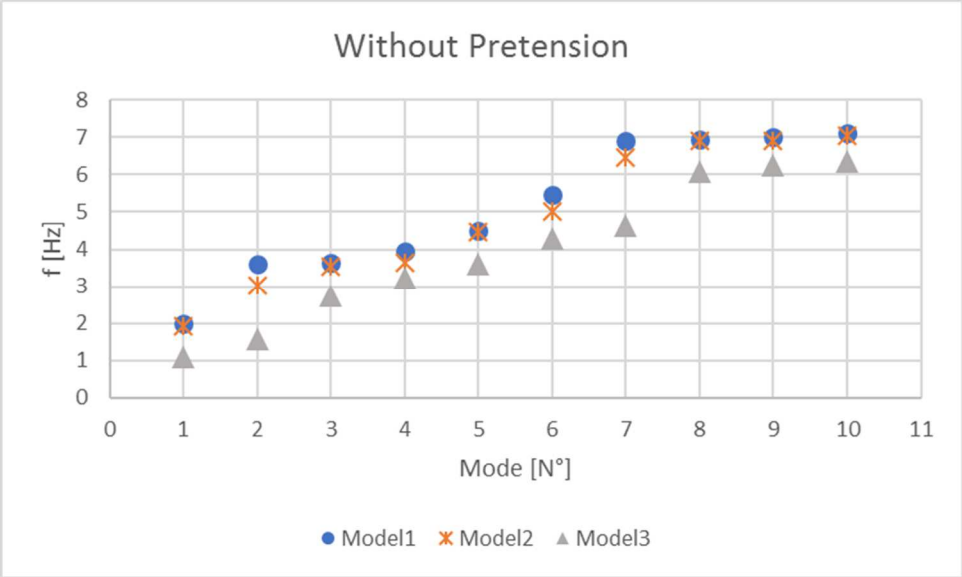

a) a)

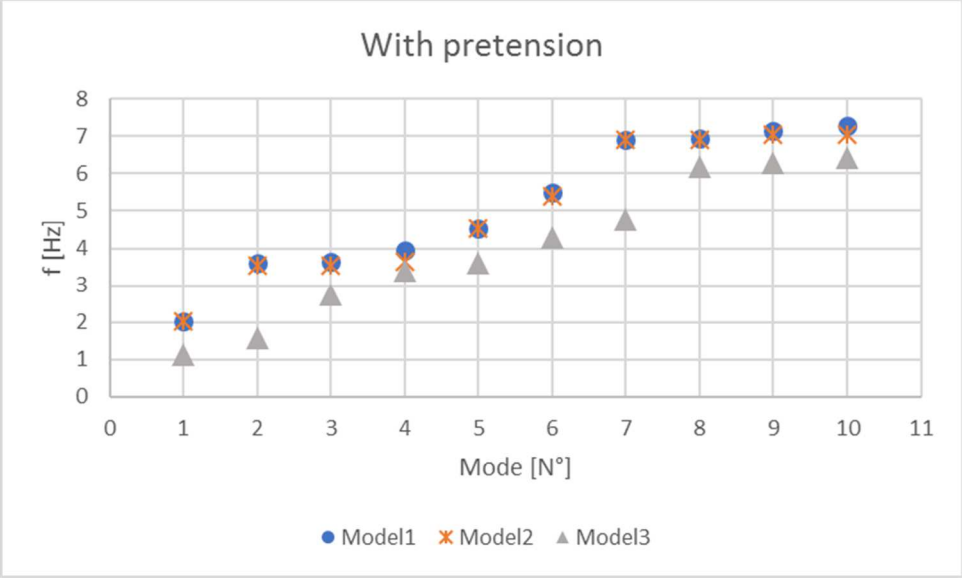

b)

Figure 3.3.13 Scatter between eigenfrequencies of the three models in the case of a) absence and b) presence of pretension.

This difference of behavior is clearer and more marked in the figures just reported, both in case of absence and in presence of pretension.

One more comment can be done with respect to the models. Only negligible differences of frequencies can be pointed out between the two load situations. This would imply that pretension do not plays a great role on the definition of structure stiffness (Figure 3.3.14)

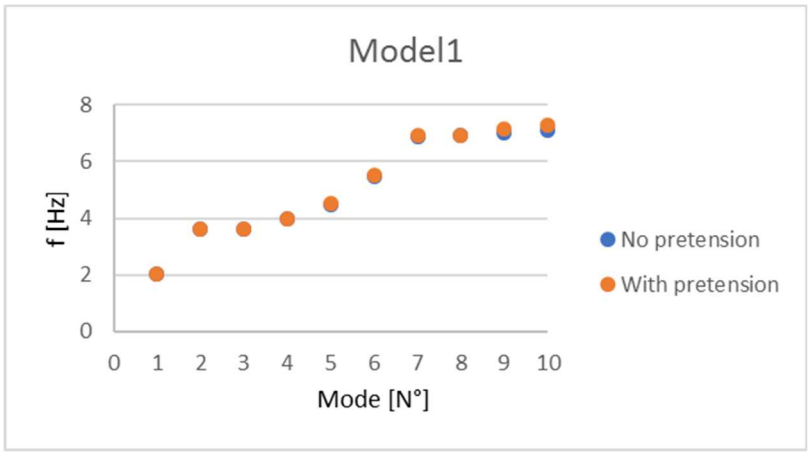

a)

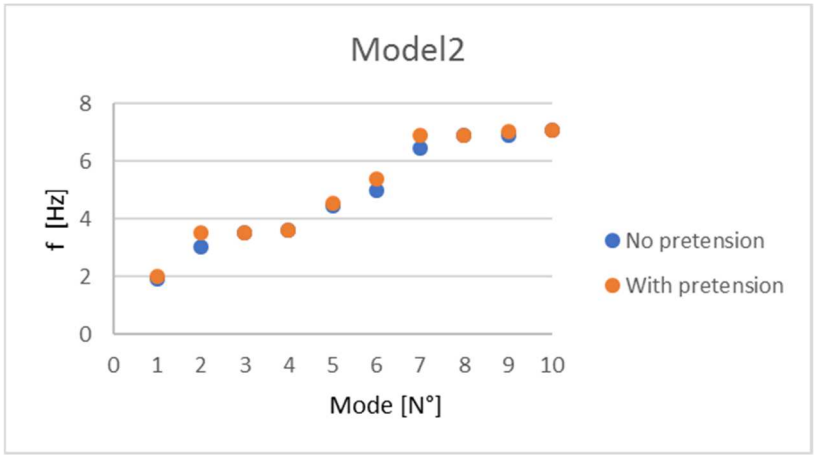

b)

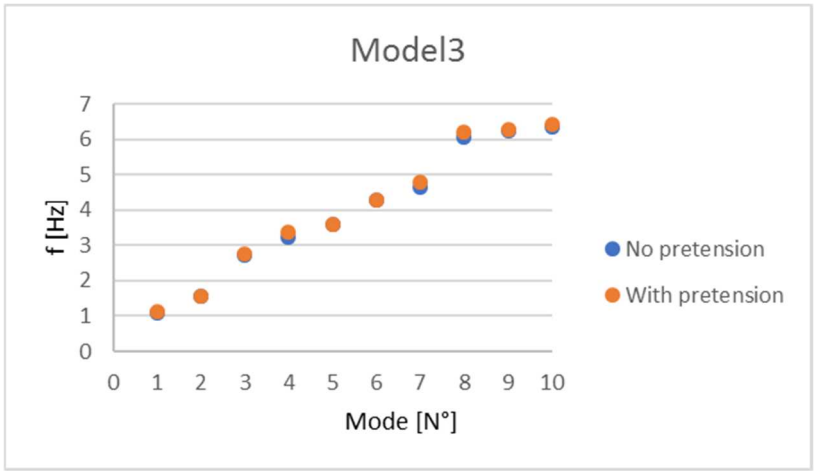

c)

Figure 3.3.14 Eigenfrequencies in the two considered situations.

Usually, pretension should have more remarkable effects. So, even in this case there was the doubt about the application of pretension in the Ansys modeling. In particular, there was doubts about the fact that Ansys took into account the initial deformed shape due to pretension. For this reason, one more verification was done.

Given similarities in values of eigenfrequencies, a similarity was needed to be in spans vertical displacements for the two loads situations as well.

Comparing data between Table 3.3.1 and Table 3.3.8, i.e. displacements for the case of absence and presence of pretension, values of vertical displacements for the deck differ for a maximum value of 4.5 *mm*, in the spans where pretension is applied. Considering the dimensions of the structure, this result was compatible with the fact that frequencies were similar.

Finally, even in this case, it has been possible to confirm that pretension was applied correctly. For sake of completeness, differences in displacements for the same nodes considered in the previous section are reported in Table 3.3.12 and Figure 3.3.15.

Table 3.3.12 Delta between vertical displacements computed for the two load cases of absence and presence of pretension in the three models

N	ΔU_z Model1 [mm]	ΔU_z Model2 [mm]	ΔU_z Model3 [mm]
1	0.00	0.00	0.00
19	0.16	0.19	0.17
37	0.16	0.18	0.16
55	2.42	2.82	2.61
73	3.69	4.33	4.06
91	3.92	4.52	4.51
109	2.95	3.30	3.32
127	0.10	0.10	0.06
145	0.63	0.73	0.73
163	0.02	0.03	0.05
181	0.15	0.19	0.23
199	0.05	0.07	0.08
205	0.00	0.00	0.00

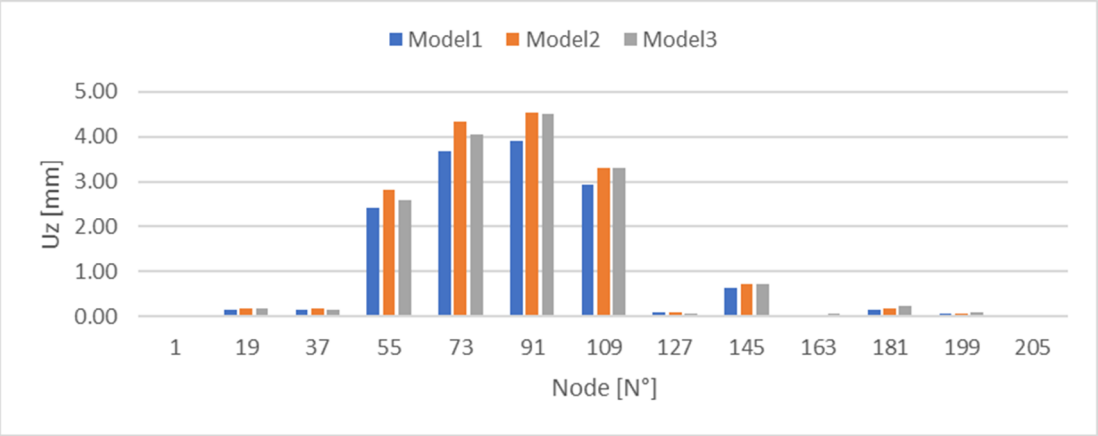

Figure 3.3.15 Graphical representation of data reported in Table 3.3.12.

For the three models, largest differences appear in the second span starting from the left in Figure 3.3.15. Elsewhere, differences are negligible. However, such small differences allow us to say that stiffness of the pre-tensioned and not pre-tensioned systems are comparable.

3.4 Validation of the modeling method

The creation of a FE model could be useful principally for two reasons, each of them related to a different phase of the life of the structure. A FE model can be used during the design phase, to assess the behavior of complex structures and validate, or not, simplified computations, based on procedures typical of structural mechanics or coming from standards and regulations. On the other hand, if a structure already exists, its FE model could be exploited to compare results obtained with numerical computations to observations made during inspecting campaigns. In such a way, it is possible to evaluate, once the model is calibrated to reproduce experimental data, which are the parameters that influence the behavior of the structure and, thus, decide which could be the best solutions to a particular issue without testing them in reality.

In our situation, we can refer to the first case. It is necessary to take into account the approximate nature of the finite elements method. Results are given using numerical methods adapted to the possibility to solve discretized problems only. Moreover, real conditions, such as natural variability of material properties, behavior of foundations and mechanical connections, make easier and obvious a certain difference between the discretized problem solution and the real problem one.

To this already large amount of variability, there is the possibility to make some modeling error. Without the possibility to compare the final results given by the finite element model with experimental results, during the design phase it is very important to check the modeling procedure step by step and make sure that everything has been done properly.

The easiest way was to check at each step if numerically results were in line with analytical ones. If main idea is to perform a dynamic analysis of the structure, it is very important that eigenmodes and eigenfrequencies are precisely determined. We are in face of a complex structure but, checking element by element and for situations for which we have analytical solutions, we can reasonably assume that the results, if correct case by case, will be meaningful even for the complete structure. So, for example, we show hereafter numerical and analytical results for two elements: one of the two main longitudinal beams with hollow rectangular section, that we will consider as simply supported and with homogeneous zero slope, and one of the transversal HEB100 elements, considered as double clamped. For the sake of completeness, it could be useful to remind analytical solutions for both cases (Eq. 3.4.1 for simply supported case and Eq. 3.4.2 for double clamped case).

$$\begin{cases} U_z(z) = C_n[\sin(\chi_n z)] \\ \omega_n = {\chi_n}^2 \sqrt{\dfrac{EJ}{\rho A}} \\ \chi_n = \dfrac{n\pi}{L} \end{cases} \qquad \text{Eq. 3.4.1}$$

$$\begin{cases} U_z(z) = C_n\left[\sinh(\chi_n z) - \sin(\chi_n z) + \dfrac{\sinh(\chi_n L) - \sin(\chi_n L)}{\cos(\chi_n L) - \cosh(\chi_n L)}(\cosh(\chi_n z) - \cos(\chi_n z))\right] \\ \omega_n = {\chi_n}^2 \sqrt{\dfrac{EJ}{\rho A}} \\ \chi_n = (n + \dfrac{1}{2})\dfrac{\pi}{L} \end{cases} \qquad \text{Eq. 3.4.2}$$

where, the subscript n indicates quantities depending on the number of considered eigenmode (ω_n is the *n-th* eigenfrequency), E is the Young's modulus, ρ is the material density, L the beam length, A the section surface, J the moment of inertia and C_n is the amplitude of the modal shape $U_z(z)$, unknown *a priori* [19].

In Table 3.4.1-Table 3.4.2 the results are compared. It is easy to assess that, practically, there are no differences among the two computations in the first case, where the discretization is very precise. In the second case, being the beam subdivided in only five elements, the degree of precision is smaller and decreases with increasing frequencies. However, the results can be considered acceptable.

Table 3.4.1 Eigenfrequencies analytically and FE computed of the simply supported beam with hollow rectangular section.

Hollow rectangular section (200x150x10 mm): simply supported beam					
A $[m^2]$	I_x $[m^4]$	I_y $[m^4]$	L $[m]$	ρ $[^{kg}/_{m^3}]$	E $[GPa]$
0.0066	0.00003682	0.000023295	53.95	8000	210
Closed form solution			FE Computation		
n	Freq x $[Hz]$	Freq x $[Hz]$	n	Freq x $[Hz]$	Freq x $[Hz]$
1	0.20	0.16	1	0.20	0.16
2	0.82	0.65	2	0.82	0.65
3	1.85	1.47	3	1.86	1.48
4	3.30	2.62	4	3.31	2.63
5	5.16	4.10	5	5.17	4.11
6	7.43	5.91	6	7.44	5.92
7	10.11	8.04	7	10.12	8.05
8	13.21	10.51	8	13.21	10.51
9	16.72	13.30	9	16.71	13.29
10	20.65	16.42	10	19.82	16.71

Table 3.4.2 Eigenfrequencies analytically and FE computed of the simply supported beam with HEB100 section.

HEB100 section: double clamped beam					
A $[m^2]$	I_x $[m^4]$	I_y $[m^4]$	L $[m]$	ρ $[^{kg}/_{m^3}]$	E $[GPa]$
0.0026	0.000004495	0.000001673	3.15	8000	210
Closed form solution			FE Computation		
n	Freq x $[Hz]$	Freq x $[Hz]$	n	Freq x $[Hz]$	Freq x $[Hz]$
1	75.82	46.25	1	73.00	44.293
2	210.61	128.49	2	232.79	129.09
3	412.80	251.84	3	403.38	254.16
4	682.39	416.30	4	657.6	428.35
5	1019.37	621.89	5	1000.4	615.44
6	1423.75	868.59	6	1505.6	864.01
7	1895.52	1156.41	7	1893.5	1130.9
8	2434.70	1485.34	8	2439.1	1506.7
9	3041.27	1855.40	9	2879.7	1855.7
10	3715.23	2266.57	10	3440.4	2293.5

CHAPTER 4
HIVOSS GUIDELINES

This chapter presents the HiVoSS guidelines for design and check of footbridges during the design phase. Even though HiVoSS stands for Human induced Vibrations on Steel Structures, this document represents a practical guide for the design of footbridges made of different materials, from reinforced or pre-stressed concrete to timber passing through steel and composite steel-concrete structures. This useful tool was conceived to give clear answers to designers that, after the case of Millennium Bridge and Passerelle Solférino, felt the necessity to consider with more attention the serviceability state of this kind of structures regarding dynamic human induced loads. In fact, once the structure is built, putting in place vibrations mitigation systems may represent an important increment of the total construction cost.

Only aspects related to the design will be covered in this chapter. For more details about measurements and vibration mitigations on existing footbridges, refer to the complete document.

4.1 The design procedure

At the moment, there are no available code regulations for vibrations performance of footbridges due to walking pedestrians.
HiVoSS guidelines propose design procedures based on results obtained during the research project RFS-CR-03019 "Advanced Load Models for Synchronous Pedestrian Excitation and Optimized Design Guidelines for Steel Footbridges (SYNPEX)" financially supported by the Research Found for Coal and Steel (RFCS). A flowchart of HiVoSS guidelines is presented in Figure 4.1.1.

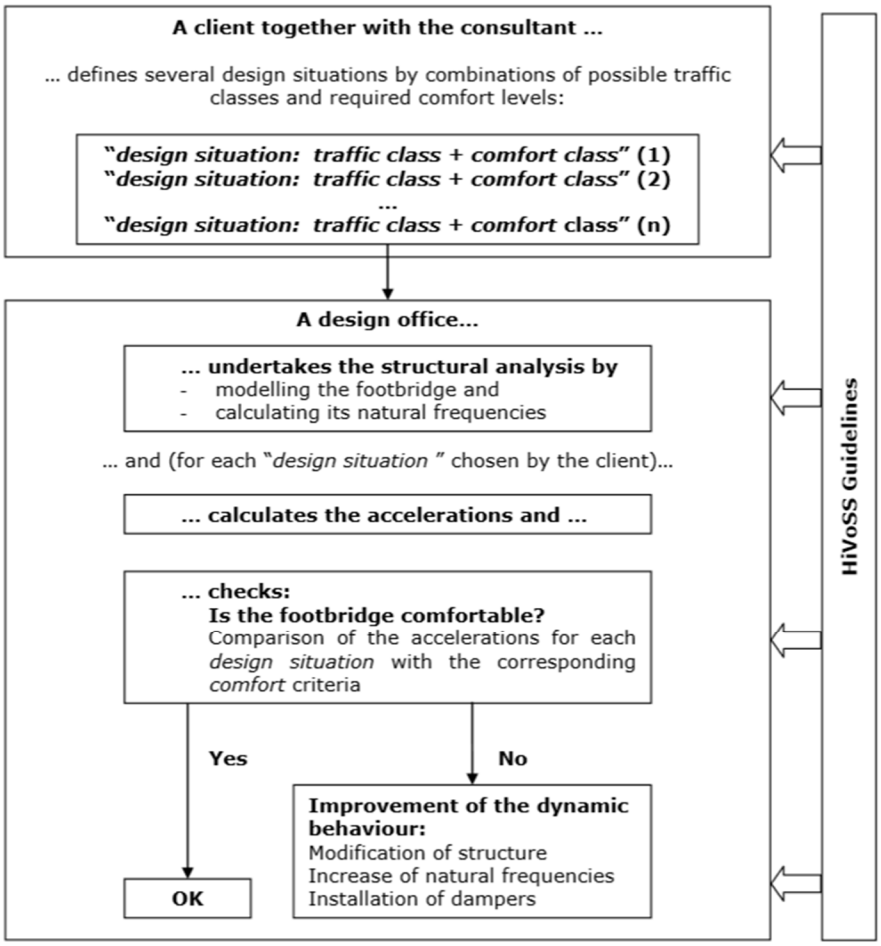

Figure 4.1.1 The design process according to HiVoSS guidelines [22]

As in every design, the first step consists in the choice of design situations defined, in this case, by both a traffic class and a comfort class. After this stage, structural analysis and computation are done from a design office with the objective to realize the structure according to all criteria, included the architectural ones. The dynamic behavior of the structure is evaluated on the basis of the acceleration of each of its points. From these values,

designers can answer the question about the comfort of the structure proceeding to the construction or improving the design.

The HiVoSS design process is given in Figure 4.1.2. The main assumption, underlined in the Background document attached to guidelines, is the fact that damping and foundation properties are unknown during design phase and, then, must be assumed based on literature data. For this reason, it is recommended that, in case of critical situations, damping devices must be already accounted during the design stage and, once the structure is built, real properties of damping and foundations must be measured to choose if they need to be installed or not.

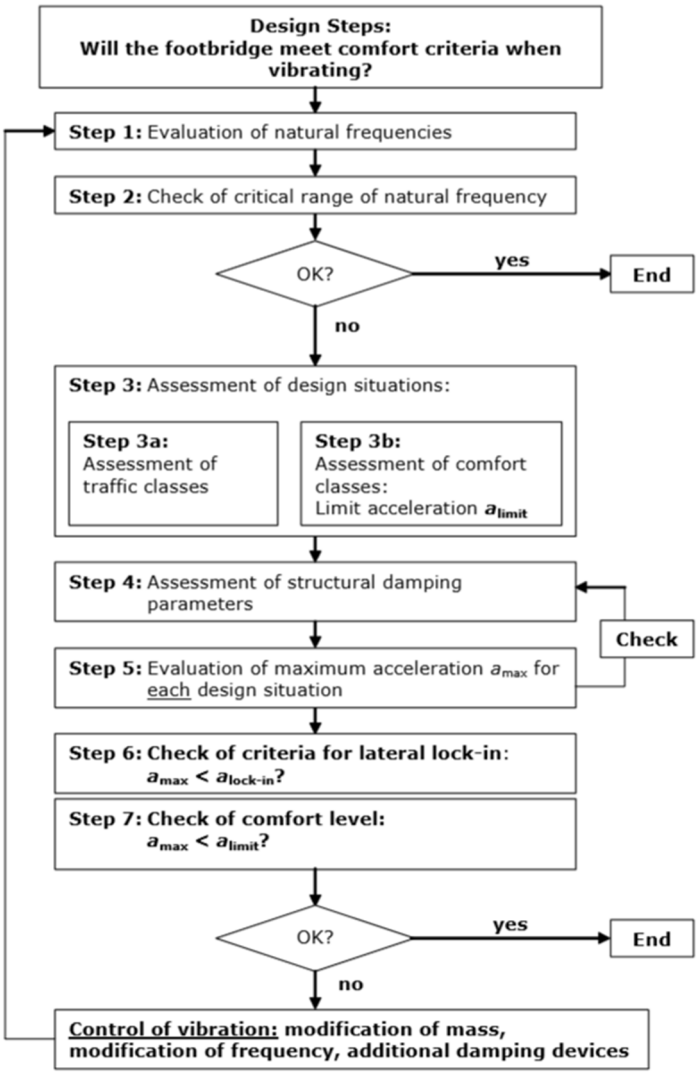

Figure 4.1.2 Design steps according to HiVoSS guidelines [22].

The design stage is subdivided in 7 Steps and in next sections, each Step will be discussed to describe the analysis that will be conducted in the next chapter.

4.2 Step 1: evaluation of natural frequencies

The evaluation of natural frequencies during design can be done in two principal ways:

- By hand calculations;
- Through FE model;

It is widely accepted that even if hand calculations and simplified methods are powerful tools, a precise computation is needed when the objective is to ensure that natural frequencies of the footbridge are outside a critical range. Obviously, the model must be sufficiently refined to well represent the real behavior of the structure. Material properties, damping coefficient and soil structure interactions must be verified after the construction of the footbridge to validate the model and allow for further checks.

4.3 Step 2: critical range of natural frequencies

In HiVoSS guidelines, it is recommended that footbridges have natural frequencies outside a critical range that varies if one considers the vertical and antero-posterior or the medial-lateral direction. In fact, in the case of walking pedestrians:

- For vertical and antero-posterior (also longitudinal) directions, the critical range is:

$$1.25\ Hz \leq f_i \leq 2.3\ Hz \qquad \text{Eq. 4.3.1}$$

- For the medial-lateral direction (also lateral), the critical range is:

$$0.5\ Hz \leq f_i \leq 1.2\ Hz \qquad \text{Eq. 4.3.2}$$

The interval for antero-posterior direction (also longitudinal) might be extended up to 4.6 Hz if the contribution of the second harmonic of the pedestrian load is considered.

In the case of running pedestrians, no critical range is given for medial-lateral direction while the one prescribed for the vertical direction is modified as follows:

$$1.9\ Hz \leq f_i \leq 3.5\ Hz \qquad \text{Eq. 4.3.3}$$

4.4 Step 3: assessment of design situation: traffic classes and comfort classes

Design is always based on some reference situations that can verify during the life cycle of the structure since a certain degree of comfort must be always guaranteed. Obviously, from the design point of view, it is important that realistic traffic conditions are modeled.

According to HiVoSS, design situations are defined through a combination of one of the 5 traffic classes given in Figure 4.4.1, and one of the 4 comfort classes listed in Figure 4.4.2.

Traffic Class	Density *d* (P = pedestrian)	Description	Characteristics
TC 1*)	group of 15 P; *d*=15 P / (*B L*)	Very weak traffic	(*B*=width of deck; *L*=length of deck)
TC 2	*d* = 0,2 P/m²	Weak traffic 	Comfortable and free walking Overtaking is possible Single pedestrians can freely choose pace
TC 3	*d* = 0,5 P/m²	Dense traffic 	Still unrestricted walking Overtaking can intermittently be inhibited
TC 4	*d* = 1,0 P/m²	Very dense traffic 	Freedom of movement is restricted Obstructed walking Overtaking is no longer possible
TC 5	*d* = 1,5 P/m²	Exceptionally dense traffic	Unpleasant walking Crowding begins One can no longer freely choose pace

Figure 4.4.1 Traffic classes defined in HiVoSS, depending on pedestrians' density [22].

Comfort class	Degree of comfort	Vertical a_{limit}	Lateral a_{limit}
CL 1	Maximum	< 0,50 m/s²	< 0,10 m/s²
CL 2	Medium	0,50 – 1,00 m/s²	0,10 – 0,30 m/s²
CL 3	Minimum	1,00 – 2,50 m/s²	0,30 – 0,80 m/s²
CL 4	Unacceptable discomfort	> 2,50 m/s²	> 0,80 m/s²

Figure 4.4.2 Comfort classes depending on the maximum acceleration [22].

Traffic classes are established in terms of pedestrians' density while comfort classes in terms of footbridges acceleration.

Considering the whole life of the structure, it is reasonable that for an event that might happen only once in the footbridge life, the designer would choose a comfort class not very high. On the contrary, for a very frequent situation, a higher degree of comfort must be guaranteed.

4.5 Step 4: assessment of structural damping

As already introduced in section 1.5, damping is a very important parameter in the evaluation of amplitude of human induced oscillations and may depend on losses of energy due to material properties, all along the structure, and on local effects of bearings or vibration control systems. The greater part of damping effects is produced inside structural elements even if, sometimes, also nonstructural elements, such as handrails and coverage of deck surface, can play a non-negligible role.

Unfortunately, none of the previous mechanisms produces dissipations that can be foreseen precisely already during the design phase and the correct estimation of energy loss can be done only after the construction of the footbridge.

Since civil engineering structures are always low damped, the usual approximation to consider a linear model of damping is widely accepted. In fact, in the viscous damping model damping effects are modeled by forces linearly proportional to velocity.

To determine the damping coefficient to be used in the equations of motion, HiVoSS gives, through Figure 4.5.1, mean and average values of damping coefficient to use in service load cases for several footbridge construction materials.

Construction type	Damping ratio ξ
Reinforced concrete	5,0%
Prestressed concrete	2,0%
Steel, welded joints	2,0%
Steel, bolted joints	4,0%
Reinforced elastomers	7,0%

Figure 4.5.1 Values of structural damping proposed by HiVoSS [22].

4.6 Step 5: determination of maximum acceleration

Once the designer moves to step 5, after the definition of one or several design situations, the parameter needed to evaluate the comfort level for a footbridge is the maximum acceleration reached by footbridge points. Indeed, acceleration is the parameter that influences the perception of the footbridge users.

In HiVoSS, three different methods to estimate the maximum acceleration are proposed. Two are based on time domain analysis while the other is a spectral design method. The logic of the analysis procedures is presented in Figure 4.6.1.

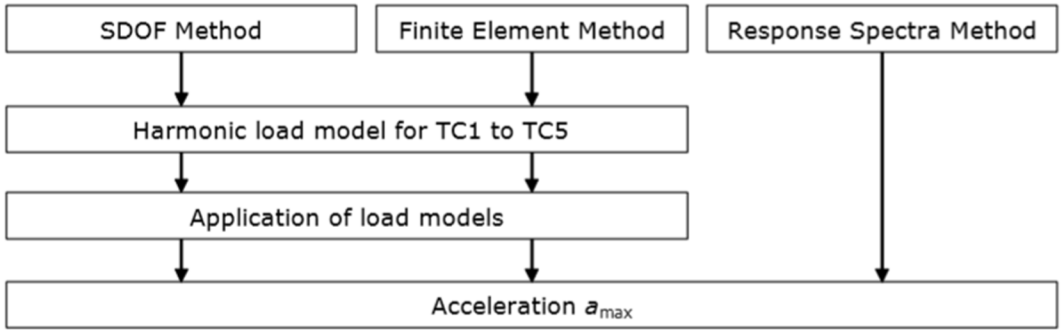

Figure 4.6.1 Proposed methods for the computation of maximum acceleration proposed bt HiVoSS [22].

For SDOF and FE methods, the determination of a_{max} is done through harmonic analysis. The third method relies on the application of an empirical formula "*based on numerical time step simulations of various pedestrian streams on various bridges geometries*" with a Monte Carlo approach.

However, we will focus on the description of the FE method that will be used with Ansys.

In this respect, key aspects are the determination of load models for traffic classes going from TC1 to TC5 and the application of the loads models.

4.6.1 Harmonic load model

In CHAPTER 1, it was possible to understand how large is the number of variables that influences the human induced loads and the difficulty to model them.
However, to provide a design procedure accounting for all the characteristics of the problem and, at the same time, for the need of a simplified method, in HiVoSS the human induced load is represented by a simple harmonic load.
First, the concept of number of synchronized pedestrians on the structure is introduced.
Inside a stream of pedestrians composed of n people walking with a random pattern, it is observed that is possible to identify an equivalent number of people n' walking with the same step frequency, perfectly synchronized (Figure 4.6.2).

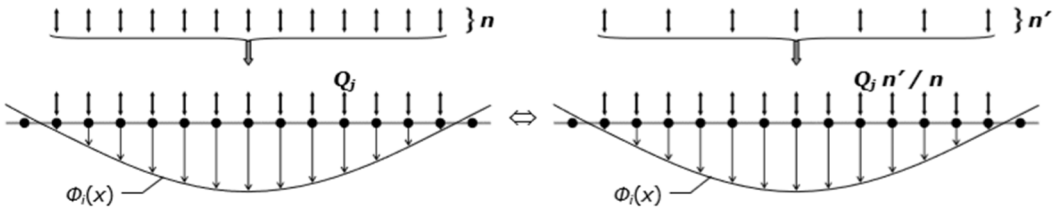

Figure 4.6.2 The equivalent number of synchronized pedestrian n' is a part of the total number of pedestrians n on the loaded surface [22].

This load can be represented as a deterministic load and it has been proved that this is sufficient to define in a quite realistic manner the degree of comfort of a footbridge.
The background document annexed to HiVoSS, after an analytic derivation for a simple case, states that n' was determined "*by regression as a function of the damping ratio and the total number of pedestrian on the footbridge*".
Two expressions of this parameter are given as function of the design traffic class:

- Traffic classes from TC1 to TC3 and $d < 1.0\ {}^{ped}/_{m^2}$: $n' = \frac{10.8\sqrt{\xi n}}{S}$; $[{}^{1}/_{m^2}]$
- Traffic classes TC4 and TC5 and $d \geq 1.0\ {}^{ped}/_{m^2}$: $n' = \frac{1.85\sqrt{n}}{S}$; $[{}^{1}/_{m^2}]$

where:

- n' is the equivalent number of synchronized pedestrians on the loaded surface;
- n is the number of pedestrian inside the stream;
- ξ id the damping coefficient;
- S is the loaded surface of the footbridge;
- d is the pedestrian density on the loaded surface.

4.6.2 Application of the load model

The harmonic load model quoted at previous section is defined as a cosinusoidal uniformly distributed load depending on time and on one of the eigenfrequencies of the structure:

$$p(t) = Pcos(2\pi f_s t)n'\psi \qquad \text{Eq. 4.6.1}$$

where:

- P is the component of the force due to a single pedestrian with a walking step frequency f_s;
- $f_s$is the step frequency, which is assumed equal to the footbridge natural frequency under consideration;
- n' is the equivalent number of pedestrians on the loaded surface S;
- S is the area of the loaded surface;
- Ψ is the reduction coefficient taking into account the probability that the footfall frequency approaches the critical range of natural frequencies under consideration.

The application of the load must be done according to a precise logic. First, the positive direction of the load must be concordant with the studied deformed shape of the structure (the HiVoSS example in Figure 4.6.3) and, second, care must be paid in the choice of frequencies for which the verification will be done. It would not have any sense performing analysis for frequencies that will never be excited by a walking pedestrian.

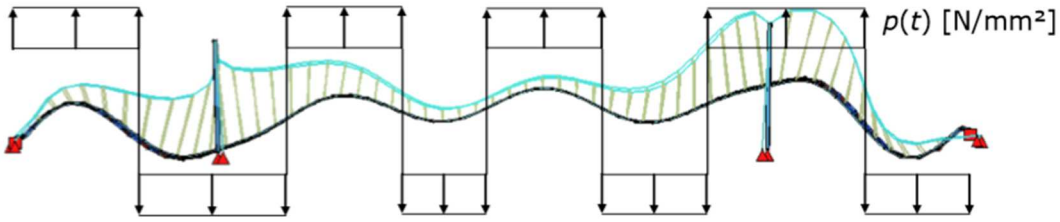

Figure 4.6.3 Example of load application for the walking pedestrians load case [22].

Thus, the Ψ coefficient is necessary to ensure that the frequency at study is inside the critical interval reported in section 4.3. Its value is computed according to Figure 4.6.4, choosing between the curve proposed for the case of vertical or longitudinal oscillations or for the case of lateral ones (Figure 4.6.4).

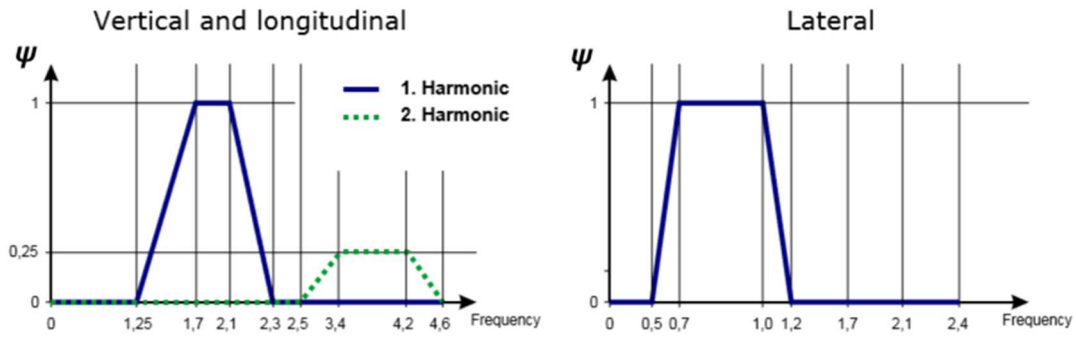

Figure 4.6.4 Graphics for the computation of the Ψ reduction coefficient [22].

Finally, the P parameter must be chosen on the base of the type of the considered modal shape. It presents three different values, each of them related to vertical, longitudinal or lateral modes (Table 4.6.1).

Table 4.6.1 Values of the P parameter as function of the type of studied oscillations [22].

	Vertical	**Longitudinal**	**Lateral**
$\boldsymbol{P}$ $[\boldsymbol{N}]$	280	140	35

The load model just described refers only to a stream of walking pedestrians on footbridges. As for running pedestrians, the design load model is reported only in Section 9 of the HiVoSS Background Document.

Here, the equivalent number of synchronized running pedestrians is equal to the number of running pedestrians crossing the footbridge *tout court*. Moreover, even though the load model is still harmonic, it is different from the case of walking pedestrians because, now, it represents a concentrated load and must be applied on the node of the considered modal shape that has the maximum displacement. The model is described by the following relationship:

$$P(t, v) = Pcos(2\pi f_s t)n'\psi \qquad \text{Eq. 4.6.2}$$

where all symbols have the same meaning as in the case of the walking pedestrians load model except for n' that, now, has not dimension and where v is the velocity of the runner over the footbridge, set to zero by default.

In this case, the interval of critical frequencies is different (compare to section 4.3) and verifications must be done only according to the vertical direction.

The P parameter, in order to well represent this different kind of induced load, (we have seen in CHAPTER 1 that the vertical component of the human induced load changes as a function of the velocity of the pedestrian), has always the value of $1250\,N$ while the determination of the Ψ coefficient is based on Figure 4.6.5.

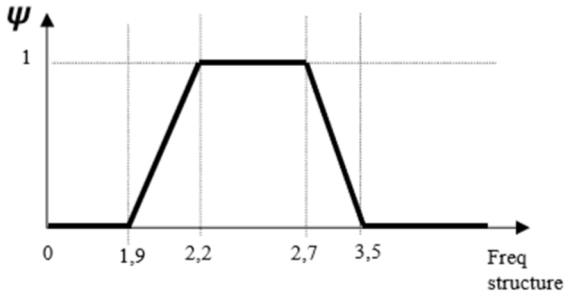

Figure 4.6.5 Graphic for the computation of the Ψ reduction coefficient for the running pedestrians load case [23].

4.7 Step 6: check of criteria for lateral lock-in

The lock-in phenomenon is something that happens in the regime where the frequency of the excitation is near to one of the natural frequencies of the structure. It causes the vanishing of the overall damping producing a sudden amplified response of the structure.

This phenomenon has been observed in case of lateral vibrations. When the footbridge slightly vibrates laterally, human body acts as negative dampers, putting energy into the system and triggering the begin of the lock- in phenomenon

This is not the focus of the work, but in HiVoSS and in its background document, two methods are proposed to verify this issue. One is based on the verification of the minimum number of people needed to start the lock-in phenomenon and the second on the determination of a limit acceleration needed before the lock in begins.

4.8 Step 7: check of comfort level

Once having made computations and verifications, the role of the designer is to check if values of accelerations respect minimum requirements of comfort classes established in design phase.

If this does not happen, four possible solution are proposed:

- Modification of the mass;
- Modification of the frequency;
- Modification of the structural damping,
- Addition of damping.

These operations are recommended already during the design phase in case of critical situations because finding a solution could be very expensive for an already built footbridge. Moreover, considering the great variability affecting the structure and the pedestrians, even

if the design shows a good behavior of the structure, it is always recommended to consider already from the design phase the possibility of installation of damping devices on the footbridge, in order to avoid problems of space and adaptation on the existing structure.
Some indications about evaluation of dynamic properties of existing footbridges, in terms of measurements, tests and instrumentations are given in the guidelines along with indications for control of vibration response. However, these two last aspects go out of the context of this work.

CHAPTER 5
DYNAMIC ANALYSIS

This section describes results obtained applying the HiVoSS prescriptions and results obtained using an innovative approach that accounts for the variability of human induced forces generated during running.

Thus, after a first introduction to the paper the approach is based on, the brief description of the Matlab code written to create a text file readable for Ansys will follow. The code, called RealRun1, has been adopted to generate time varying loads on mesh nodes and updating their position at each load step, as the runner moves on the footbridge.

However, before presenting results for the case of running human, according to Hivoss and as result of the Matlab code, a preliminary check was done for the case of a group of 15 walking persons according to Hivoss. It is confirmed that this load case, for the natural frequency lying in the HiVoSS interval of critical frequencies for walking pedestrians, induces only relevant arches displacements.

5.1 The running pedestrian induced load

In CHAPTER 1 the description of the load induced by walking people was made in a very accurate way. Through the study of several papers, the main features of the load, such as an important inter- and intra-subject' variability and its stochastic nature, were clarified. A few key factors are recalled here.

The walking pedestrian induced load, also known as Ground Reaction Force (GRF), is characterized by three different components: vertical, longitudinal and lateral. The determination of their exact time histories has been a very important research topic in the last few decades and still today, for biomechanical reasons, it is the object of more accurate studies. The difficulty of the matter is related to the fact that it is not easy to sample this kind of loads without taking into account boundary conditions that may be represented by stiffness of plates or treadmills, shoes, interaction with other pedestrians and so on. However, a good agreement for the M shape of the GRF vertical component for walking pedestrian is generally reached (Figure 5.1.1).

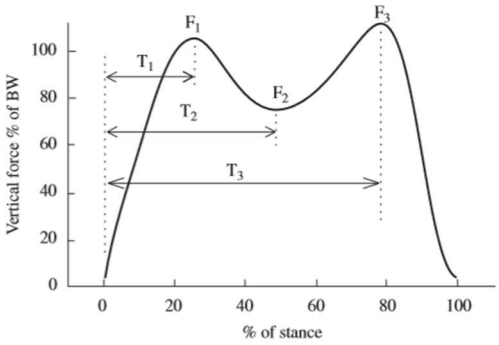

Figure 5.1.1 Time history of GRF vertical component for a walking pedestrian [46].

It was already showed that this special shape is due to the way in which the bodyweight and inertial loads are transmitted to the ground during the gait cycle. However, Figure 5.1.1 represents only the load induced by one single step. Since steps follow each other's during a walk and since there is a time in which both feet touch the ground in the so-called double support phase, more studies were conducted to determine some probable relation between the velocity of the pedestrian and the duration of support. It was found that, as speed increases, the duration of support decreases and finally becomes so short that, when the pedestrian starts to run, the double support phase does not exist anymore. Besides, also the time history shape of the load was found to be dependent on the speed. In Figure 5.1.2 the difference between vertical components of the human induced load when walking or running is clarified.

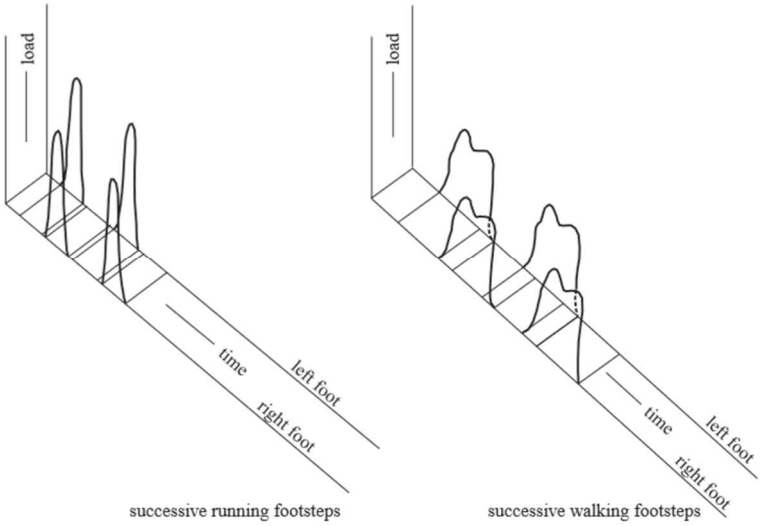

Figure 5.1.2 Vertical components of GRFs for both feet and two different velocities [45]. On the left the case of the running pedestrian: no double support phase and no more M shape of the load.

Unfortunately, so far there was not the need to analyze GFRs of running pedestrians and this lead to a consequent lack of information and description of this special load. In effect, after the cases of Millennium Bridge and Passerelle Solférino, the attention of the academic community was focused on GRFs induced by walking pedestrians with the aim to find design methods taking into account at the same time the difficulty to model this stochastic load and the need for an easily applicable design method. The results have been cast in form of guidelines as, for example, HiVoSS, described in CHAPTER 4, and SETRA "Technical guide for assessment of vibrational behavior of footbridges under pedestrian loading", where the case of running pedestrians is barely and superficially treated.

However, during the last years, a new interest on this problem arose. Due to the growing number of competitions organized in urban environments, footbridges need to have an adequate comfort level also under these conditions. Thus, researches are done around the world with the purpose to provide a reliable design method capable to address the engineers' concerns. A very interesting work was done by *Racic and Morin* [47], that is the base of the load time history used to perform the transient analysis of the structure.

They created an extended database of continuous signals of vertical running loads generated by individuals in motion on flat stationary surfaces and provided two mathematical models to reproduce measurements. The first model is based on the classical deterministic perfectly periodic approach usually applied for walking loading, while the second accounts for the stochastic nature of the load. Using this second model, *Racic and Morin* produced a numerical generator of synthetic force-time series capable to simulate the load and its variability. It must be specified that, since measurements were done on stiff treadmills, *the*

model give significant results when the bridge motion is not perceptible by the runner. However, in any case, the realistic reproduction of running forces based on observation is a key aspect to consider for the comfort level of a footbridge.

For the creation of the database of vertical load time histories, *Racic and Morin* used two different treadmills in order to be able to collect data for speeds going from 0.1 to 25 km/h. The experimental procedure prescribed the record of at least 64 successive footfalls for different values of speeds after the first at which jogging, rather than walking, was more comfortable for subjects. The increment of speed was done by successive steps of 0.5 km/h and all signals were sampled at 200 Hz.

Finally, 458 vertical running force-time histories (an example in Figure 5.1.3) were collected involving 45 volunteers of different sex, body mass, height and age.

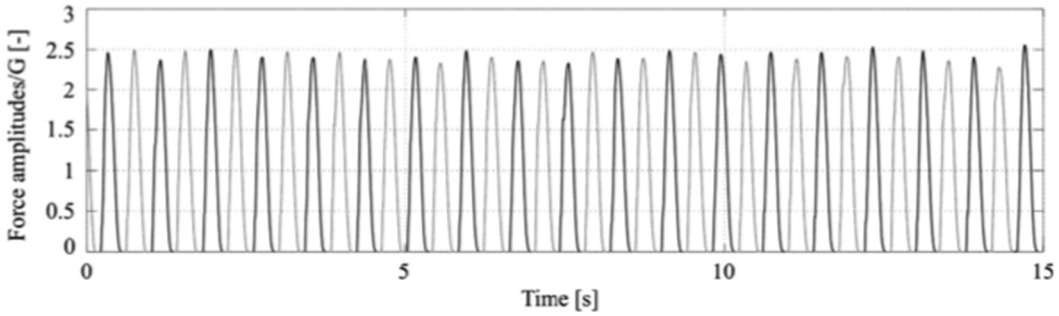

Figure 5.1.3 Force signal generated at a speed of 8 km/h [47].

Then, they tried to reproduce the signal exploiting the approach based on Fourier's series, where the load can be represented as the sum of sinus functions as follows:

$$F(t) = G\sum_{i=1}^{m}\alpha_i \sin(2\pi i f_r t - \varphi_i) \qquad \text{Eq. 5.1.1}$$

where:

- $F(t)$ represents the total force at time t;
- G is the body weight;
- α_i are the "dynamic load factors" (DLFs);
- f_r is the running frequency;
- $\varphi_i$are phase angles.

It was demonstrated that this approach can only provide an approximate representation of the running vertical force and, even considering a random uniform distribution of φ_i in the interval $[-\pi;\pi]$, the sum of Fourier harmonics is different from the real force-time history signal (Figure 5.1.4).

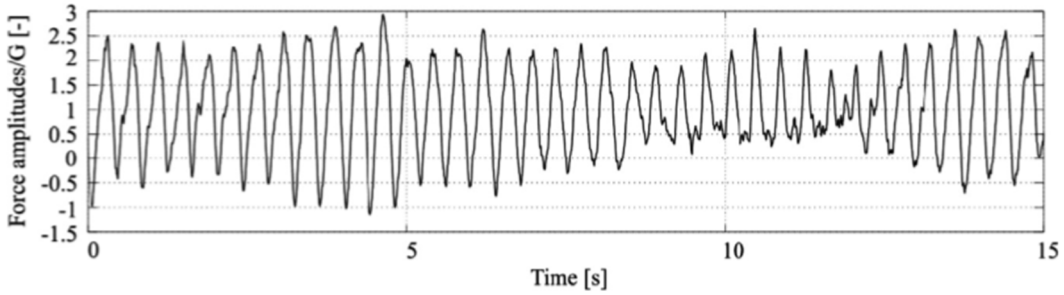

Figure 5.1.4 The force-time history reproduced using the spectrum of a real time history and a random uniform distribution of φ_i in the interval $[-\pi; \pi]$ [47].

Then, by taking advantage of existing numerical generator of electrocardiogram (ECG) signals, *Racic and Morin* used a dynamic time warping (DTW) method, initially developed for speech recognition, to obtain the template load cycle in the most correct and representative form by minimization of the sum of squared differences between different "aligned" load cycles (Figure 5.1.5). We recall that a complete load cycle is considered between two identical moments of the load time history. Here, it is considered between the two moments in which a foot hits the ground. Thus, the load cycle is composed of a contact phase and a "flying phase".

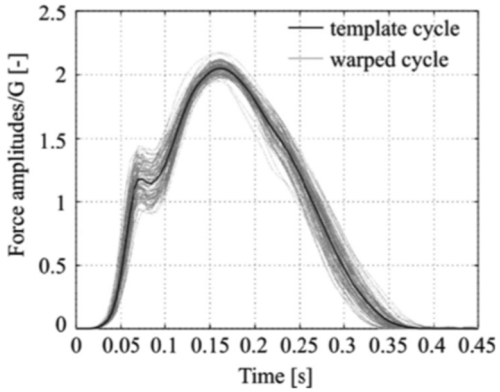

Figure 5.1.5 Determination of the template cycle and the warped cycles [47].

The general shape of the template load cycle can be modelled as the sum of four Gaussian functions:

$$Z(t) = \sum_{i=1}^{4} A_i e^{-(t-t_i)^2/2\delta_i^2} \qquad \text{Eq. 5.1.2}$$

where:

- $Z(t)$ is the curve fit;
- A_i is the height of the *j*th Gaussian peak;
- t_i is the position of the center of the peak;

– δ_i controls the width of the Gaussian bell functions.

If the complete duration of a load cycle is determined by the parameter τ_k and it is computed, along with the three previous parameters, through the stochastic method presented in [47] on the base of data collected in the database of measurements, then the computed force time history is very representative of a real signal.

For example, in Figure 5.1.6, a comparison between a measured and a synthetic force-time signal is showed. The similarity is excellent if compared with the synthetic signal produced through the Fourier method in Figure 5.1.4.

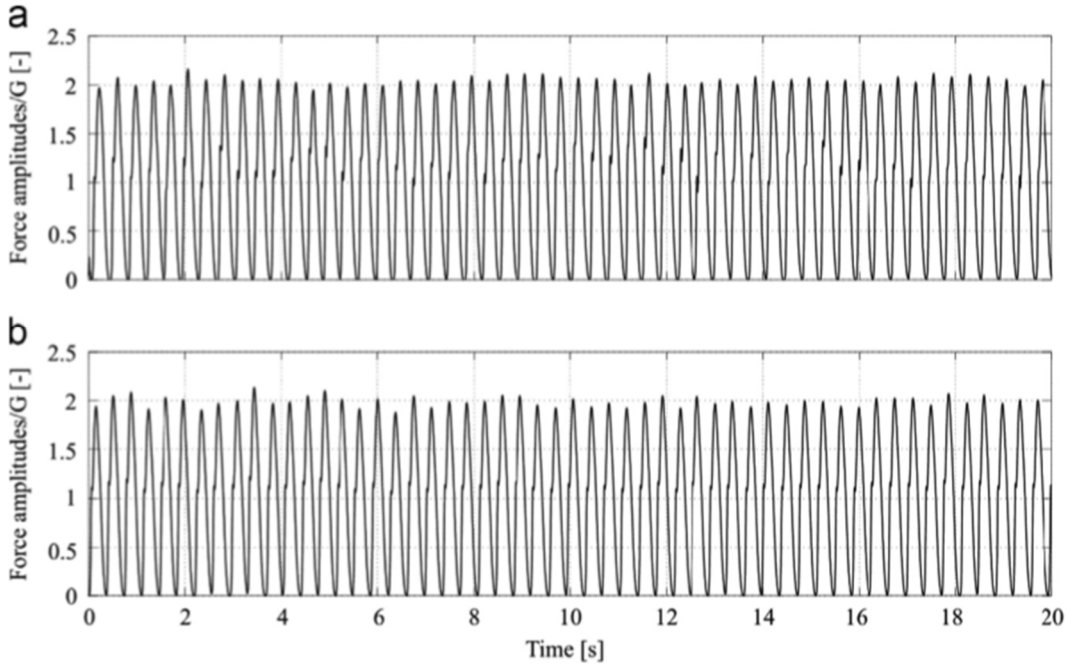

Figure 5.1.6 a) Measured and b) an example of synthetic force-time series [47].

Moreover, using this procedure it is possible to consider also the typical variability of human induced loads. The quoted numerical generator can produce synthetic signals that are slightly different even if the input parameters, step frequency and duration of the run, are identical. In particular, Figure 5.1.7 illustrates two examples of force signals generated using twice the numerical generator with the same values for input parameters: $f_r = 3Hz$ and $T = 40\ s$.

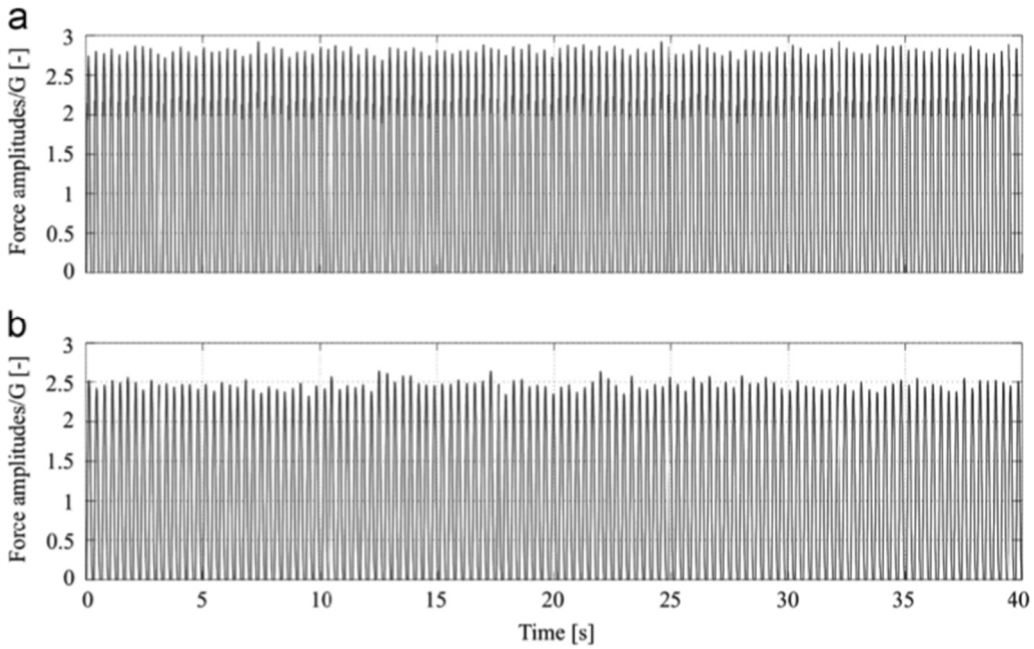

Figure 5.1.7 Examples of artificial force signals generated for the same set of input parameters $f_r = 3Hz$ and $T = 40\ s$ [47].

5.1.1 Arising issues

In the previous section, the determination of the running pedestrian load time-history through the use of mathematical model has been presented. However, this cannot be exploited for the execution of a dynamic analysis.

The load time history realized by a running pedestrian (provided by Professor Racic) has been obtained through the numerical generator described in [47] and reported in Figure 5.1.8.

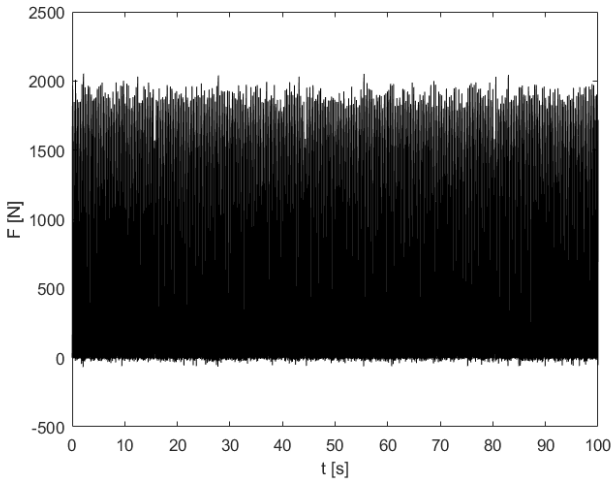

Figure 5.1.8 Force time history produced by a running pedestrian during an interval of 100s [47].

It represents the time evolution of the pedestrian induced load which step frequency coincides with the natural frequency of the structure that we aim to study for a duration of 100 s. The sampling frequency is 200 Hz.

Nevertheless, the load time history is not directly usable in the format of a force function of the time to perform a transient dynamic analysis in Ansys Mechanical APDL.

In fact, to this aim, Ansys requests the application of loads through the realization of "load steps" in which loads must be defined according to precise rules of the Ansys programming language.

In addition, considering the length of the footbridge under consideration, only few seconds of the load time history are necessary.

But, if these two problems could be solved in a relatively not complex manner, in our case, the plot of the time history represents the evolution of the load only as function of the time, losing sight of it moves in space.

Thus, wishing to represent correctly the load, it is necessary to consider the pedestrian displacement along the structure as the second time-dependent variable of the excitation. This variable is closely linked to the realization of load cycles, since the application point of the load changes each time that a load cycle is completed. If a load cycle is identified by a contact phase and a flying one, the distance between two consecutive application points of the load is exactly the pedestrian stride length.

But, since the footbridge has been modeled through finite elements, loads need to be applied only on mesh nodes. In effect, in order to define concentrated loads, Ansys requests to specify their application points by asking the identification number of the interested node. In the case under consideration, it is not necessarily said that the pedestrian has a stride length

coincident with the distance between two consecutive nodes, nor his trajectory coincident with a mesh-line.
For these reasons, each time that the application point needs to be updated, i. e. at the end of each load cycle, the pedestrian vertical induced load needs to be transformed in equivalent nodal forces and bending moments to be applied on nearer nodes.
Finally, all the operations just described might lead to provide an input file readable by Ansys Mechanical APDL. Thus, other than solving the mechanical problem, it is necessary to write the input file at the same time.
The generation of the Matlab code RealRun1 has been useful for both the objectives. Ideas and driving principles for its realization are presented in the next section. Details about the code and its implementation are specified in APPENDIX C

5.2 RealRun1

The numerical code RealRun1, written in Matlab language, generates a text file according to code rules of Ansys Mechanical APDL for the execution of a transient analysis of the footbridge loaded by a running pedestrian. The code is adopted for the generation of nodal loads time histories induced by one running person, based on a load time history of the type presented in section 5.1.
The fundamental assumption made for the creation of the code was to consider the possibility for the runner to move only on a rectilinear trajectory parallel to the axis of the footbridge but not necessarily coincident with one of the mesh lines along the y-direction. Thus, the forces transmitted by the runner must be transformed in nodal loads, and their variability, both in time and in space, must be considered.
The most important conceptual steps at the base of the code can be synthetized in the following list:

1. Definition of some fundamental variables:
    a. Time duration to cross the footbridge;
    b. Coefficients α e β of the Rayleigh damping;
    c. Coordinates of the first contact point on the footbridge;
    d. The array of nodes, not part of the mesh grid of the deck, to be neglected-in the determination of mesh nodes potentially affected by the trajectory. To illustrate the case in which a deck node will be neglected, the reader can refer to Figure 5.2.1. The reason of this choice is related to the fact that shape functions are adapted for use on regular mesh grids only (point 6);

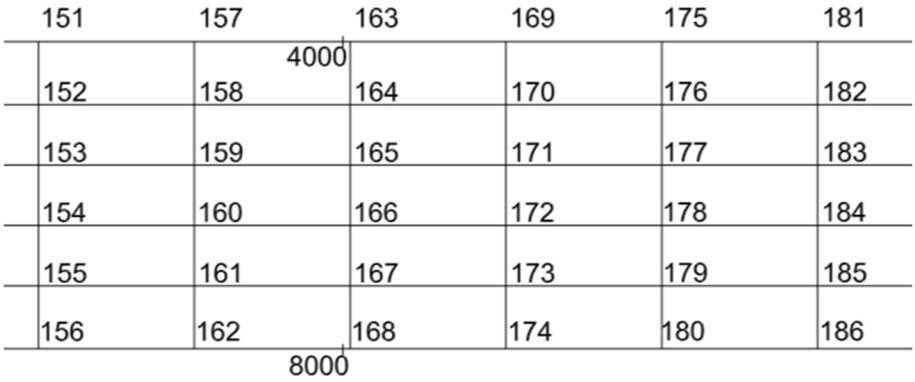

Figure 5.2.1 Some nodes belonging to the mesh grid of the deck are reported. Nodes 4000 and 8000, where H-shaped struts elements link to the deck, will not be loaded by nodal loads obtained through the use of shape functions.

2. Reading of the load time history that must be post-processed;
3. Reading of the Ansys input file to store deck nodes and their coordinates;
4. Generation of the needed load time history from the read load time history of the load as a function of the computed time to cross the footbridge and correction of oscillations of the load during the time in which cycles should represent the flying phase (Figure 5.2.2);

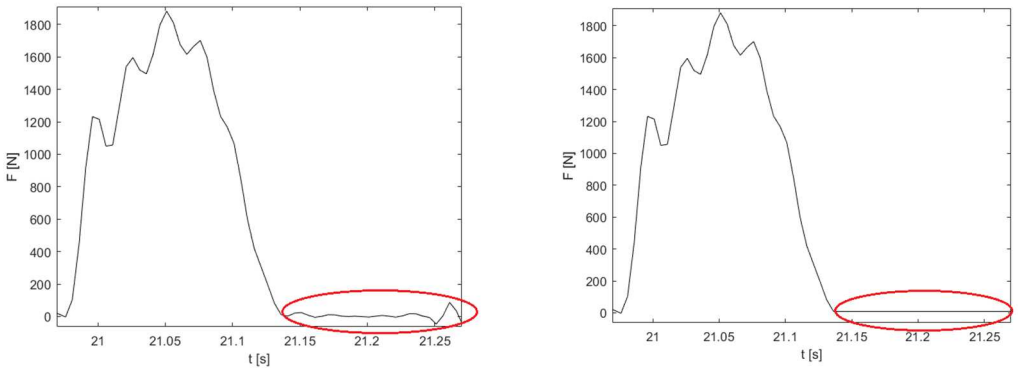

a) b)

Figure 5.2.2 Result of the load time history post-processing for one load cycle: a) before post-processing; b) after post-processing.

5. Definition of coordinates of points along the trajectory and determination of coordinates of nodes over which the load will be transmitted at each load cycle;
6. Computation, for each load cycle, of nodal loads using shape functions to transform the runner induced pedestrian load. The shape functions transform the vertical load induced by the pedestrian in a generic point of the deck in vertical forces and bending moments in longitudinal and transversal direction, acting on the nodes of

the mesh grid surrounding the vertical load. Figure 5.2.3 describes the way the shape functions are exploited.

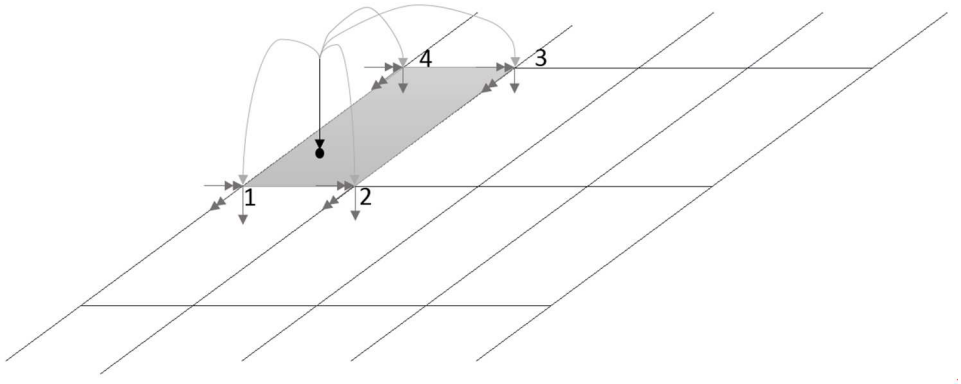

Figure 5.2.3 Graphical representations of the role of shape functions: the vertical load induced from the pedestrian is transformed in nodal forces and bending moments.

7. Generation of the text file readable by Ansys for the execution of a transient analysis under the varying nodal loads.

The chart flow for the generation of the code is presented in Figure 5.2.4, but reader can refer to APPENDIX E for a detailed explanation of the code.

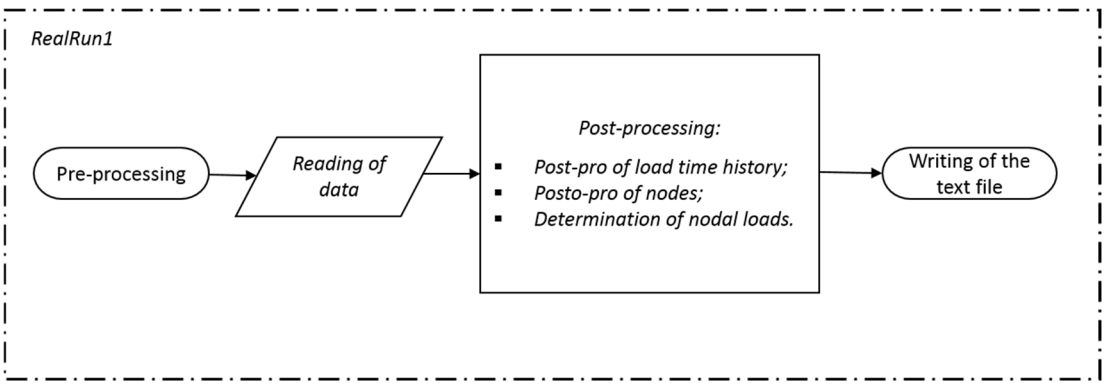

Figure 5.2.4 Chart Flow for the generation of RealRun1.

5.3 Walking pedestrians' analysis: Hivoss

According to Hivoss guidelines and as already stated in CHAPTER 4, to verify the degree of comfort of a footbridge subjected to walking pedestrians induced loads it is necessary to establish the following features of the problem:

– Traffic Class or people density over the footbridge;

- Natural frequencies of the footbridge in the interval $1.25 \leq f_i \leq 2.5\ Hz$, coincident with the interval of human walking frequencies;
- Damping coefficient;
- Prescribed comfort Class or maximum accepted acceleration;

The verification procedure prescribes "*the application of the following harmonic load:*

$$p(t) = Pcos(2\pi f_s t)n'\psi \qquad \text{Eq. 5.3.1}$$

uniformly distributed on the footbridge deck and applied with positive direction according to the considered modal deformed shape. Modulus of the distributed load is determined on the base of the geometry of the structure and of the following variables:

- P is the component of the force due to a single pedestrian with a walking step frequency f_s;
- f_s is the step frequency, which is assumed equal to the footbridge natural frequency under consideration;
- n' is the equivalent number of pedestrians on the loaded surface S;
- S is the area of the loaded surface;
- Ψ is the reduction coefficient taking into account the probability that the footfall frequency approaches the critical range of natural frequencies under consideration.

All the quoted parameters have been determined and reported in Table 5.3.1. The length and width of the footbridge deck are $L = 54\ m$ and $B = 3.15\ m$.

One of the aims of this master thesis is to compare the results obtained through the Hivoss guidelines and those coming from a finer model for the running pedestrian case. Thus, the design check for walking pedestrians is done only for the lower degree of excitation. The check was done to have an insight on the footbridge behavior and confirm that only arches oscillations are caused by this load case.

The TC1 traffic class was chosen and the reduction coefficient was determined for the second eigenfrequency of the structure, laying in the critical interval of frequencies.

Table 5.3.1 Parameters for the computation of the modulus of the distributed load according to Hivoss guidelines for the case of walking pedestrians.

Parameter	Value	Note	References
$\boldsymbol{d}\ [{}^{\boldsymbol{P}}/_{\boldsymbol{m^2}}]$	0.088	Traffic class 1 $d = \frac{n}{BL}$, with $n = 15$	Section 4.4, Figure 4.4.1
$\boldsymbol{f_i = f_s}\ [\boldsymbol{Hz}]$	1.56	Eigenfrequency in the critical interval	APPENDIX D, Table D. 3, eigenmode 2 with pretension
$\boldsymbol{\xi}$ [%]	0.4	Damping coefficient	Section 4.5, Figure 4.5.1
$\boldsymbol{a_{max}}\ [{}^{\boldsymbol{m}}/_{\boldsymbol{s^2}}]$	0.50	Comfort Class 1	Section 4.4, Figure 4.4.2
$\boldsymbol{P}\ [\boldsymbol{N}]$	280		Section 4.6, Table 4.6.1
$\boldsymbol{n'}[{}^{\boldsymbol{1}}/_{\boldsymbol{m^2}}]$	0.0155	$n' = \frac{10.8\sqrt{\xi n}}{S}$	Section 4.6
$\boldsymbol{S}\ [\boldsymbol{m^2}]$	170.1	$S = BL$	
$\boldsymbol{\Psi}\ [-]$	0.68	Linear interpolation	Section 4.6 Figure 4.6.4

Considering the data listed in Table 5.3.1, the modulus of the harmonic distributed load generated by walking pedestrians according to Hivoss guidelines is equal to:

$$p = 2.96\ {}^{N}/_{m^2} \qquad \text{Eq. 5.3.2}$$

Concentrated vertical loads applied on each node of the deck grid were computed by multiplying the distributed load by the influence area of each node. Moreover, as suggested by Hivoss guidelines, the positive direction of loads follows the modal shape. Figure 5.3.1 shows the considered modal shape and the applied loads.

Modal shape of f_s $[Hz]$	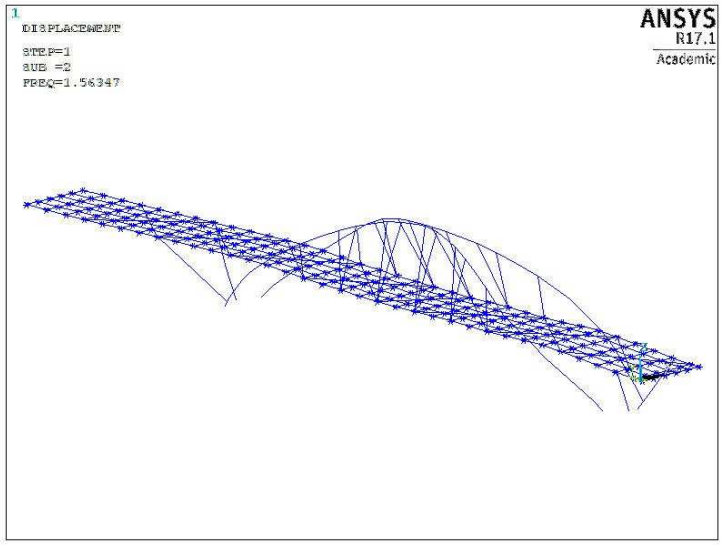 a)
Load distribution	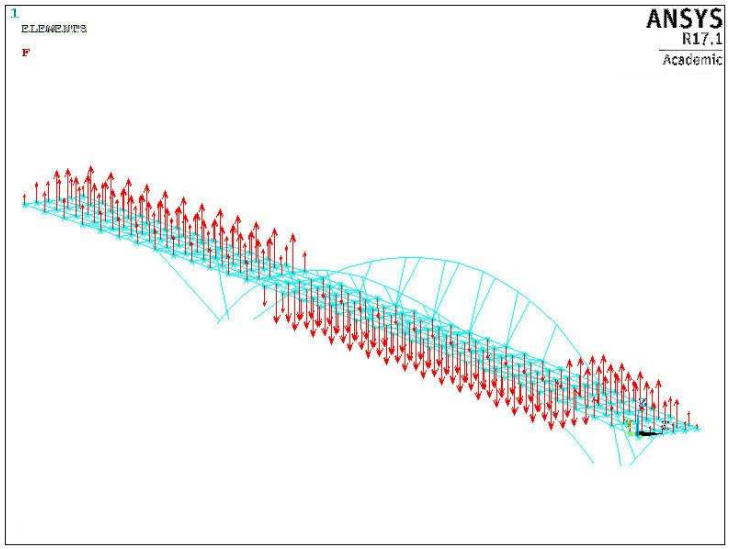 b)

Figure 5.3.1 Analyzed modal shape of the footbridge in a); applied distributed load in b) for the case of the walking pedestrians.

5.3.1 Harmonic analysis: results

According to Hivoss guidelines, a harmonic load must be applied to the structure. A harmonic analysis is performed with Ansys and this procedure can be implemented through three different numerical methods:

- Full;
- Reduced;
- Mode Superposition.

Each of the three methods have the following restrictions:

- All loads must vary sinusoidally in time;
- All loads must have the same frequency;
- Non linearities are not considered;
- Transient effects are not computed.

The simplest method is the Full. Even if it is the most precise among the others, it is the most time consuming. In fact, displacements and stresses are computed step by step using the entire system of matrices without any approximation.

As for the method to establish load frequencies, Ansys asks the analyst to choose for an interval of frequencies where a given number of computations will be done. In this work, 100 subdivisions were adopted. The interval including the frequency at study is

$$0.5 \leq f_s \leq 2.5\ Hz \qquad \text{Eq. 5.3.3}$$

Since the evaluation of the comfort level is established as a function of the maximum limit acceleration and Ansys only gives displacements as output for this kind of analysis, it is necessary to compute accelerations from displacements.

Let us consider the simplest case of a single degree of freedom system (SDOF) subjected to a harmonic force. The equation of motion describing its behavior is:

$$\ddot{x}(t) + 2\xi\omega_1\dot{x}(t) + \omega_1^2 x(t) = \frac{F}{k}\omega_1^2 sin(\omega t) \qquad \text{Eq. 5.3.4}$$

Where:

- $x(t)$; $\dot{x}(t)$; $\ddot{x}(t)$ are displacement, velocity and acceleration;
- ξ is the damping coefficient;
- ω_1 is the fundamental frequency of the SDOF;
- F is the amplitude of the force;
- k is the stiffness of the SDOF;
- ω is the frequency of the harmonic force.

The solution of the equation is:

$$x(t) = e^{-\xi\omega_1 t}\left(Acos\left(\omega_1 t\sqrt{1-\xi^2}\right) + Bsen\left(\omega_1 t\sqrt{1-\xi^2}\right)\right) + x_p(t) \qquad \text{Eq. 5.3.5}$$

Ansys give displacements of the steady state response, here represented by $x_p(t)$, the particular integral of the equation of motion. For the SDOF system under harmonic load it can be analytically determined:

$$x_p(t) = \frac{F}{k}N(\beta)sen(\omega t - \phi) \qquad \text{Eq. 5.3.6}$$

Where:

- $N(\beta) = {1}/{\sqrt{(1-\beta^2)^2 + 4\xi^2\beta^2}}$ is the magnification factor;
- $\beta = {\omega}/{\omega_1}$ is the frequency ratio;
- $\phi = arctg({2\xi\beta}/{1-\beta^2})$ is the phase angle between the excitation and the response.

Thus, to obtain the acceleration of the system, it is sufficient to differentiate two times the analytical expression obtained for displacements with respect to time. Acceleration is directly proportional to displacements and to the square of the exciting frequency:

$$\ddot{x}_p(t) = -\omega^2 \frac{F}{k} N(\beta) sen(\omega t - \phi) = -\omega^2 x_p(t) \qquad \text{Eq. 5.3.7}$$

This result can be extended to multi degrees of freedom (MDOF) systems and this procedure will be used to obtain maximum accelerations of nodes in the footbridge at study.
The analytical solution $\ddot{x}_p(t)$ is obtained using the complex exponential and is the projection, on the imaginary axis of the "Argand's plane", of the complete complex solution:

$$\ddot{x}_p(t) = -\omega^2 \frac{F}{k} N(\beta) e^{i(\omega t - \phi)} \qquad \text{Eq. 5.3.8}$$

Following this solution approach, Ansys gives displacements results in term of real, imaginary and amplitude values of displacements. Nodes for which results are analyzed are showed in Figure 5.3.2.

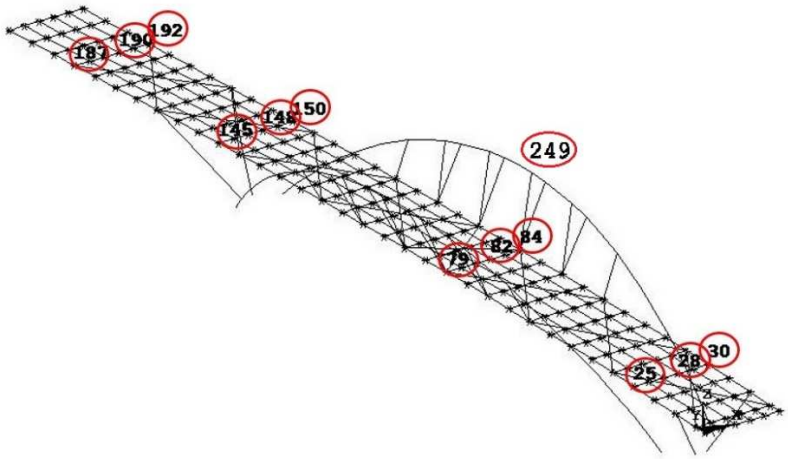

Figure 5.3.2 Position of nodes for which results have been extracted and reported here.

Except for the smallest span, three nodes are chosen for every span of the footbridge.
The resonance curves of amplitude, real and imaginary values for node 84, the one that presents the largest displacements in vertical direction on the deck, are reported in Figure 5.3.3.
The peak of the response appears when the load has the frequency equal to the eigenfrequency of the structure. The maximum value of displacements is equal to 1.2 *mm*. As

a consequence, the acceleration generated by the passage of 15 people over the footbridge according to Hivoss is equal to 0.115 $^{m}/_{s^2}$.

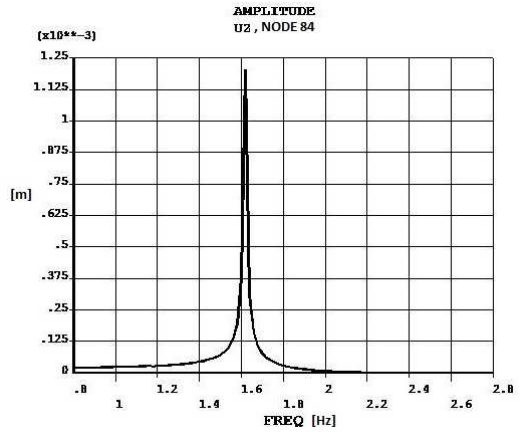

a)

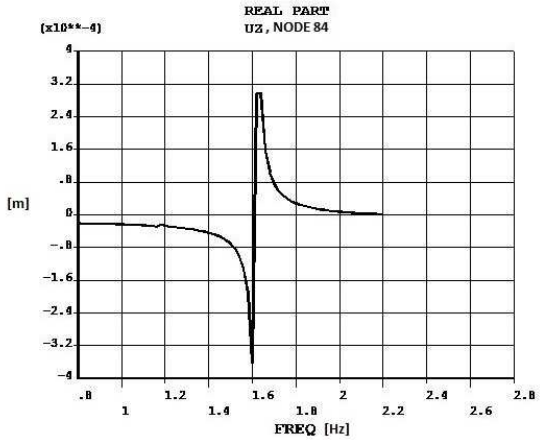

b)

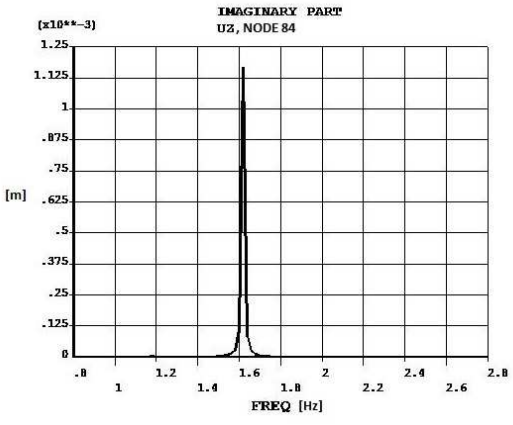

c)

Figure 5.3.3 Resonance curves of a) amplitude, b) real part and c) imaginary part of vertical displacements for node 84 for the case of walking pedestrians.

The numerical values of displacements and accelerations computed for each of the studied nodes are listed in Table 5.3.2 and Figure 5.3.4.

Table 5.3.2 Numerical values of amplitude, real part, imaginary part and acceleration for each of the considered nodes after verification according to Hivoss guidelines for the walking pedestrians case.

Node	$max\{\lvert z(f)\rvert\}$ $[mm]$	$R(z(f))$ $[mm]$	$Im(z(f))$ $[mm]$	$max\{\lvert \ddot{z}(f)\rvert\}$ $[^{m}/_{s^2}]$
25	0.12	-0.02	-0.12	0.01
28	0.11	-0.02	-0.10	0.01
30	0.12	-0.03	-0.12	0.01
79	1.16	0.29	1.12	0.11
82	1.20	0.29	1.17	0.11
84	1.21	0.30	1.17	0.11
145	0.16	-0.03	-0.16	0.01
148	0.15	-0.02	-0.15	0.01
150	0.16	-0.03	-0.15	0.01
187	0.07	0.05	-0.04	0.006
190	0.07	0.06.	-0.03	0.006
192	0.06	0.06	-0.02.	0.006

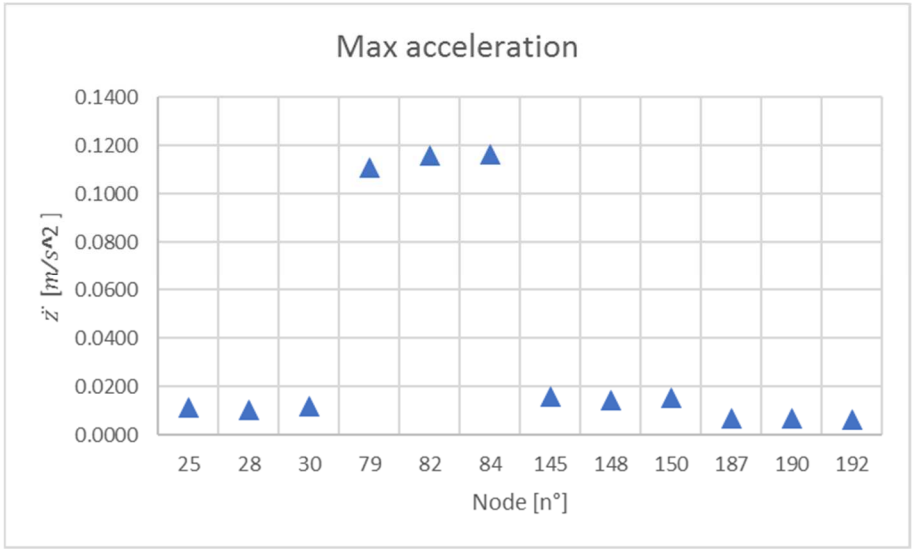

Figure 5.3.4 Graphical representation of accelerations reported in Table 5.3.2 for all the considered nodes.

Since the acceleration limit for comfort class 1 is equal to 0.5 $^{m}/_{s^2}$, Figure 5.3.4 shows that for the TC1 (Traffic Class 1=15 people) the degree of comfort is acceptable whichever the position of the receiver is on the deck of the footbridge.
Accelerations of nodes 79, 82, 84, on the central span, are one order of magnitude larger than the ones of other spans nodes.

However, given the modal shape, it was important to study the behavior of arches. Resonance curves of amplitude in x and z direction for the arch top node 249 (in Figure 5.3.2) displacements are reported in Figure 5.3.5, while numerical values of displacements and accelerations maxima are given in Table 5.3.3.

As foreseeable from the modal shape, arches present largest displacements and, as consequence, greatest accelerations. Normally, these values are not object of verifications, since pedestrians could not feel arches vibrations if they walk on the deck. However, for the given dimensions of the structure, these values of displacements and accelerations can be perceived by view, considered as a sign of safety lack and could generate some fatigue problem.

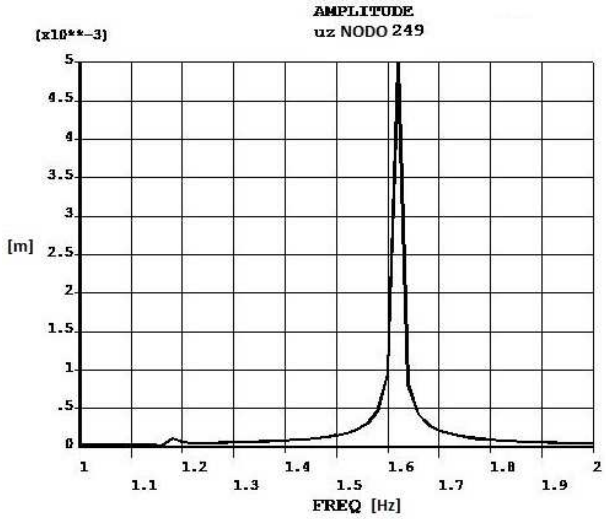

a)

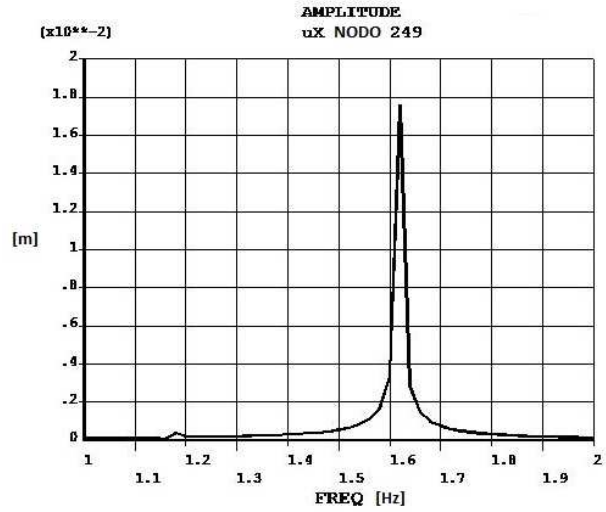

b)

Figure 5.3.5 Amplitude response curves for a) x-displacements and b) z-displacements of arch top node 249 in the load case of walking pedestrians.

Table 5.3.3 Numerical values of amplitude, real part, imaginary part and acceleration for the arch top node 249 after verification according to Hivoss guidelines for the walking pedestrians case.

Node	**Direction**	$max\{\lvert z(f)\rvert\}$ $[mm]$	$R(z(f))$ $[mm]$	$Im(z(f))$ $[mm]$	$max\{\lvert \ddot{z}(f)\rvert\}$ $[^{m}/_{s^2}]$
249	*z*	4.99	-2.10	-4.52	0.47
249	*x*	17.6	-7.39	-16.0	1.68

5.4 Running pedestrian' analysis: Hivoss

The procedure of Hivoss guidelines for the running pedestrians differs from that for walking pedestrians first for the critical interval of frequencies:

$$1.9 \leq f_s \leq 3.5\ Hz \qquad \text{Eq. 5.4.1}$$

For this reason, the chosen frequency has been $f_s = 3.38\ Hz$.
A second difference concerns the load model. In the case of the running pedestrian it is expressly specified that "*the proposed load model is a single load P(t,v) which is moving across the bridge with a certain velocity v of the joggers…The single load P(t,v) calculates to:*

$$P(t,v) = Pcos(2\pi f_s t)n'\psi \qquad \text{Eq. 5.4.2}$$

Parameters related to this load model and used in the harmonic analysis according to Hivoss guidelines are presented in Table 5.4.1. The number of runners has been taken equal to one to compare results coming from this analysis with the ones obtained using RealRun1.

Table 5.4.1 Parameters for the computation of the modulus of the concentrated load according to Hivoss guidelines for the case of ne running pedestrian.

Parameter	Value	Note	References
$\boldsymbol{d}\ [^{\boldsymbol{P}}/_{\boldsymbol{m^2}}]$	5.8 E-3	Traffic class 1 $d = \frac{n}{BL}$, with $n = 1$	Section 4.4, Figure 4.4.1
$\boldsymbol{f_i = f_s}\ [\boldsymbol{Hz}]$	3.38	Eigenfrequency in the critical interval	APPENDIX D, Table D. 3, eigenmode 4 with pretension
$\boldsymbol{\xi}$ [%]	0.4	Damping coefficient	Section 4.5, Figure 4.5.1
$\boldsymbol{a_{max}}\ [^{\boldsymbol{m}}/_{\boldsymbol{s^2}}]$	0.50	Comfort Class 1	Section 4.4, Figure 4.4.2
$\boldsymbol{P}\ [\boldsymbol{N}]$	1250		Section 4.6,
$\boldsymbol{n'}[^{\boldsymbol{1}}/_{\boldsymbol{m^2}}]$	1	$n' = n$	Section 4.6
$\boldsymbol{S}\ [\boldsymbol{m^2}]$	170.1	$S = BL$	
$\boldsymbol{\Psi}\ [-]$	0.15	Linear interpolation	Section 4.6 Figure 4.6.5

The computed value of the load modulus is:

$$P = 187.5\ N \qquad \text{Eq. 5.4.3}$$

Figure 5.4.1 shows the modal shape considered and the load applied at node 73, where the modal shape presents larger displacements.

Deformed shape of f_s $[Hz]$	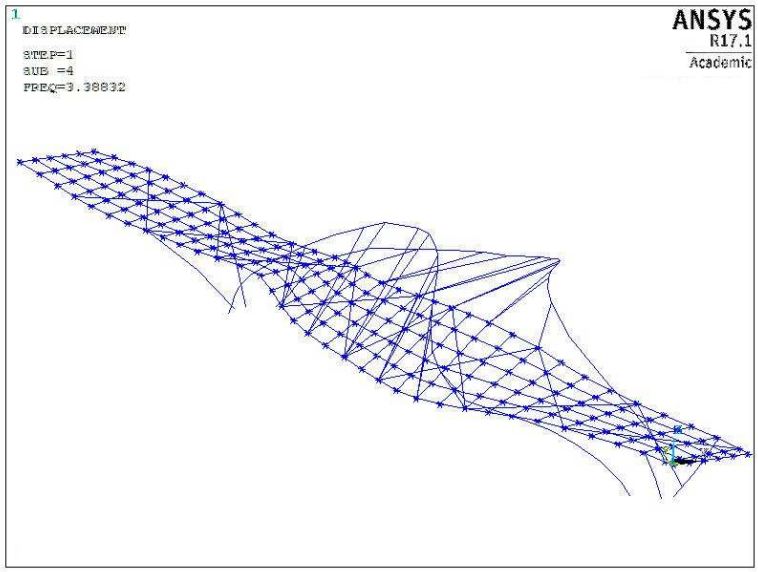 a)
Distribution of loads	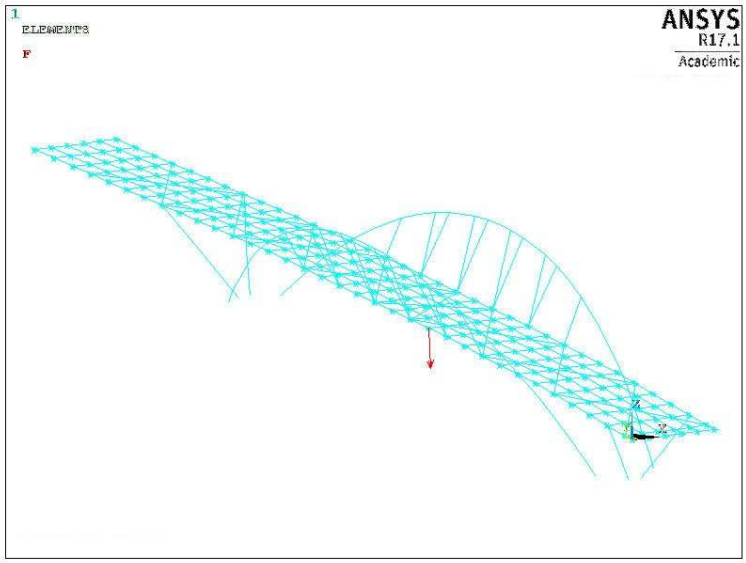 b)

Figure 5.4.1 Analyzed modal shape of the footbridge in a); applied concentrated load in b) for the case of the running pedestrian

5.4.1 Harmonic analysis: results

The solution is given in terms of amplitude and real and imaginary parts of displacements. The resonance curves are for the node 84 (Figure 5.4.2).

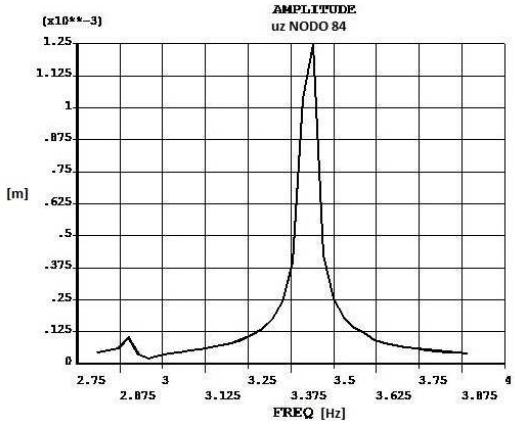

a)

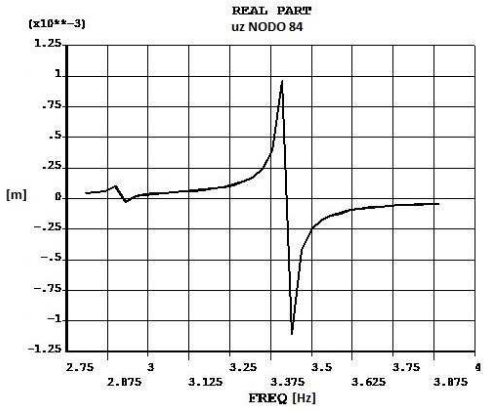

b)

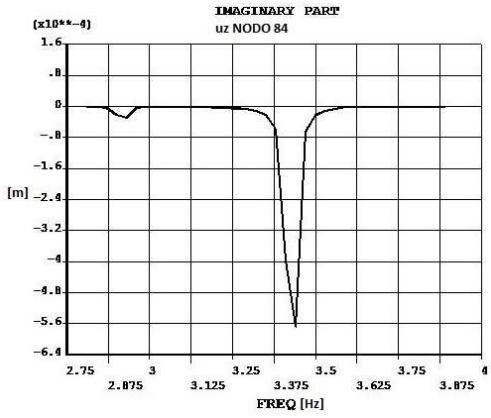

c)

Figure 5.4.2 Resonance curves of a) amplitude, b) real part and c) imaginary part of vertical displacements for node 84 for the case of running pedestrian.

The vertical displacement of node 84, equal to 1.3 *mm* is comparable to the one caused by the walking pedestrians load case (1.2 *mm*). However, the frequency considered for the running pedestrian is larger than for the quoted load case and the computed acceleration is equal to

0.562 $^{m}/_{s^2}$, above the threshold for ensuring comfort class 1 (0.5 $^{m}/_{s^2}$) but still guarantying a medium degree of comfort ($a_{max} < 1\,^{m}/_{s^2}$)

Numerical values of amplitude of displacements as well as their real and imaginary part for important nodes are reported in Table 5.4.2.

Table 5.4.2 Numerical values of amplitude, real part, imaginary part and acceleration for each of the considered nodes after verification according to Hivoss guidelines for the running pedestrian case.

Node	$\boldsymbol{max}\{\lvert \boldsymbol{z}(\boldsymbol{f})\rvert\}$ $[\boldsymbol{mm}]$	$\boldsymbol{R}(\boldsymbol{z}(\boldsymbol{f}))$ $[\boldsymbol{mm}]$	$\boldsymbol{Im}(\boldsymbol{z}(\boldsymbol{f}))$ $[\boldsymbol{mm}]$	$\boldsymbol{max}\{\lvert \ddot{\boldsymbol{z}}(\boldsymbol{f})\rvert\}[^{\boldsymbol{m}}/_{\boldsymbol{s}^2}]$
25	0.21	0.18	0.09	0.09
28	0.03	-0.03	-0.02	0.01
30	0.21	-0.18	-0.09	0.09
79	1.27	1.12	0.59	0.57
82	0.24	-0.22	-0.10	0.10
84	1.25	-1.11	-0.57	0.56
145	0.07	0.07	0.03	0.03
148	0.007	0.007	0.002	0.003
150	0.04	-0.04	-0.02	0.02
187	0.18	0.15	0.10	0.08
190	0.16	-0.15	-0.05	0.07
192	0.37	-0.34	-0.15	0.16

The graphical representation of nodes accelerations (Figure 5.4.3) highlights that at edge nodes they are larger than at mid transversal nodes, especially for nodes of the central span (79, 82, 84). This indicates a *torsional effect* induced by the presence of the harmonic load.
In fact, even if accelerations are represented in amplitude and without sign, the presence of a torsional effect can be confirmed taking into account the modal shape.

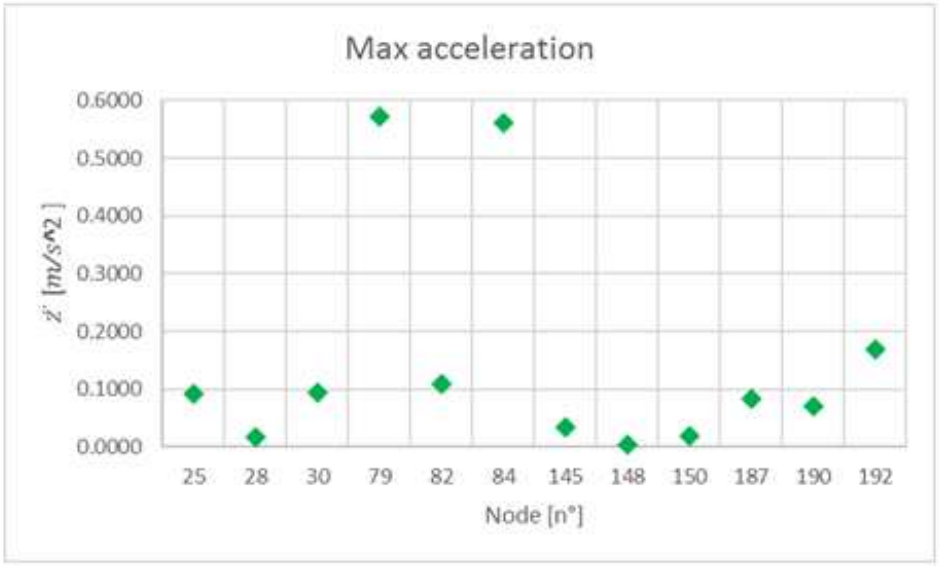

Figure 5.4.3 Graphical representation of accelerations reported in Table 5.4.2 for all the considered nodes

For the modal shape at $f = 3.38\,Hz$, arches seem to have displacements comparable to the ones of the deck (Figure 5.4.1 a)) and a check was made to verify their behavior. The analyzed node is the arch top node (n° 249), the same studied for the walking people load case. In Figure 5.4.4, the amplitude resonance curves are reported for x and z displacements.
Displacements in x-direction are one order of magnitude larger then z-displacements ($10^{-3}\ vs\ 10^{-4}\ m$). However, both are smaller than displacements that appear in the case of 15 walking pedestrians. The maximum value of displacements, in both cases is in x-directions but, in this load case, has a value of 2.21 mm (Table 5.4.3), while for the previous case it was of 17.6 mm (Table 5.3.3).

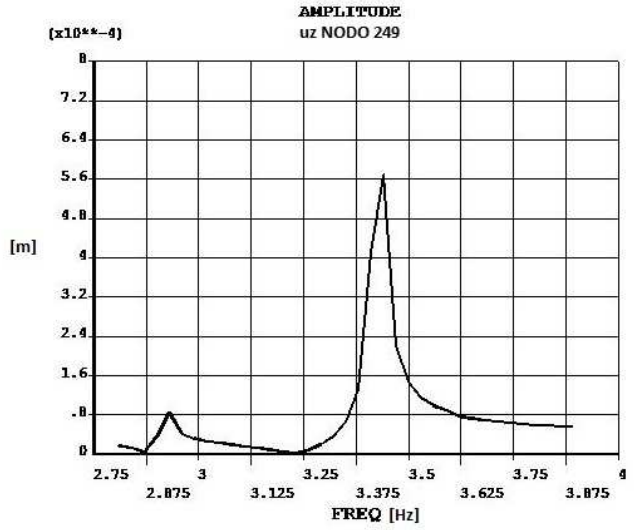

a)

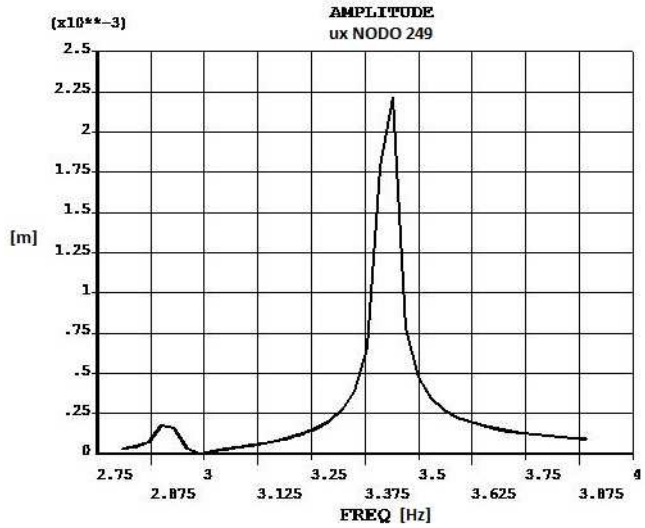

b)

Figure 5.4.4 Amplitude response curves for a) x-displacements and b) z-displacements of arch top node 249 in the load case of running pedestrian.

Table 5.4.3 Numerical values of amplitude, real part, imaginary part and acceleration for the arch top node 249 after verification according to Hivoss guidelines for the running pedestrian case.

Node	**Direction**	$max\{\lvert z(f)\rvert\}$ $[mm]$	$R(z(f))$ $[mm]$	$Im(z(f))$ $[mm]$	$max\{\lvert \ddot{z}(f)\rvert\}$ $[m/s^2]$
249	*z*	0.57	-0.51	-0.24	0.25
249	*x*	2.21	-1.98	-0.99	0.99

Even if the frequency at study in this case is two times larger than the one studied in the case of walking pedestrians and, thus, square of the related angular frequency is four times larger, accelerations of the arch top node 249 are smaller. The threshold of Comfort Class 2, that defines a medium degree of comfort with a maximum value of $1\ ^{m}/_{s^2}$ for accelerations, is not exceeded (Table 5.4.3). Anyway, we should remember that verifications according to Hivoss should be done only for the deck, i.e. the vibration path from where pedestrians could perceive vibrations.

5.5 Running Human's analysis: RealRun1

As already stated in section 5.2, the Matlab code RealRun1 produces a text file that Ansys uses as input to execute a transient analysis. The pedestrian load varies in time inside each load cycle and its application point must be updated at each contact between a foot of the runner and the footbridge. These features of the load are illustrated in Figure 5.5.1

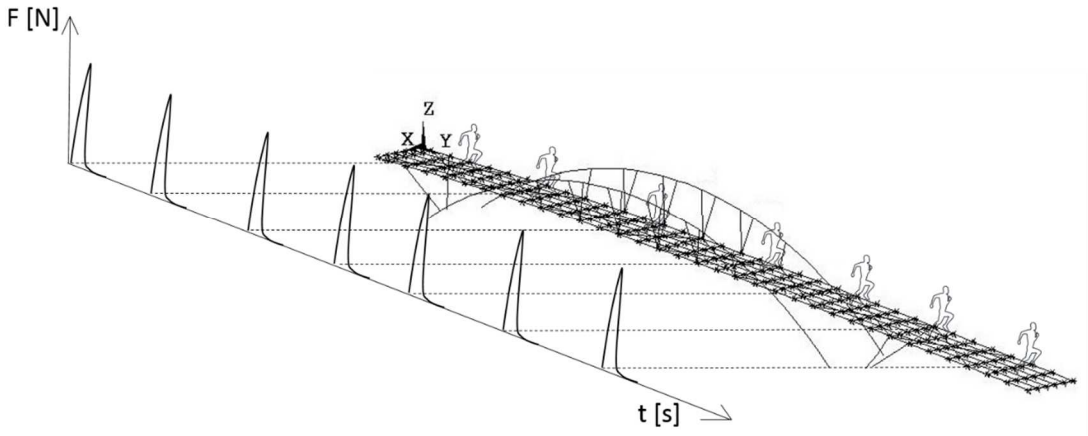

Figure 5.5.1 Graphical representation of the running pedestrian in some points of the footbridge and representation of relative induced forces. Load changes in time but also the point of application is modified.

In order to make comparison between results obtained through RealRun1 and by applying prescriptions of HiVoSS guidelines, the frequency of contact between runner's feet and structure has been considered equal to $3.38\ Hz$. Considering the discussion in CHAPTER 1, the contact frequency between the runner and the structure can be related to a speed of the runner equal to 6.6 $^{m}/_{s}$ and, since the length of the footbridge deck is $L = 54\ m$, the time needed to cross the bridge is $8.17\ s$. Thus, only the first 28 load cycles were extracted from the initial load time history (Figure 5.5.2).
The first contact point of the pedestrian with the footbridge has the coordinates reported in Table 5.5.1, given in the global reference system showed in Figure 5.5.1.

Table 5.5.1 First contact point between the running pedestrian and the footbridge.

$x\ [m]$	$y\ [m]$	$z\ [m]$
0.2	0.1	0

They were chosen in order to have almost the same position of the harmonic load used in the harmonic analysis once in the complete run. A shift of 0.2 m from the edge of the deck seems to be reasonable to represent the runner behavior. The pedestrian's trajectory is rectilinear, and the coordinate x remains constant during the whole time history.

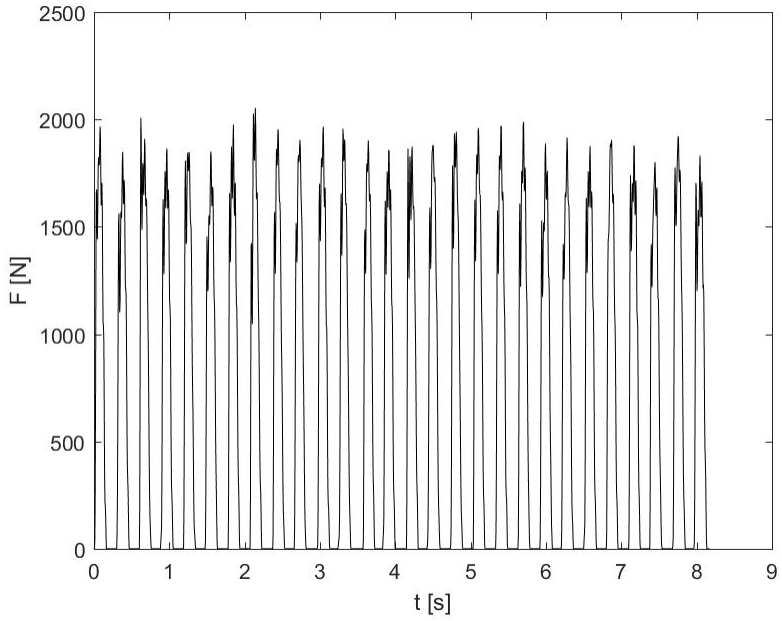

Figure 5.5.2 Load cycles needed to cross the entire length of the footbridge.

The Rayleigh damping model described in section 1.5 is adopted. To compute the $\boldsymbol{\alpha}$ and $\boldsymbol{\beta}$ damping parameters, it was assumed that, for the first eigenfrequency of the studied model in the case of applied pretension ($f_1 = 1.13\ Hz$, refer to Table D. 3 in APPENDIX D) and the studied eigenfrequency ($f_4 = 3.38\ Hz$), the damping coefficient ξ was equal to the one prescribed by Hivoss guidelines, i.e. 0.4 %. Using Eq.1.5.8 and Eq. 1.5.9, the computed values of $\boldsymbol{\alpha}$ and $\boldsymbol{\beta}$ are:

$$\begin{cases} \boldsymbol{\alpha} = 0.0425 \\ \boldsymbol{\beta} = 0.0283 \cdot 10^{-2} \end{cases} \qquad \text{Eq. 5.5.1}$$

The numerical integration of equations of motion has been done in Ansys exploiting the Newmark's method based on the constant average acceleration algorithm. The coefficients of the algorithm to be input to Ansys are reported in Table 5.5.2.

Table 5.5.2 Values of Newmark's parameters

Newmark's Parameter	Value
$\boldsymbol{\alpha}$	$\frac{1}{4}$
$\boldsymbol{\delta}$	$\frac{1}{2}$
$\boldsymbol{\gamma}$	0

Parameters α and δ ensure the constant average acceleration while γ ensures the unconditional stability of the numerical method. Details about the numerical method used are reported in APPENDIX C, section C.3, synthetized from the *Theory Reference Manual* of Ansys [3].

Ansys computes results of the transient analyses in terms of displacements, accelerations, velocities, stresses, strains, etc. as function of the time but, only for the first two quantities, an analysis is done in section 5.5.1. Moreover, spectra of accelerations have been computed through a Matlab postprocessing of Ansys output data and reported too.

5.5.1 Transient analysis: results

In this section, we will consider the whole-time history of displacements and accelerations of some deck nodes since it is not possible to know *a priori* in which time interval the maxima values to which refer for a design case will be. So, plots and values of displacements and accelerations directly extracted from Ansys for a time period of 25 seconds will be reported. The time in which the pedestrian is on the footbridge goes from zero to 8.17 s while, until 25 s, the footbridge is unloaded and in free vibration regime.

Since results indicate that the behavior of nodes belonging to the same transversal line of the mesh grid is similar, only nodes 25, 79, 145 and 187 will be analyzed (Figure 5.5.3).

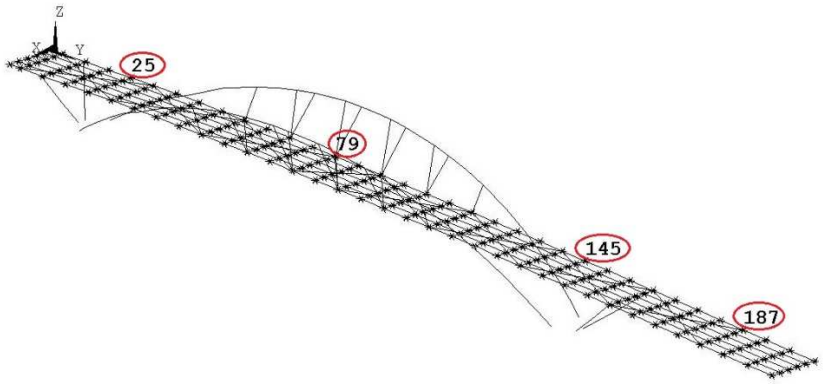

Figure 5.5.3 Position of nodes for which transient analysis results have been extracted and reported.

Figure 5.5.4 and Figure 5.5.5 a), show displacements and accelerations of node 25, on the second span in the direction of the run. The largest oscillations are in the first part of the signal because the pedestrian is still on the second span until 1.38 *s*.

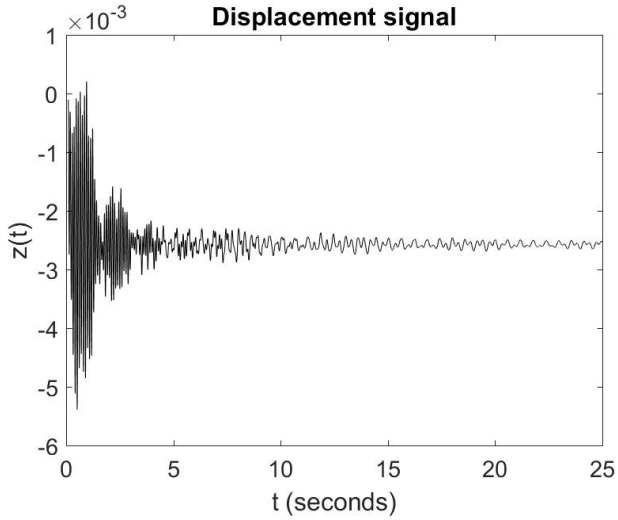

Figure 5.5.4 Z-displacement time history of node 25.

The related accelerations show a similar behavior. The moment in which both displacements and accelerations become negligible is around 4.9 *s*, i.e. when the pedestrian completely crosses span number 3.

The spectrum of accelerations is reported in Figure 5.5.5 b). It shows that the response of the structure is more affected by frequencies far beyond the pedestrian running frequency and it allows to justify the low amplitude of displacements: resonance is not activated.

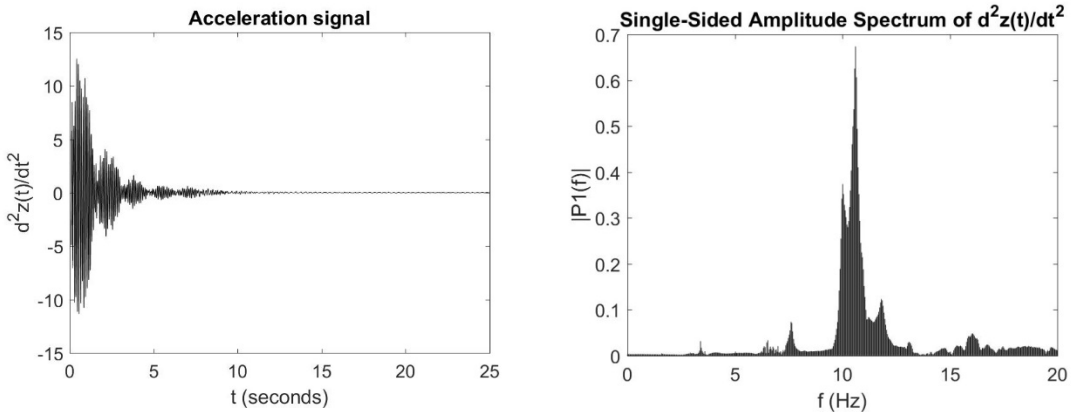

a) b)

Figure 5.5.5 a) Z-acceleration time history of node 25 and b) related spectrum.

On the other hand, node 79, that is located on the third and central span, is subjected to vibrations with an almost constant amplitude during the entire passage over the footbridge. They start to damp out, slowly, only after the pedestrian leaves the footbridge at $t \approx 8\ s$ (Figure 5.5.6).

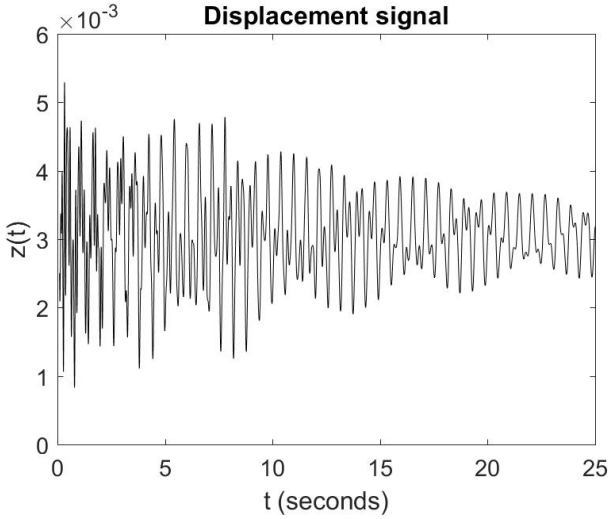

Figure 5.5.6 Z-displacement time history of node 79.

On the contrary, accelerations show a behavior similar to that of node 25 (Figure 5.5.7 a)). This may indicate that the central span is more sensitive to excitations lying in the two first spans rather than in the fourth and fifth span. In this case, the spectrum of accelerations (Figure 5.5.7 b)) shows contributions by a larger number of frequencies with a high level of noise.

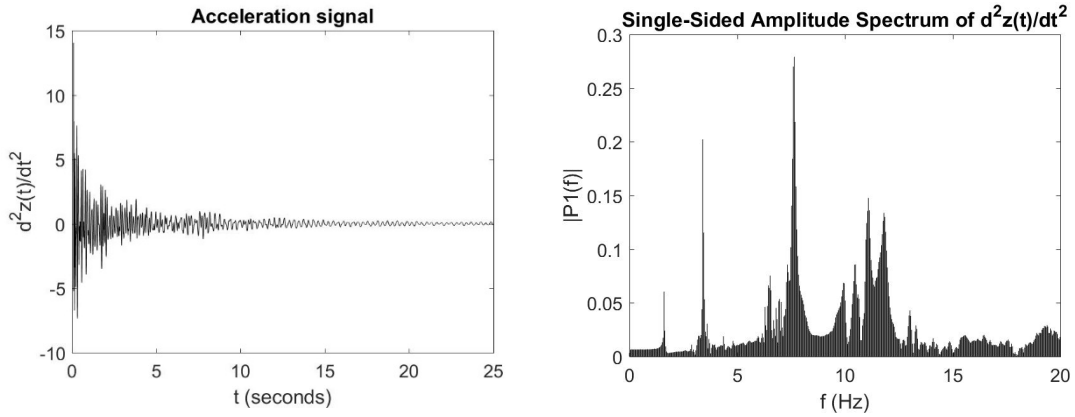

a) b)

Figure 5.5.7 a) Z-acceleration time history of node 79 and b) related spectrum.

Node 145 represents a middle way between node 25 and node 79. Located on the fourth span, it is subjected to the influence of the load since the first load steps and especially, when the runner is on the central span ($1.38\ s \leq t \leq 4.9\ s$ in Figure 5.5.8).

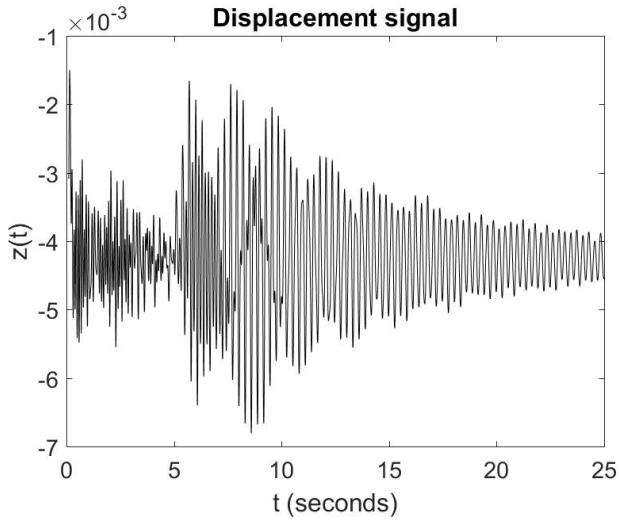

Figure 5.5.8 Z-displacement time history of node 145.

But, when the runner starts to be on span 4, in correspondence of $t > 4.9\ s$, displacements and accelerations (Figure 5.5.9 a)) increase. The behavior of this span will be affected also when the pedestrian is on the fifth and last span and, also in this case, damping acts slowly. With respect to other spans, the spectrum (Figure 5.5.9 b)) shows a decrease in the values of frequencies influencing the structure response but, at the same time, the noise is reduced and this explains why the acceleration signal has a more regular shape.

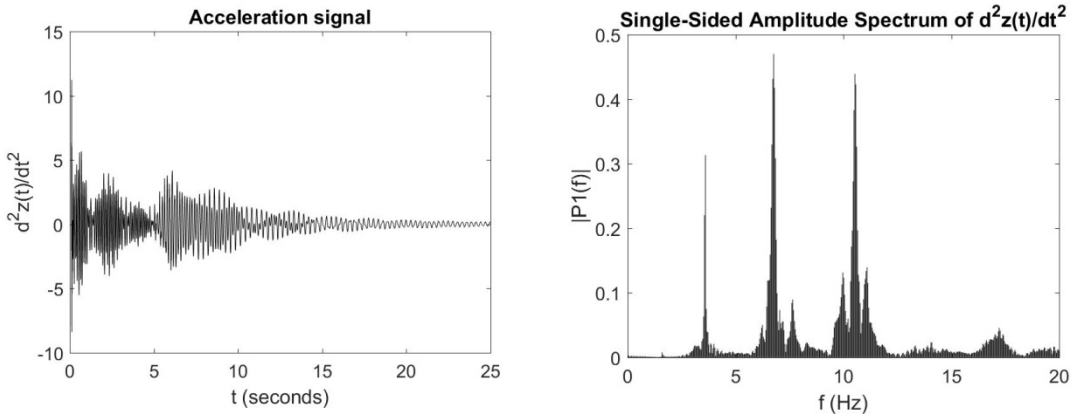

a) b)

Figure 5.5.9 a) Z-acceleration time history of node 145 and b) related spectrum.

Finally, in Figure 5.5.10 and Figure 5.5.11 a), displacements and accelerations of node 187 increase considerably when, after 7 s, the pedestrian starts to cross the last span, where node 187 is located. The amplification of the response is clearly induced by the resonance of the structure with the running frequency of the pedestrian. Spectrum of accelerations (Figure 5.5.11 b)) shows that the run excites not only the first harmonic but also the second ($f_1 = 3{,}38\ Hz$ and $f_2 = 3{,}76\ Hz$). The resonance situation is accompanied by a low level of noise and regular signals of both displacements and oscillations.

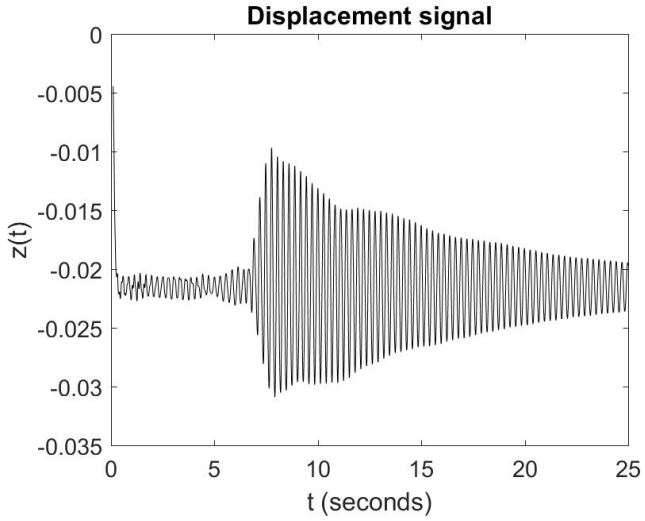

Figure 5.5.10 Z-displacement time history of node 187.

In addition, among the others, the span where node 187 is located was the one that had the largest values of vertical displacements under static condition. Now, other than having the largest values of oscillations amplitude (about 20 mm), it also has the slowest damping process.

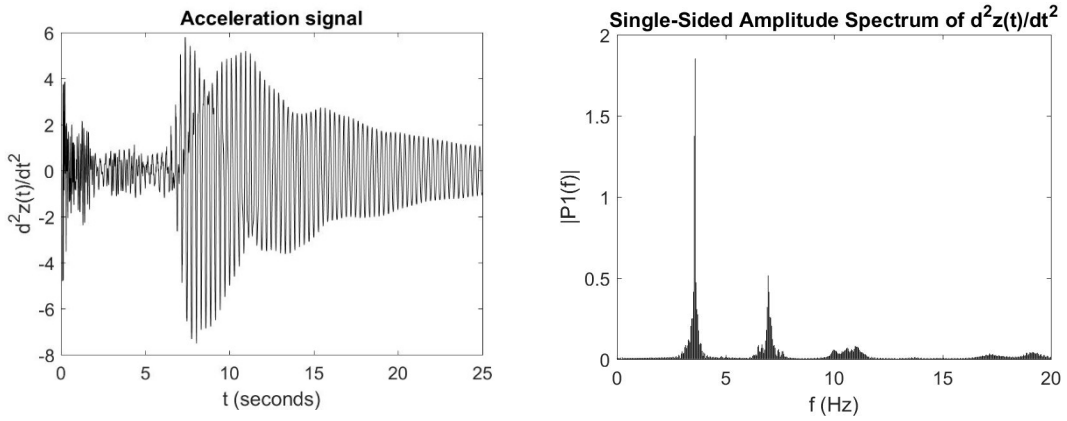

a) b)

Figure 5.5.11 a) Z-acceleration time history of node 187 and b) related spectrum.

For the sake of completeness, Table 5.5.3 reports values of interest in the design phase of the footbridge for all nodes studied with the HiVoSS procedure. Column 2 lists maxima values of amplitude reached during the time interval of interest. Columns 3, 4, 5 e 6 list values of the maximum and minimum of the cycle with maximum amplitude and time at which they take place. Finally, maxima values of accelerations are in column 7, followed by the related time of realization.

Table 5.5.3 Extreme values from the transient analysis.

Node	$Ampl_{max}$ $[mm]$	t_{max} $cycle\ [s]$	z_{max} $[mm]$	t_{min} $cycle\ [s]$	z_{min} $[mm]$	$\ddot{z}_{max}$ $[m/s^2]$	$t(a_{max})$ $[s]$
25	5.33	0.57	-0.09	0.52	-5.42	12.28	0.52
28	9.14	0.47	1.51	0.52	-7.63	16.94	0.42
30	5.13	0.47	-0.15	0.52	-5.27	12.26	0.43
79	4.20	0.33	5.32	0.28	1.12	8.13	0.29
82	5.91	0.33	4.78	0.28	-1.13	17.29	0.11
84	3.50	0.34	5.04	0.27	1.55	7.17	0.11
145	4.63	8.23	-2.08	8.31	-6.71	5.66	0.60
148	4.49	8.22	-3.50	8.31	-7.99	3.93	5.94
150	4.14	8.21	-2.19	8.31	-6.33	4.14	0.65
187	20.42	7.75	-10.44	7.92	-30.86	-7.75	8.05
190	21.38	7.78	-11.95	7.91	-33.34	6.07	8.19
192	20.51	7.79	-11.84	7.91	-32.36	7.48	8.46

In general, accelerations appear rather large. Even though maxima of displacements stay around 5 *mm*, except for the case of the node on the last span, a running pedestrian induces

these displacements in a small amount of time and, as a consequence, he generates accelerations that may cause high discomfort for walking or standing pedestrians

Largest amplitudes of oscillations are related to spectra showing frequencies near to the eigenfrequency of the structure. But, if this is quite normal, results would induce to think that HiVoSS provide a design method that does not maximize the effects of a running pedestrian. In fact, accelerations obtained through the two methods show an excessive discrepancy: considering vertical accelerations of all nodes listed in Table 5.4.2 and Table 5.5.3, the mean value determined through HiVoSS was around 0.15 $^{m}/_{s^2}$ with a peak of 0.57 $^{m}/_{s^2}$ while, using RealRun1, the mean value was around 7.8 $^{m}/_{s^2}$ with a peak of 17.29 $^{m}/_{s^2}$.

HiVoSS guidelines suggest to place the harmonic load on the node having the maximum vertical displacement for the considered modal deformed shape. However, according to the study we have just done, through RealRun1, rather we see that maxima oscillations in terms of displacements appear in correspondence of the node that had the largest vertical displacements under the static load case (node 187) and that HiVoSS always underestimate accelerations by an order of magnitude. In addition to that, in correspondence of the more oscillating node, the structure tends to synchronize with both the first and the second harmonic of the load.

Before drawing final conclusions in next CHAPTER 6, however, it must be specified that the load model provided by *Racic and Morin* [47] assumes that the runner should not perceive vibrations so that the absence of human structure interactions can be guaranteed. In effect, perception of vibrations may induce the pedestrian to change his running rhythm and, in the worst cases, to stop and wait for vibrations to end.

So, it would be worthwhile to check if the highlighted correlation between larger vertical displacements in the static load case and greater risk of resonance for a given node can be confirmed by applying RealRun1 on existing structures with problems of vibrations induced by running pedestrians.

CHAPTER 6
CONCLUSIONS

The case study adopted in this work was a steel footbridge that will be built in Louvain La Neuve (Belgium) in a few months. Two inclined arches with linearly variable L-shaped section sustain through ten steel tendons per side the central span of the deck, made of five spans.

This work aimed to compare the results of dynamic analysis done on the footbridge using two different models for a running pedestrian. At the same time, since footbridge at study is still at the design stage, it also aimed to provide a first judgment about its degree of serviceability under this load case.

The reason to choose the running pedestrian load case was guided by the fact that today there are still not clear indications to handle the case of running pedestrian even if a growing concern among engineers from all around the world is arising due to the increasing number of urban running competitions.

To reach the objectives of the thesis, several steps were necessary.

The starting point was the creation of the finite element model of the footbridge, through the software Ansys Mechanical APDL.

The following step was to conduct preliminary analyses to determine which parameters influenced the structure response and which zones could be affected by possible variations of the geometry. In particular, two more models of the footbridge with slight differences in the arches geometry were studied: Model1, with vertical arches having hollow rectangular cross sections, and Model2, with inclined arches but still hollow rectangular cross section.

A comparison of results coming from the static analysis of the three models subjected only to the gravity load showed that change in the geometry of arches has the most important influence on the series of nodes in the span where tendons are applied. In particular, the mid-span node vertical displacement of Model1 and Model3 (the model representing the real

structure, with inclined arches having L-shaped section) are respectively the 77.58% and 54.54% larger than displacements of Model2.

However, even if spans adjacent to the central span, that is also the most influenced, are only slightly affected by variations of arches geometry, these modifications have the same impact on vertical displacements of nodes belonging to other spans (around +7% for the second and the fourth span and +1.75% for first and fifth span). The fifth span has the mid-node vertical displacement around 20 mm in the three cases, almost equal to the ratio of deflection limit under permanent loads $l/_{500} = 22.8\ mm$.

In addition, one more important effect of geometry modifications was on displacements of arches nodes. In fact, it was observed that the inclination of arches and the modification of their section increased both vertical and horizontal displacements. In the three cases, arches displaced towards the deck in the vertical direction, with a maximum displacement of the arches top nodes of 7.32 mm for Model3. The behavior was different for Model1 and Model2 or Model3 in the horizontal direction. In Model1, arches deformed reducing the distance between each other by 2.58 mm per side while, in the second case, the distance was increased with a maximum value of 15 mm per side for Model3.

The determination of pretension to be applied on suspension tendons allowed to make a step further and demonstrated that this kind of load must be non-uniformly applied for all the Models in order to generate almost zero vertical displacements when the structure is subjected to gravity load only. So, values of pretension were reported and the tendons length variations needed to apply pretension have a minimum and a maximum value of 3.1 mm and 4 mm respectively.

Then, a modal analysis, needed also to select the eigenfrequencies for the dynamic analysis checks, showed that modifications in arches geometry affected the values of eigenfrequencies more than pretension. In fact, making a comparison among the three models, Model1 and Model2 showed larger but similar values of eigenfrequencies and different modal shapes with respect to Model3. This has lower values of eigenfrequencies and a larger number of modal shapes involving arches vibrations. On the other hand, considering for each model the comparison between the cases of pretension applied or not, eigenfrequencies do not change for the two situations even though modal shapes are slightly different.

In the three cases, vertical, torsional and lateral mode shapes were present. For the model representing the footbridge as designed, the mode having eigenfrequency equal to 3.38 Hz was a torsional eigenmode and it was chosen for the running pedestrian load case verifications. According to the European HiVoSS (Human induced Vibrations on Steel Structures) guidelines, this value of eigenfrequency is in the interval of frequencies that can be excited by running pedestrians ($1.9\ Hz \leq f_i \leq 3.5\ Hz$).

Results, obtained through the harmonic analysis done applying the harmonic load model of the guidelines for a single running pedestrian crossing the footbridge at a speed of 6.66 $^{m}/_{s}$, indicate amplitude values of vertical displacements ranging from 0.1 mm to 1.21 mm for nodes laying on one of the two longitudinal beams of the deck. However, the parameter to establish the serviceability limit state of a footbridge, according to HiVoSS, is the maximum value of acceleration and, in this case, it is reached in one node of the central span with a value of 0.562 $^{m}/_{s^2}$, that is above the threshold ensuring the best comfort class (0.5 $^{m}/_{s^2}$) but still guarantying a medium degree of comfort ($a_{max} < 1\,^{m}/_{s^2}$). Also, according to the harmonic analysis, the arch top node shows a critical behavior in the horizontal direction, where displacements and accelerations amplitudes are around one order of magnitude larger than in z-direction (2.21 mm versus 0.57 mm and 0.99 $^{m}/_{s^2}$ versus 0.25 $^{m}/_{s^2}$) even being under alarming thresholds.

Finally, these results were compared to the ones obtained from a transient analysis where the running pedestrian is described as a moving and time-varying load according to the load model proposed by *Racic and Morin* [47] and produced through the Matlab code RealRun1, specifically written for the purpose.

To this aim, some challenges have been overpassed. In particular, the load time history provided by Professor Vitomir Racic, was post-processed to take into account the position of the pedestrian moving over the footbridge as a second time-dependent variable of the load. Each load cycle, in fact, represents a load applied at a different contact point between the runner and the structure. Moreover, the need to consider that contact points do not necessarily coincides with mesh nodes, pushed us to find a method for the determination of nodal vertical forces and bending moments applicable on nodes surrounding the load application point Results were extracted for the same nodes analyzed in the harmonic analysis even though, in this case, the computed maxima values of nodal vertical accelerations were always larger, reaching peaks of 17.0 $^{m}/_{s^2}$. Moreover, transient analysis results showed that, differently from the results of the harmonic analysis, maxima displacements were not reached on the central span of the footbridge but on the span that under the static load case presented largest displacements, i.e. span number 5.

In addition, another comparison between the two load models can be performed in terms of the spectrum of accelerations of the node laying on the last span. Other than the first harmonic, also the second harmonic characterizing the human induced load gives an important contribution to the structure response.

These two aspects are not taken into account by the HiVoSS guidelines that, first, suggest placing the harmonic load on the node that has the largest value of vertical displacement in the considered modal shape and, second, recommend the computation of a reduction factor

involved in the load modulus determination taking into account only the first harmonic of the load.

Thus, conclusions that can be drawn from the work could refer both to the structure design and to the proposed load model for running pedestrian's verifications.

As for the design, arches excessive displacements and oscillations in the horizontal direction, along with the several modal shapes involving arches eigenmodes, may suggest that a small modification could be proposed. From the static analysis, the best compromise is represented by Model2, with hollow rectangular sections for arches. Should this be not sufficient or not acceptable from the aesthetic point of view, then maintaining the L-shaped cross sections could be possible by linking arches through transversal elements. In that case, it would be necessary moving the support of the arches at the Lauzelle-side nearer to the edge support and maintain the same arch curvatures to have a sufficient clear height above the deck. Moreover, this solution could also have a positive effect on the fifth span, whose length could be reduced due to the shift of the supports represented by the H-shaped struts elements.

For the load model, it must be specified that the one provided by *Racic and Morin* [47] assumes that the runner should not perceive vibrations so that the absence of human structure interactions can be guaranteed. However, it would be worthwhile to check if the highlighted correlation between larger vertical displacements in the static load case and greater risk of resonance for a given node can be confirmed by applying RealRun1 on existing structures with problems of vibrations induced by running pedestrians. This behavior may depend on the fact that the involved modal shapes have large displacements in the same span of the deformed shape under gravity loads, but this is not necessarily the same for other footbridges. Moreover, it could also be useful to investigate the effect of the second harmonic of the load.

Further developments of RealRun1 could be represented by the possibility to generate input files simulating the run of several pedestrians on different trajectories or with different velocities Furthermore, an approach like the one we used in this work could became the solution to design problems existing today. The design process could be integrated by transient simulations that will became more and more less expensive with the tools that will be available in next years.

Finally, it is clear that the load model proposed by HiVoSS must be improved. A more solid load model is needed, for example, to take into account peaks of accelerations due to impulsive effects at the moment in which the pedestrian touches for the first time the deck, or to consider more than one harmonic of the load.

Bibliography and references

[1] A. McRobie, G. Morgenthal, Risk management-induced dynamics of foobridges, in: *Proceedings of the Intrnational Conference on the Design and Dynamic Behaviour of Footbridges*, Paris, France, November 20-22, 2002.

[2] Ansys Mechanical APDL Documentation, Command Reference, Release 17.1.

[3] Ansys Mechanical APDL Documentation, Theory Reference, Chapter 15, Analysis Procedure, Release 17.1.

[4] C. Cremona, Dynamic investigations of the Solferino footbridge, Proceedings of IOMAC '09, 3rd International Operational Modal Analysis Conference, 4th-6th May 2009, Portonovo, Italy.

[5] C. L. Vaughan, B. L. Davis, J. C. O' Connor, *Dynamics of Human Gait*, Kiboho Publishers, Cape Town, 1999.

[6] DETAN ROD SYSTEMS,Technical Product Information, *Halfen GMBH,* Germany, 2016.

[7] Dictionary of Medical Terms, 4th edition, A&C Black, London, 2004

[8] E. Ayyappa, Words about words: the terminology of human walking, bipedal exchange, *Monograph of the American Academy of Orthotists and Prosthetists Gait Society*, Vol. 1-2, American Academy of Orthotists and Prosthetists Gait Society, Alexandria, USA, 1994.

[9] E. Lai, M.G. Mulas, Uncoupled approaches for walking-induced vertical vibration of a lively footbridge, *Insights and Innovation in Structural Engineering, Mechanics and Computation*, Zingoni (Ed.), Taylor & Francis Group, London, 2016.

[10] E. Lai, Pedestrian-Footbridge Dynamic Interaction: Uncoupled Analysis Using a MSD Model, PhD Thesis, Department of Civil and Environmental Engineering, Doctoral School in Structural, Seismic and Geotechnical Engineering, Politecnico di Milano, Milano, Italy, 2016

[11] E. P. Hanavan, *A Mathematical Model of the Human Body*, Aerospace Medical Research Laboratory, Wright-Petterson Air Force Base, Ohio, USA, 1964.

[12] E. T. Ingólfsson, C. T. Georgakis, J. Jönsson, Pedestrian-induced lateral vibrations of footbridges: A literature review, *Engineering Structures* 45 (2012) 21-52.

[13] F. Perotti, Dipense del corso di Dynamics of Structures, Politecnico di Milano, A. A. 2014-2015.

[14] F. W. Galbraith, M. V. Barton, Ground loading from footsteps, *Journal of the Acoustic Society of America* 48 (5) (1970) 1288-1292.

[15] G.P. Tilly, D. W. Cullington, R. Eyre, Dynamic behaviour of footbridges, IABSE Surveys S-26/84, IABSE Periodica, No 2/84, 1984, pp 13-24.

[16] H. Grundmann, H. Kreuzinger, M. Schneider, Dynamic calculations of footbridges, *Bauingenieur* 68 (1993) 215-225 (in German).

[17] H. Hatze, A mathematical Model for the computational determination of parameter values of anthropometric segments, *Journal of Biomechanics* 13 (1980)833-843.

[18] H. Vernet, A critical analysis of the Passerelle Léopold-Sédar-Senghor, Paris, Proceedings of Bridge Engineering (2) (2011), University of Bath, Bath, UK.

[19] Harris Cyril M., "Shock & Vibration Handbook, Third Edition", McGraw-Hill, Inc.,New York, 1988

[20] HiVoSS (Human induced Vibrations of Steel Structures): *Design of Footbridges – Background document*, 2008.

[21] HiVoSS (Human induced Vibrations of Steel Structures): *Design of Footbridges – Guideline*, 2008.

[22] HiVoSS (Human induced Vibrations of Steel Structures): Design of Footbridges – Guideline, 2008.

[23] HiVoSS (Human induced Vibrations of Steel Structures): Design of Footbridges – Background document, 2008.

[24] ISO, *Bases for Design of Structures-Serviceability of Buildings Against Vibrations*, ISO 10137, International Standardization Organization, Geneva, Switzerland, 1992.

[25] J. E. Wheeler, Prediction and control of pedestrian induced vibration in footbridges, *ASCE Journal of the Structural Division* 108 (ST9) (1982) 2045-2065.

[26] J. L. Humar, *Dynamics of Structures*, CRC Press/Balkema, Leiden, 2012.

[27] J. M. W. Brownjohn, A. Pavic, P. Omenzetter, A spectral density approach for modelling continuous vertical forces on pedestrian structures due t walking, *Canadian Journal of Civil Engineering* 31 (2004) 65-77.

[28] J. Perry, *Gait Analysis: Normal and Pathological Function*, Thorofare, New York, 1992.

[29] J.M.W. Brownjohn, P.-Q. Xia, Dynamic assessment of curved cable-stayed bridge by model updating, *Journal of Strucutral Engineering* 126 (2) (2000) 252-260.

[30] L. Romano, Vibrazione delle Strutture da ponte, Genova, 2012.

[31] M. G. Gardner-Morse, D. R. Huston, Modal identification of cable-stayed pedestrian bridge, *Journal of Structural Engineering* 119 (11) (1993) 3384-3404.

[32] M. Mimram. Passerelle Solférino Paris. Basel, Berlin, Boston: Birkhäuser, F. Fromonot, 2001.

[33] N. Messenger, Moving the human machine: understanding the mechanical characteristics of normal human walking, *Physics Education* 29 (1994) 352-357.

[34] P. Dallard, A. J. Fitzpatrick, A. Flint, S. Le Bourva, A. Low, R.M. Ridsdill-Smith, M. Willford, The London Millennium Footbridge, *Structural Engineer* 79 (22) (2001) 17-33.

[35] P. Dallard, T. Fitzpatrick, A. Flint, A. Low, R. Ridsdill-Smith, The Millennium Bridge, London: problems and solutions, *The Structural Engineer* 79 (8) (2001) 15-17.

[36] P. Dallard, T. Fitzpatrick, A. Flint, A. Low, R. Ridsdill-Smith, M. Willford, M. Roche, London Millennium Bridge: pedestrian-induced lateral vibration, *Journal of Bridge Engineering* 6 (6) (2001) 412-417.

[37] P. E. Eriksson, Vibration of Low-Frequency Floors- Dynamic Forces and Response Prediction, PhD Thesis, Unit for Dynamics in Design, Chalmers University of Technology, Göteborg, Sweden, 1994.

[38] R. W. Clough, J. Penzien, *Dynamics of Structures,* McGraw-Hill, New York, 1993.

[39] S. Živanović, A. Pavic, P. Reynolds, Probability-based prediction of multi-mode vibratio response to walking excitation, *Engineering Structures* 29 (2007) 942-954.

[40] S. Živanović, A. Pavic, P. Reynolds, Vibration serviceability of footbridges under human-induced excitation: a literature review, *Journal of Sound and Vibration* 279 (2005) 1-74.

[41] T. Fitzpatrick, P. Dallard, S. Le Bourva, A. Low, R. Ridsdill-Smith, M. Willford, Linking London: The Millennium Bridge, Report No L12.32, The Royal Academy of Engineering, London, June 2001.

[42] T. Fitzpatrick, R. R. Ridsdill-Smith, Stabilising the London Millennium Bridge, Ingenia (August 2001) 18-22.

[43] T. Kärnä, Damping methods to mitigate wind-induced vibrations, Rakenteiden Mekaniikka (*Journal of Structural Mechanics*) 42, (1) (2009) 38-47.

[44] T. P. Andriacchi, J. A. Ogle, J.O. Galante, Walking speed as basis for normal and abnormal gait measurements, *Journal of Biomechanics* 10 (1977) 261-268.

[45] T. S. Keller, A. M. Weisberger, J. L. Ray, S. S. Hasan, R. G. Shiavi, D. M. Spengler, Relationship between vertical ground reaction force and speed during walking, slow jogging and running, *Clinicla Biomechanics* 11 (1996) 253-259.

[46] V. Racic, A. Pavic, J. M. W. Brownjohn, Experimental identification and analytical modelling of human walking forces: Literature review, *Journal of Sound and Vibration* 326 (2009) 1-49.

[47] V. Racic, J.B. Morin, Data-driven modelling of vertical dynamic excitation of bridges induced by people running, *Mechanical Systems and Signal Processing* 43 (2014) 153-170.

[48] V. T. Inman, H. J. Ralston, F. Todd, *Human walking*, Williams & Wilkins, Baltimore, USA, 1981.

[49] Y. Matsumoto, S. Sato, T. Nishioka, H. Shiojiri, A study on design of pedestrian over-bridges, *Transaction of JSCE* 4 (1972) 50-51.

Sitography

[I] https://structurae.net/photos/42152-solferino-footbridge-paris

[II] https://structurae.net/photos/161419-leopold-sedar-senghor-footbridge

[III] blogpontsdeparis.blogspot.be/2011/04/dun-pont-une-passerelle-de-solferino.html

APPENDIX A
STRUCTURAL BOARD

Appendix A contains some structural details of the studied structure extracted from boards kindly offered by the engineering office McCarré.
The reported board is subdivided in four windows. Window A represents a lateral elevation of the footbridge where it can be appreciated for all its length. On the left-hand side, the Courbevoie District support is represented. In the same window, deck slopes are reported span by span.
Window B shows a vertical cut at the mid-section of the central span of the footbridge. Here, dimensions and details about arches sections and deck width are reported.
In Window C information such as HEB section dimensions and deck coverage are reported.
Finally, in window D, a more detailed cut of the deck is presented where dimensions of the longitudinal beams at the edges of the deck with hollow rectangular cross section are reported.
Some architectural views of the footbridge are reported in the lowest part of the board.

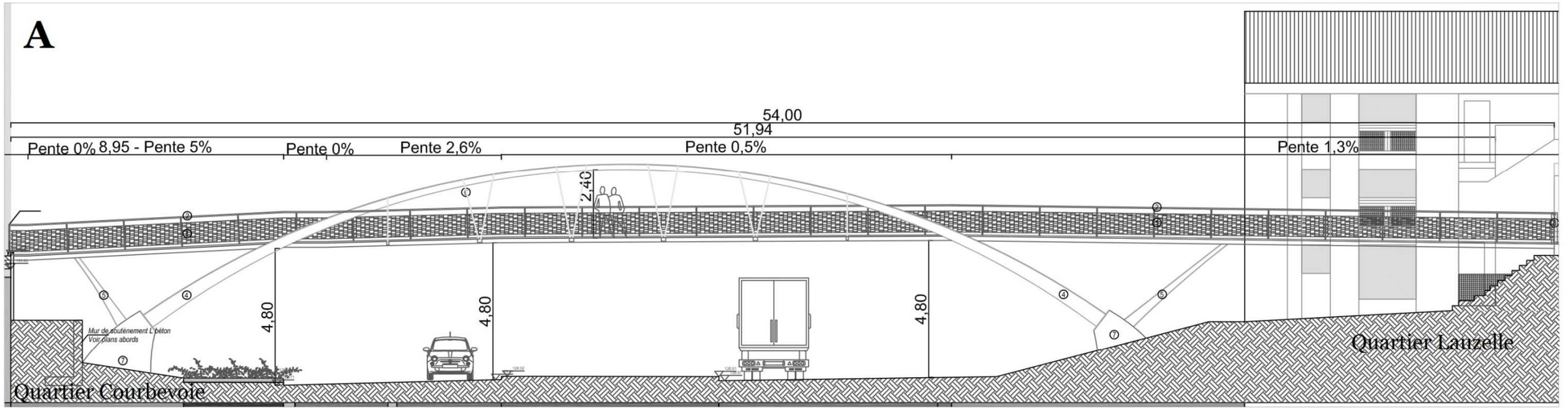
A
54,00
51,94
Pente 0%
8,95
Pente 5%
Pente 0%
Pente 2,6%
Pente 0,5%
Pente 1,3%
2,40
4,80
4,80
4,80
Mur de soutènement L béton
Voir plans abords
Quartier Courbevoie
Quartier Lauzelle
B
Arc
Tôles courbées
Section au sommet : 500x200x20mm
Suspente tablier / arc
Tige Ø25mm
240
120
294
Assemblage boulonné
15°
Arc: Tôles courbées
Section à la base:
Platine d'ancrage
Epaisseur 10mm
Socle
Culée béton gris clair
Béton préfabriqué
C
Assemblagepar plat boulonné
Capot métallique démontable
Pour protection gorge lumineuse
Platelage tablier
Bois synthétique anti-dérapant
Sous-structure platelage
HEB100 tous les 1,60m
Main courante
Tube 60x30x4mm
Cornière métallique 40x40x5mm
Raidisseur garde-corps
Double plat métallique tous les 2m
Garde-corps :
Métal tissé
Sous-structure : câbles Ø2cm
D
Plat boulonné
entre montants du garde-corps
Structure tablier
Tube métallique 200x150x10mm
Platelage tablier
Bois synthétique anti-dérapant
Sous-structure platelage
Fer T métalliques 100x100x11mm tous les 0,60m
120
294
Main courante
Tube 60x30x4mm
Raidisseur garde-corps
Double plat métallique
Garde-corps :
Métal tissé
Sous-structure : câbles
Projet
Demande de permis d'urbanisme
Passerelle Lauzelle - Courbevoie - Boulevard de Wallonie
M C ▪ CARRÉ
INGÉNIEURS & ARCHITECTES
AVENUE ALBERT EINSTEIN 11A
B-1348 LOUVAIN-LA-NEUVE
Maître d'Ouvrage
Les Jardins de Courbevoie S.A.
Avenue des communautés, 100
1200 Woluwe-Saint-Lambert
Représentée par : Mr Jean-Luc Son, REIM sarl
Adresse chantier
Boulevard de Wallonie
Architecte
Gaëtan Cordi
Objet du plan
Détails et références
Modifications
Indice
date
objet de la modification
date: 25/04/2013
échelles: 1/20 - 1/2
plan PU-04

APPENDIX B
NODES BOARD

The Finite elements model of the footbridge has been generated through Ansys Mechanical APDL. According to the direct generation method, that will be explained in Appendix C, it was necessary to define the mesh grid node by node and element by element. For this reason, it was necessary to establish a convention in order to know where each node was located without the necessity to look at the complete model.

Then, through the board reported in this Appendix B, we want to clarify the adopted convention. The board of nodes for only the model with vertical arches has been reported.

First of all, it must be specified that Ansys do not need to handle nodes numbered in sequential way. Then, the mesh grid of the deck is reported in window A. Nodes on the deck have been numbered in a sequential order on each transversal mesh line and from the left (Courbevoie district side) to the right. They start from one, in correspondence of the origin of the reference system and they reach number 210 at the opposite side of the deck.

In the same window, it is possible to observe also other nodes, but they are better represented in windows from B to E.

As for windows B and C, they allow to observe easily the presence of nodes going from 501 to 523. They have been used to orient the transversal element of the deck, that are inclined to follow slopes of the deck. Moreover, some among the 8 nodes multiples of 1000 are visible. They are the nodes in which H struts elements and arches are linked to the deck.

Nodes going from 236 to 262 and from 336 to 362 belong to the arches. Their position is showed in plane, in windows from A to C, and in elevation, in windows D and E.

Finally, nodes from 263 to 266 and from 363 to 366 have been used for the generation of H strut elements (plane view: windows B and C; elevation: windows D and E).

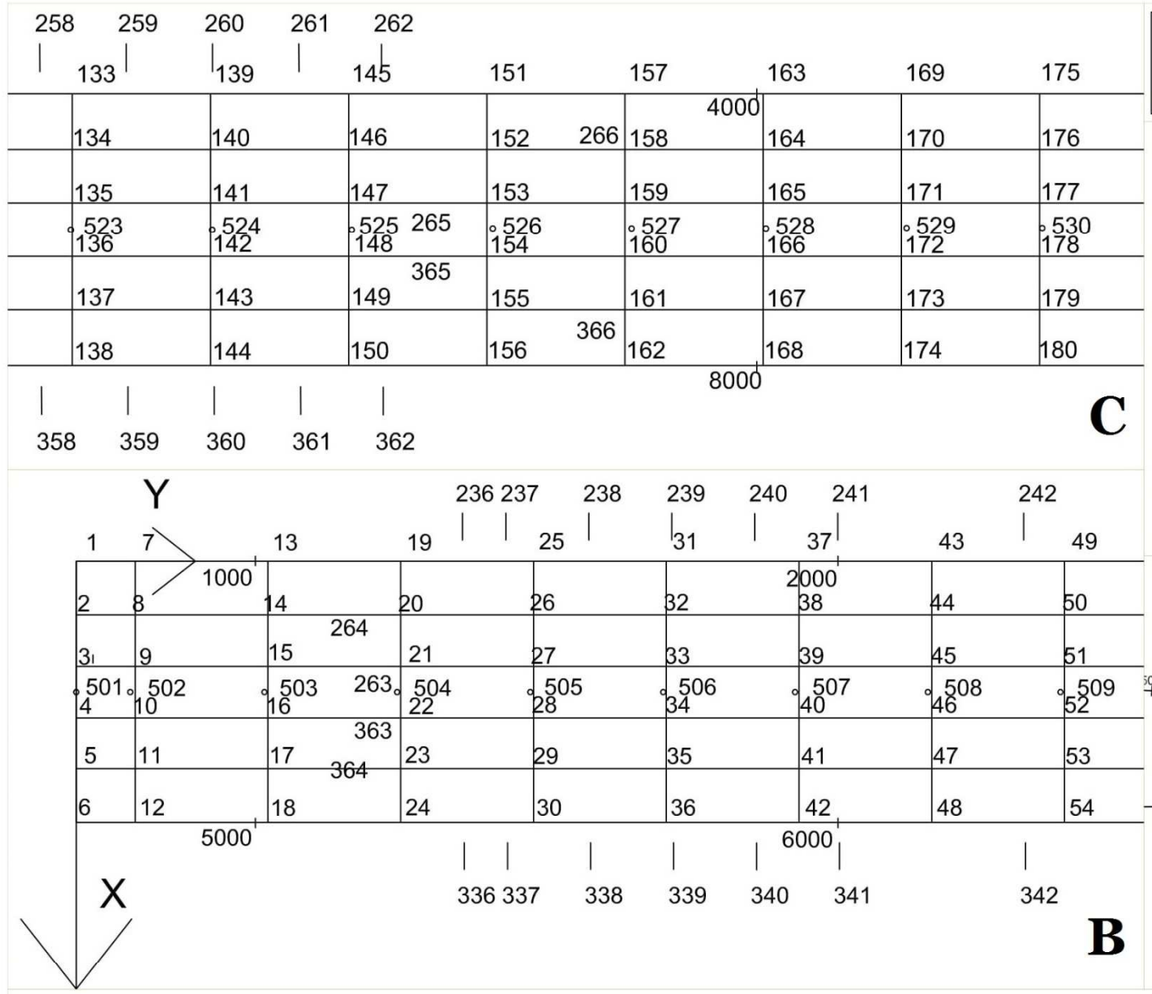

Appendix B: M.sc. Thesis-Dynamic analysis of a steel footbridge crossed by running pedestrians.	Author: Michele Pisani
	Plan: Nodes numbering convention used in Ansys modeling
	Project: Passerelle Lauzelle-Courbevoie-Boulevard de Wallonie/ McCarré

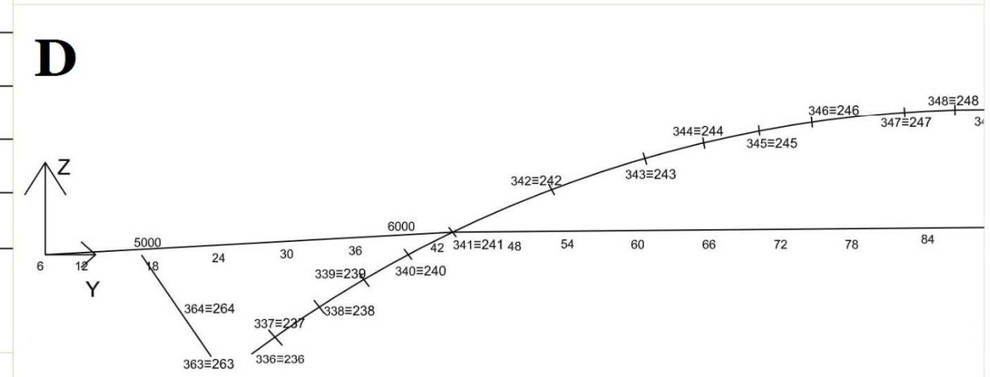

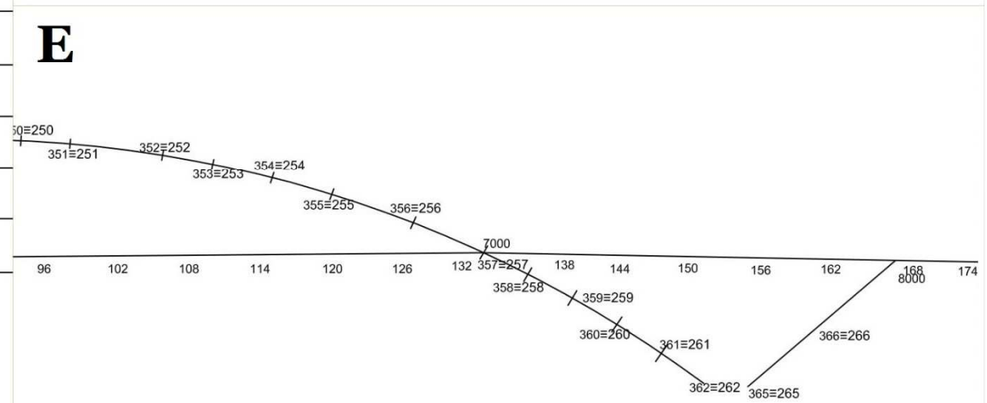

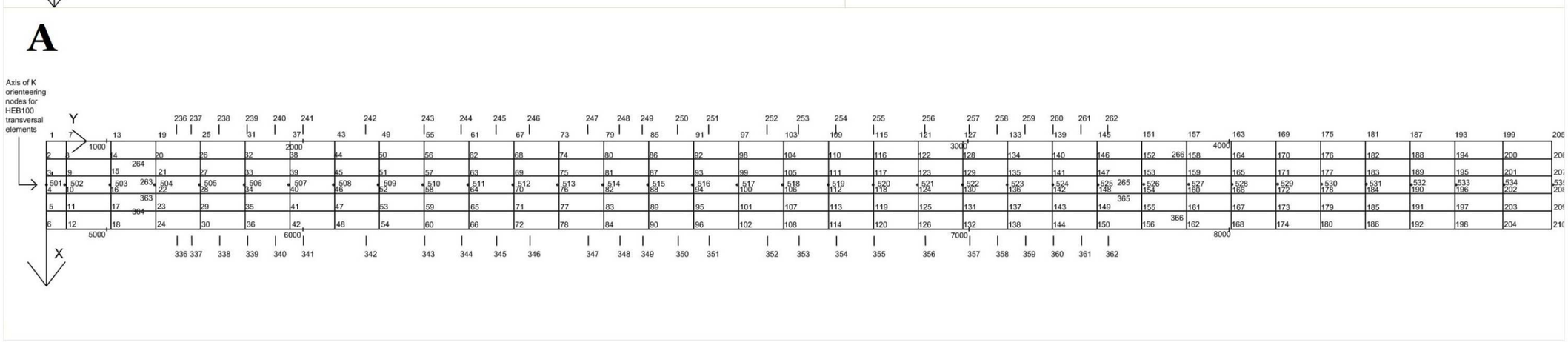

APPENDIX C
ANSYS MECHANICAL APDL

As described in paragraph 3.1, Ansys Mechanical APDL was adopted to model the footbridge. In this section, the model derivation from the practical point of view is presented. As already stated, the use of APDL involves the need to generate the model and perform the analyses through a code written in text file format and following the rules of the Ansys parametric language. Some base notions of this language are presented in the following.

There are three different phases to generate the model and analyze the results. It is common for all FE software (one other example may be Abaqus CAE) to divide in different phases the modeling process.

The first part of every Ansys code must be the so-called Pre-Processor phase. The Pre-Processor is the phase in which the user sets in place material properties, constitutive laws, geometry of the structure, loads and boundary conditions. In Ansys, meshing is inside the Pre-Processor and do not need a separated phase (as in Abaqus CAE).

If loads and boundary conditions are not defined in the Pre-Processor phase, they can be defined in the Solution part of the code. This phase is the one in which the user defines all the rules to run the analysis and the possible initial conditions. Different options can be chosen: static, modal, harmonic, transient, spectrum or buckling analysis. For all of them other options can be selected concerning, for instance, computation method, number of iterations and so on.

All the results can be visualized trough the last part of the code, called General Post-Processing Phase. To plot and list results for element or nodal solutions, commands are available too. Anyway, visualization of results is easier if done through the GUI and, for this reason, the */POST1* command (necessary to enter this phase using the parametric language) was not inserted in the case at study.

The detailed description of the first two code phases within the input file are listed below. Reference is made to the ANSYS APDL Manual [2].

To enter the *Pre-Processor*, the command */PREP7* is adopted. Three equal commands *ET* follow, each selecting an element type suitable to better describe the behavior of the structure. The three commands and related elements are:

- *ET,1,BEAM188*, with rigid section, shear stress output related to torsion and flexure and cubic shape functions. This element type is based on the Timoshenko theory, particularly recommended for beams from slender to relatively stubby dimensions. The element has six degrees of freedom per node. Input data are cross-section properties, material properties and three nodes. The end nodes (I and J) are mandatories, the third node (K) is used to define the orientation of the element around the axis going from node I to J (Figure C.1);

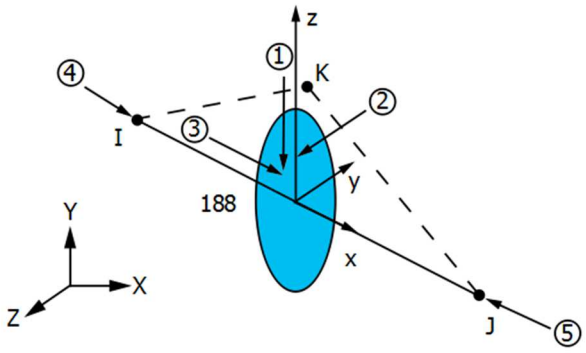

Figure C.1 BEAM188 Geometry [2].

- *ET,2,LINK180*, with rigid section. This element type is adopted to model trusses, sagging cables, links, springs and so on. It has three degrees of freedom per node, that describe nodal translation along x, y and z-axis. It is possible to model tension-only behavior. The element is defined through the following input data: two nodes (I and J), section properties and material properties (Figure C.2).

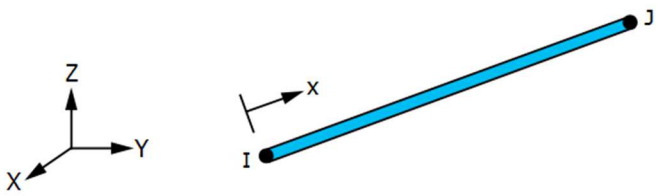

Figure C.2 LINK180 Geometry [2].

- *ET,3,MASS21,* can have up to six degrees of freedom to describe translations and rotations of a lumped mass. They can be reduced to 3 setting *keyoption* 3 equal to 2

to neglect rotations for a 3-D element (Eq C. 1). It is defined by a single node (I). Setting *keyoption* 1 equal to 1 the mass is defined as the product of a volume time a density. Volume is defined as a real constant and density as a material property (Eq C. 2). This procedure is useful to visualize lumped masses in the elements plot.

$$[M_e] = \begin{bmatrix} a & & \\ & a & \\ & & a \end{bmatrix} \qquad if\ KEYOPT(3) = 2 \qquad \text{Eq C. 1}$$

$$a = \rho V \qquad if\ KEYOPT(1) = 1 \qquad \text{Eq C. 2}$$

The second type of command in the input file defines real constants (R), that are used to define volumes of lumped masses. The constants will be later recalled with the pointer REAL, when mass elements are defined.
The step concerning sections definition requires two different procedures for constant and tapered sections. It is necessary to consider already at this point the presence of tapered elements even if they are not still defined. Without giving here information about the choice of command variables (section C.1 for more details), for elements that have a constant section the following commands are used:

SECTYPE, secID, type, subtype, name, refinekey
SECDATA, val1, val2, val3, val4, val5, val6
SECOFFSET, location

In *SECTYPE*, *secID* is the section definition number to be recalled when defining an element, *type* allows to choose among different types of sections, *subtype* is an ulterior specification for the section type, *name* is the user defined name of the section and *refinekey* sets the mesh refinement of the beam section, set to zero by default and not changed for our cases.
In *SECDATA, val-i* are geometrical values to give as prescribed by the guide, depending on the *type* and the *subtype* of selected section.
SECOFFSET allows the user to establish the origin of the section and the location of the nodes in the section. An example is given in Figure C.3.

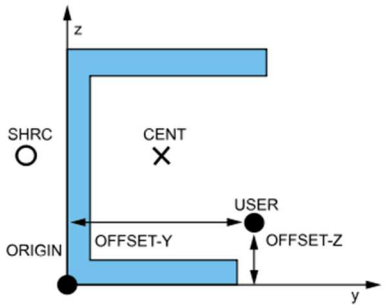

Figure C.3 Properties of SECOFFSET [2].

It is important to underline that, in most cases, offset of section origin has been set to be coincident with the center of gravity of the section. In the case of HEB100 and T elements, all in the deck, the offset has been changed to have the correct positioning of beams: inferior face of HEB100 must be adjacent to the inferior face of hollow rectangular beam while the superior surface of T elements must be adjacent to the superior face of HEB100 beams (APPENDIX A). Moreover, in the third model, for L arches sections, the offset has been set to the point in which cables are anchored on arches, i.e. $z = 9\ cm$ and $y = 1\ cm$ in Figure C.4.

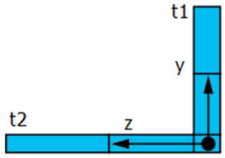

Figure C.4 Offset in L shaped section [2].

On the other hand, for tapered elements, the definition of section as previously described is not sufficient and it is necessary to define a second section, with the same characteristics, different geometrical values and in the same way as before. In this case a third step is required:

SECTYPE, *newsecID*, *TAPER*
SECDATA, *secID1*, *xsec1*, *ysec1*, *zsec1*
SECDATA, *secID2*, *xsec2*, *ysec2*, *zsec2*

This sequence defines the initial and final sections of the tapered element and the distance between the two sections, that defines the inclination angle of linking facets.
Materials definition follows in the Pre-Processor. It is not necessary to define all characteristics of materials but only the ones needed, already showed in Table 2.2.5.

MP, DENS, *matID*, *density_val*

MP, EX, *matID*, *Youngmodulus_val*
MP, NUXY, *matID*, *Poissonratio_val*

For isotropic materials, it is not necessary to define elastic properties in more than one direction.
The long list of nodes definition comes after:

N, *IDnode*, *x*, *y*, *z*

Values of *IDnode* and coordinates are obtained using conventions described in paragraph 3.2 and Figure 3.2.2.

At the end of the Pre-Processing phase, we arrive to the direct generation of mesh elements. Their definition is done recalling an element type, the material and the section from which they are made of:

TYPE, *etypeID*
MAT, *matID*
SECNUM, *secID*

Where *etypeID*, *matID* and *secID* are used to recall the element features defined above.
These features will be assigned to all the generated elements until other features will be recalled. Generating an element means linking a number of nodes with a finite element. In general, the generation command *E* could accept from one up to eight nodes: it depends on the required input for the accessed *ET*. For beam and link elements, two nodes are mandatory and, for the former, a third node is needed to orient the element. For mass elements, only one node is necessary.

E, *IDnodeI*, *IDnodeJ*, *IDnodeK, IDnodeL*, *IDnodeM*, *IDnodeN, IDnodeO*, *IDnodeP*

Finally, before entering the solution phase, to complete the modeling of the structure, boundary conditions and constraints are implemented.

D, *IDnode*, *label1*, *val1*, *val2*, *NEND*, *NINC*, *label2*, *label3*, *label4*, *label5*, *label6*

D is the command that assigns boundary conditions. For structural applications, *label1* could be a degree of freedom in displacements or rotation. For the node *IDnode*, it is set to *val1*. *val2* is for the case in which the degree of freedom allows a complex component. Other labels

can be set if the same boundary condition applies also to other degrees of freedom. If the user wants to apply the same boundary conditions to other nodes, they can be applied up to the node *NEND* with an increment of *NINC*

CP, *setID*, *label, IDnodeI*, *IDnodeJ*

The command *CP* allows coupling degrees of freedom (*label*) of a set of nodes going from two (*IDnodeI* and *IDnodeJ*) up to seventeen. This command has been used to constraint displacements of deck nodes to arches nodes. The first node of the coupled set is the retained node while the degrees of freedom of the second node are removed.

At this point the model should be ready. The *\SOLU* command starts the *Solution* phase. Given the complexity of the structure, different options and relative commands are adopted to execute a nonlinear static analysis in three time steps. At the begin of each time step the acceleration of gravity to model the self-weight of the structure is defined. Pre-tension effects are activated as well as geometrical nonlinearities. In the first time step, two coupled commands make the time step different from the others:

INISTATE, SET, MAT, *matID*
INISTATE, DEFINE, , , , , *val*

With this command an initial stress value, i.e. a pretension value, is assigned to elements having *matID* material.
After the nonlinear static analysis, the results are stored with the *UPCOORD* command and the modal analysis of the structure is performed with related commands.

The *Post.Processing* phase, finally, was not implemented in the input file and results were observed and evaluated using the Graphic User Interface.

C.1 Samples of one Ansys Input file

```
/PREP7                                          ! Enter the Preprocessor
ET,1,BEAM188,,1,3,2,,,
                                                ! KEYOPT(2)=1=Section is assumed to
                                                !be rigid (classical beam theory)
                                                ! KEYOPT(3)=3=shape functions: CUBICHE
                                                ! KEYOPT(4)=2=shear stress output=torsion
                                                ! and flexure related

ET,2,LINK180,,1,,,,,                            ! KEYOPT(2)=1=Section is assumed
to be rigid


  ET,3,MASS21,1,,2                              ! KEYOPT(1)=1=Interpret real constants as
                                                !volumes and rotary inertias/density
                                                !(Density must be input as a material property)
                                                ! KEYOPT(3)=2=3-D mass without rotary inertia

!! ------ Definition of real constant SETS ------ !!

R,2,0.02016                                     ! Volume of lumped masses on longitudinal
                                                !edge of the footbridge
R,3,0.004473                                    ! Volume of lumped masses on transversal
                                                !edge of the footbridge (V1=V6)
R,4,0.008946                                    ! Volume of lumped masses on transversal
edge of the footbridge (V2=V3=V4=V5)
R,7,0.014553                                    ! Volume of lumped masses on transversal
                                                ! edge of the footbridge (V7=V12)
...
...
...
SECTYPE,1,BEAM,HREC,LATBEAM,0                   !Definition of deck's lateral beam
                                                !section
SECDATA,0.15,0.20,0.01,0.01,0.01,0.01
SECOFFSET,CENT                                  !Beam origin will be offset to the
                                                !section CENTER OF GRAVITY
```

...
...
...
!! Definition of tapered sections for archs elements !!
...
...
...
SECTYPE,17,BEAM,L
SECDATA,0.3,0.55,0.02,0.02
SECOFFSET,USER,0.09,0.01

SECTYPE,18,BEAM,L
SECDATA,0.307,0.537,0.02,0.02
SECOFFSET,USER,0.09,0.01

SECTYPE,170,TAPER
SECDATA,17,2.68071,4.654,-2.23
SECDATA,18,2.78021,5.176,-1.851
...
...
...
!!Definition of cable elements !!

SECTYPE,41,LINK
SECDATA,0.000490625 !Section of cables linking deck and
!archs, D=0.025 m
SECCONTROL,0,1 !KEYOPT(0)=0=value of added
!mass per unit length
!KEYOPT(1)=1=tension only behaviour
...
...
...
!!!Definition of Steel (isotropic)!!!

MP,DENS,1,8000 !Density [kg/m^3]
MP,EX,1,210000000000 !Young's modulus [KN/m^2]
MP,NUXY,1,0.3

```
...
...
...
!!!Definition of wood for deck covering!!!
MP,DENS,7,1050                                          !Density [kg/m^3]
...
...
...
! Definition of mesh nodes for left lateral beams

!!Left longitudinal beam nodes!!
N,1,0,0,0
N,7,0,0.71087,0.0131
N,13,0,2.31087,0.09304
N,19,0,3.91087,0.17298
N,25,0,5.51087,0.25292
N,31,0,7.11087,0.33287
N,37,0,8.71087,0.41281
...
...
...
!Definition of Element types!

TYPE,1
MAT,1
SECNUM,1

!!ETYPE left longitudinal beam!!

E,1,7
E,7,1000
E,1000,13
E,13,19
E,19,25
E,25,31
E,31,37
E,37,2000
E,2000,43
```

```
E,43,49
E,49,55
E,55,61
...
...
...
!! -- Definition of mass elements to take into account wood deck covering -- !!

TYPE,3
MAT,7

!! Masses for equal inter-axes between transversal beams!!

!! Edge masses!!
REAL,2
E,13
E,19
E,25
...
...
...
!Definition of supports at beam ends

D,2,UZ,0,,,,UX,UY,,ROTY,ROTZ,
D,3,UZ,0,,,,UX,UY,,ROTY,ROTZ,
D,4,UZ,0,,,,UX,UY,,ROTY,ROTZ,
...
...
...
!Definition of constraints between arches and deck!
CP,1,UX,241,2000
CP,2,UY,241,2000
CP,3,UZ,241,2000
...
...
...
!!!!BEGIN SOLUTION!!!!
```

```
/SOLU
!Non linear Static Analysis!

ANTYPE,STATIC
nlgeom,on                                          !large displacement on!
pstres,on                                          !include prestress effect!
nropt,full
OUTRES,ALL,ALL
solcontrol,on,on
KBC,0                                              !KCBC,0=Loads are linearly
                                                   !interpolated (ramped) !
ematwrite,yes
!---------------- load steps non linear analysis ----------------

!------ load step 1 -------
g=9.81                                             !Definition of gravity acceleration!
ACEL,,,g                                           !ACEL generate, in absence of other
                                                   !loads, g positive in opposite to positive
                                                   ! direction of Z.!
                                                   !So it is not correct to write -g !
!!Definition of Pretension!!

INISTATE,SET,MAT,2
INISTATE,DEFINE,,,,,305580000

INISTATE,SET,MAT,3
INISTATE,DEFINE,,,,,295080000

INISTATE,SET,MAT,4
INISTATE,DEFINE,,,,,284580000

INISTATE,SET,MAT,5
INISTATE,DEFINE,,,,,298580000

INISTATE,SET,MAT,6
INISTATE,DEFINE,,,,,292580000

TIME,10                                            ! we need to give a value of time at each
```

!load step (two load step cannot have
! the same value of time)!
DELTIM,1,0.001,1 ! It is the duration of a substep. With
! this value of time, we will have at
!least 10 substeps!

ematwrite,yes
solve
!----------- load step 2 --------
...
...
...
!----------- load step 3 --------
...
...
...
!----------- modal analysis
/solu
antype,modal
ematwrite,yes
upcoord,1.0,on
pstres,on
modopt,lanb,100,0.1,10
mxpand,,0.1,10
psolve,eiglanb
finish
/solu
upcoord,1.0,on
expass,on
psolve,eigexp
finish
save
finish

C.2 Sample of Ansys Input file produced with RealRun1 for the transient analysis

```
/SOLU

ANTYPE,TRANS,NEW            !make a nonlinear static analysis before using this input

                                        !!LOAD STEP n° 1!!

NLGEOM,OFF
TIME,0.29500
AUTOTS,ON
DELTIM,0.00250,0.00250,0.00250
OUTRES,NSOL,ALL
OUTRES,V,ALL
OUTRES,A,ALL
TIMINT,ON
ALPHAD, 0.042500
BETAD, 0.000282
TRNOPT,FULL,,,,,NMK
TINTP,0
                !!****Loads Definition****!!

                !!*****__Nodal Loads definition__*****!!

*DIM,NF1N1,TABLE,60,1,1,TIME
NF1N1(1)=-0.00000,-0.79938,-6.66057,-66.30471,-223.26347,-435.37273,-578.84311,
          -584.40951,-521.48369,-503.10362,
NF1N1(11)=-554.69094,-616.40609,-636.47193,-624.34414,-623.79102,-654.54371,
          -686.41376,-672.50456,-610.08291,-558.15766,
NF1N1(21)=-567.08796,-594.70541,-551.97281,-442.78839,-368.08395,-362.46286,
           -338.24304,-237.42172,-124.89200,-75.66813,
NF1N1(31)=-69.41268,-50.62261,-16.51091,-0.00000,-0.00000,-0.00000,-0.00000,
           -0.00000,-0.00000,-0.00000,
NF1N1(41)=-0.00000,-0.00000,-0.00000,-0.00000,-0.00000,-0.00000,-0.00000,
          -0.00000,-0.00000,-0.00000,
NF1N1(51)=-0.00000,-0.00000,-0.00000,-0.00000,-0.00000,-0.00000,-0.00000,
```

```
            -0.00000,-0.00000,-0.00000,

NF1N1(1,0)=0.00000,0.00500,0.01000,0.01500,0.02000,0.02500,0.03000,0.03500,
              0.04000,0.04500,
NF1N1(11,0)=0.05000,0.05500,0.06000,0.06500,0.07000,0.07500,0.08000,0.08500,
              0.09000,0.09500,
NF1N1(21,0)=0.10000,0.10500,0.11000,0.11500,0.12000,0.12500,0.13000,0.13500,
              0.14000,0.14500,
NF1N1(31,0)=0.15000,0.15500,0.16000,0.16500,0.17000,0.17500,0.18000,0.18500,
              0.19000,0.19500,
NF1N1(41,0)=0.20000,0.20500,0.21000,0.21500,0.22000,0.22500,0.23000,0.23500,
              0.24000,0.24500,
NF1N1(51,0)=0.25000,0.25500,0.26000,0.26500,0.27000,0.27500,0.28000,0.28500,
              0.29000,0.29500,

F,1,FZ,%NF1N1%

...
...
...

ALPHAD, 0.042500
BETAD, 0.000282
 LSWRITE
SAVE
SOLVE

FDELE,1,FZ
FDELE,1,MX
FDELE,1,MY
FDELE,2,FZ
FDELE,2,MX
FDELE,2,MY
FDELE,8,FZ
FDELE,8,MX
FDELE,8,MY
FDELE,7,FZ
FDELE,7,MX
```

```
FDELE,7,MY

                    !!LOAD STEP n° 2!!

...
...
...

                    !!LOAD STEP n° 108!!

NLGEOM,OFF
TIME,32.03389
AUTOTS,ON
DELTIM,0.00250,0.00250,0.00250
OUTRES,NSOL,ALL
TIMINT,ON
ALPHAD, 0.042500
BETAD, 0.000282
TRNOPT,FULL,,,,,NMK
TINTP,0

LSWRITE
SAVE
SOLVE

FINISH
SAVE

/EOF
```

C.3 Time integration method

The Newmark's method of constant acceleration method was chosen to perform the transient analysis. This is one of the implicit numerical methods for direct integration in time. The main idea is to solve the system of the equations of motion only for discrete values of time. The procedure is well described in [3]. To proceed, equations of motion must be used in the discretized form:

$$\boldsymbol{M}\ddot{\boldsymbol{x}}_{n+1} + \boldsymbol{C}\dot{\boldsymbol{x}}_{n+1} + \boldsymbol{K}\boldsymbol{x}_{n+1} = \boldsymbol{F}_{n+1} \quad \text{Eq C. 3}$$

where:

- $\boldsymbol{M}$ is the mass matrix;
- $\boldsymbol{C}$ is the damping matrix;
- $\boldsymbol{K}$ is the stiffness matrix;
- $\boldsymbol{F}_{n+1}$ is the force vector at time $t + \Delta t$;
- $\ddot{\boldsymbol{x}}_{n+1}$ is the vector of nodal accelerations at time $t + \Delta t = t_{n+1}$;
- $\dot{\boldsymbol{x}}_{n+1}$ is the vector of nodal velocities at time $t + \Delta t = t_{n+1}$;
- $\boldsymbol{x}_{n+1}$ is the vector of nodal displacements at time $t + \Delta t = t_{n+1}$;

Exploiting an approach at the finite differences, accelerations and velocities vectors are computed as follows:

$$\dot{\boldsymbol{x}}_{n+1} = \dot{\boldsymbol{x}}_n + [(1-\delta)\ddot{\boldsymbol{x}}_n + \delta\ddot{\boldsymbol{x}}_{n+1}]\Delta t \quad \text{Eq C. 4}$$

$$\boldsymbol{x}_{n+1} = \boldsymbol{x}_n + \dot{\boldsymbol{x}}_n\boldsymbol{\Delta t} + [\left(\tfrac{1}{2} - \alpha\right)\ddot{\boldsymbol{x}}_n + \alpha\ddot{\boldsymbol{x}}_{n+1}]\Delta t^{\boldsymbol{2}} \quad \text{Eq C. 5}$$

where:

- α and δ are the Newmark's integration parameters;
- $\ddot{\boldsymbol{x}}_n$ is the vector of nodal accelerations at time t_n;
- $\dot{\boldsymbol{x}}_n$ is the vector of nodal velocities at time t_n;
- $\boldsymbol{x}_n$ is the vector of nodal displacements at time t_n.

Finally, the integration procedure consists in the solution of the system of Eq. 5.5.1, Eq. 5.5.2 and Eq. 5.5.3. The three unknowns are $\dot{\boldsymbol{x}}_{n+1}$, $\dot{\boldsymbol{x}}_{n+1}$and $\ddot{\boldsymbol{x}}_{n+1}$ and they are computed thanks to the known quantities at time t_n. For this reason, at each cycle of calculation, results of the considered step will represent initial conditions for the following. As for the first time integration interval, initial condition must be given as well.

So, making use of Eq. 5.5.2 and Eq. 5.5.3 in Eq. 5.5.1, displacements at t_{n+1} are computed through:

$$(a_0\boldsymbol{M} + a_1\boldsymbol{C} + \boldsymbol{K})\boldsymbol{x}_{n+1} = \boldsymbol{F}_{n+1} + \boldsymbol{M}(a_0\boldsymbol{x}_n + a_2\dot{\boldsymbol{x}}_n + a_3\ddot{\boldsymbol{x}}_n) + \boldsymbol{C}(a_1\boldsymbol{x}_n + a_4\dot{\boldsymbol{x}}_n + a_3\ddot{\boldsymbol{x}}_n)$$

Eq C. 6

where:

- $a_0 = \frac{1}{\alpha\Delta t^2}$
- $a_1 = \frac{\delta}{\alpha\Delta t}$
- $a_2 = \frac{1}{\alpha\Delta t}$

- $a_3 = \frac{1}{2\alpha} - 1$
- $a_4 = \frac{\delta}{\alpha} - 1$
- $a_5 = \frac{\Delta t}{2}(\frac{\delta}{\alpha} - 2)$

Then, the program determines the other two unknowns taking advantage of the following equations:

$$\dot{\boldsymbol{x}}_{n+1} = a_1(\boldsymbol{x}_{n+1} - \boldsymbol{x}_n) - a_4\dot{\boldsymbol{x}}_n - a_5\ddot{\boldsymbol{x}}_n \quad \text{Eq C. 7}$$

$$\ddot{\boldsymbol{x}}_{n+1} = a_0(\boldsymbol{x}_{n+1} - \boldsymbol{x}_n) - a_2\dot{\boldsymbol{x}}_n - a_3\ddot{\boldsymbol{x}}_n \quad \text{Eq C. 8}$$

The Newmark's procedure for direct time integration of equations of motion can be classified inside the class of unconditionally stable numerical methods under special conditions. This means that the amplification of errors due to computations during the time integration could be limited independently from the value of time step size Δt chosen to make the integration. To ensure the unconditioned stability of the method, then, the special conditions mentioned above are about the Newmark's parameters:

$$\begin{cases} \delta = \frac{1}{2} + \gamma \\ \alpha \geq \frac{1}{4}(1+\gamma)^2 \\ \gamma \geq 0 \end{cases} \quad \text{Eq C. 9}$$

These parameters are automatically computed by Ansys if, through the command TINP, the value of γ is given. For our purposes, it was equal to 0.

APPENDIX D
NATURAL MODES

Appendix D reports tables of deformed shapes of natural modes determined through the modal analysis in section 3.3.3.
Table D. 1, Table D. 2 and Table D. 3 report the modal shapes of the first 10 footbridge modes for models 1 to model 3 respectively, in both cases of absence and presence of pretension. We recall that differences between the three models are related to their geometry. Model1 presents vertical arches with rectangular hollow cross section, Model2 has inclined arches and rectangular hollow cross section. Model3 has inclined arches with L shaped cross sections.

Values of natural frequencies for each modal shape are reported in columns 2 of the quoted tables. For each mode, two values of eigenfrequencies are reported: one for the modal shape illustrated in column 3, for the case of no pretension applied (WO-P), and one for the modal shape illustrated in column 4, for the case of applied pretension (W-P).

All the models have lateral, vertical, torsional and mixed modes of vibrations. The pretension and the variation of the arches geometry induce variation of eigenfrequencies and modal shapes at the same time.
For a detailed analysis about modal shapes, the reader can refer to section 3.3.3.

Table D. 1 Eigenfrequencies and modal shapes for the Model1.

Mode	Frequency [Hz]	Modal shape w/o pretension	Modal shape with pretension
1	WO-P: 2.006 W-P: 2.070	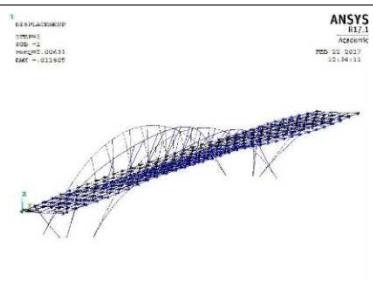	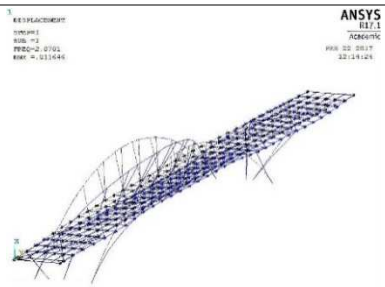
2	WO-P: 3.593 W-P: 3.590	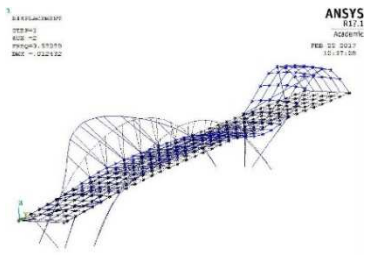	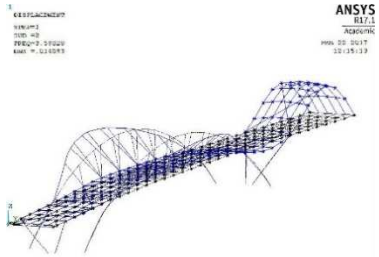
3	WO-P: 3.630 W-P: 3.622	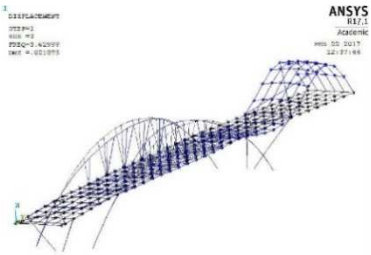	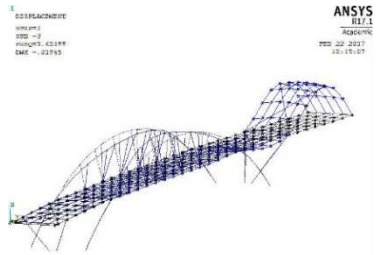
4	WO-P: 3.961 W-P: 4.379	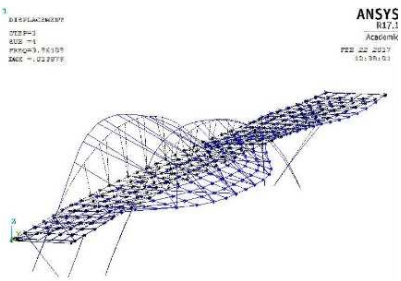	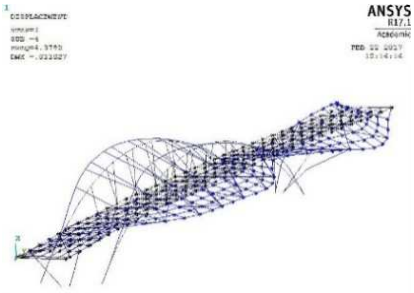
5	WO-P: 4.497 W-P: 4.751	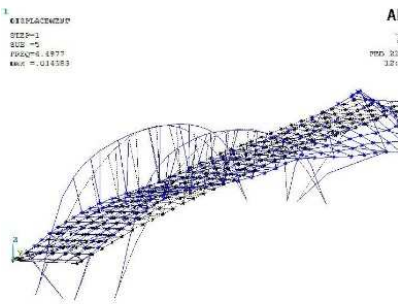	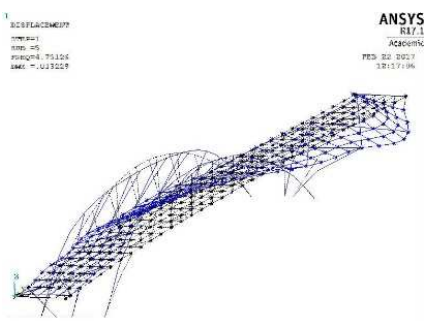

Mode	Frequency [Hz]	Modal shape w/o pretension	Modal shape with pretension
6	WO-P: 5.470 W-P: 5.965	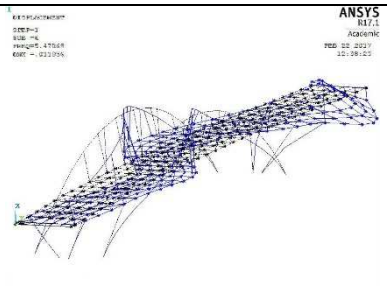	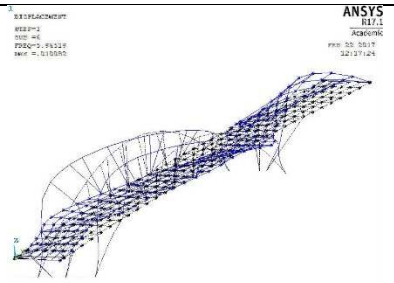
7	WO-P: 6.896 W-P: 6.876	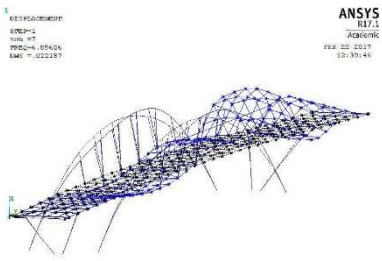	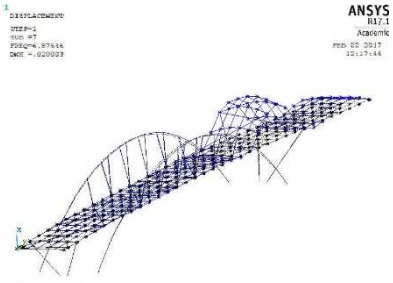
8	WO-P: 6.937 W-P: 6.945	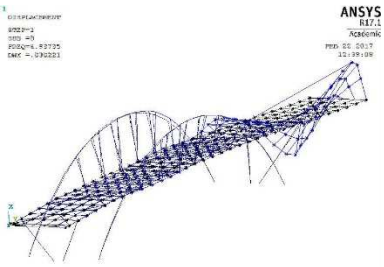	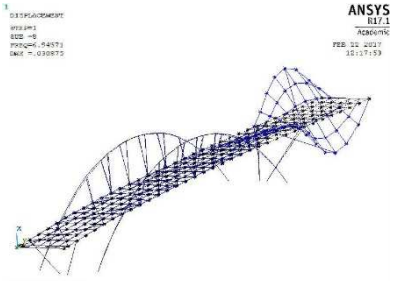
9	WO-P: 7.009 W-P: 7.272	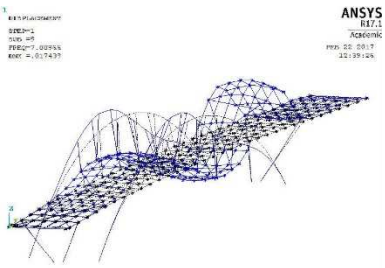	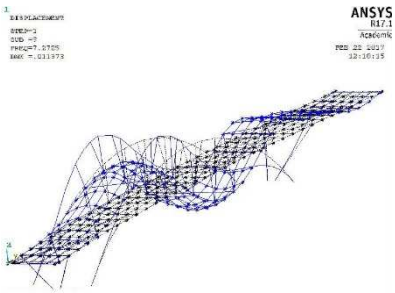
10	WO-P: 7.124 W-P: 9.078	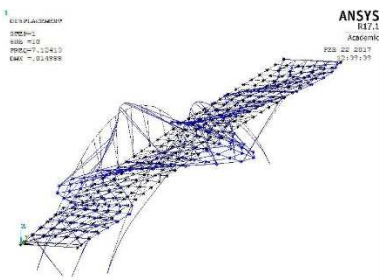	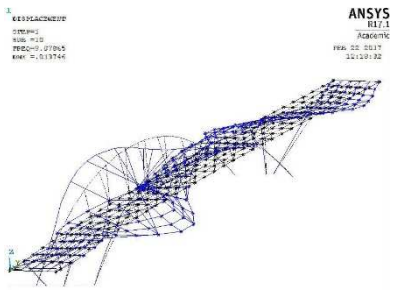

Table D. 2 Eigenfrequencies and modal shapes for the Model2.

Mode	Frequency [Hz]	Modal shape w/o pretension	Modal shape with pretension
1	WO-P: 1.910 W-P: 2.052	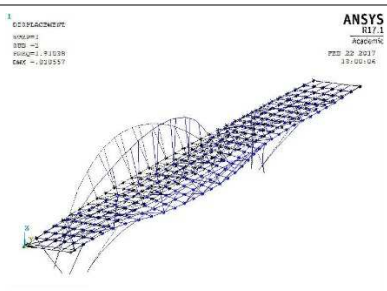	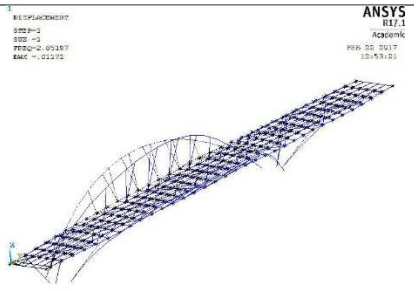
2	WO-P: 3.037 W-P: 3.533	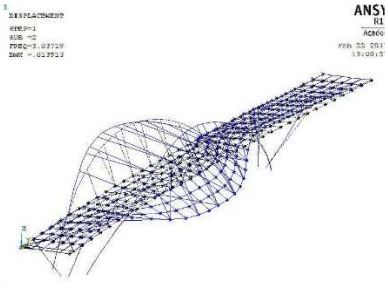	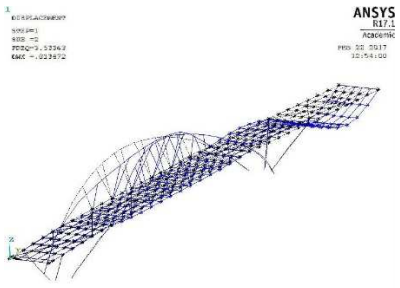
3	WO-P: 3.536 W-P: 3.619	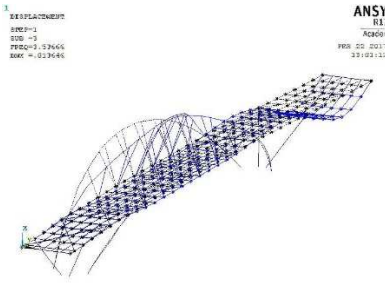	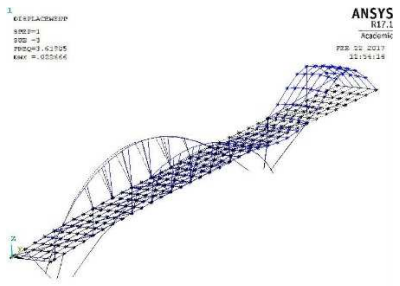
4	WO-P: 3.629 W-P: 4.287	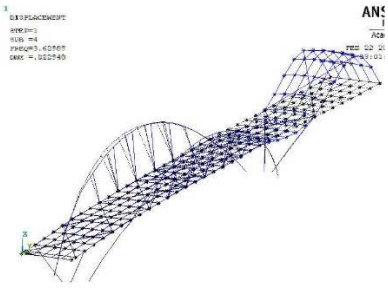	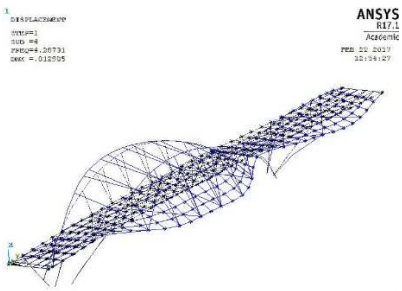
5	WO-P: 4.457 W-P: 4.705	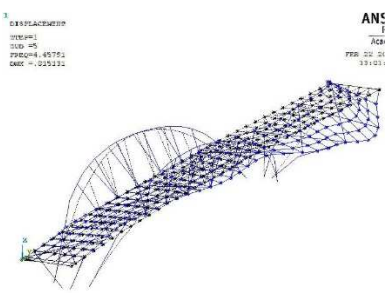	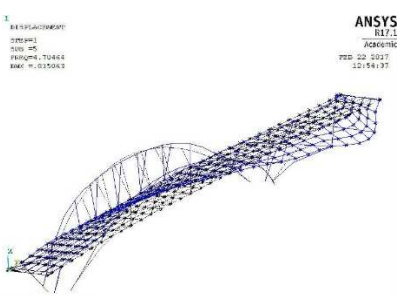

Mode	Frequency [Hz]	Modal shape w/o pretension	Modal shape with pretension
6	WO-P: 5.014 W-P: 5.862	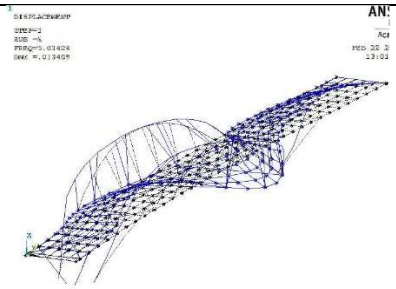	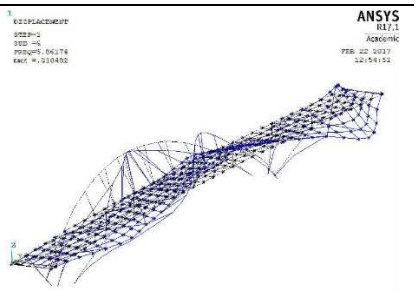
7	WO-P: 6.470 W-P: 6.862	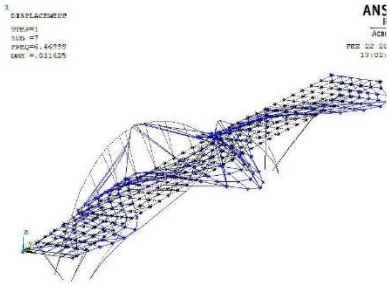	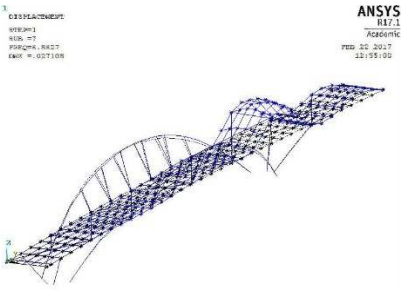
8	WO-P: 6.904 W-P: 6.948	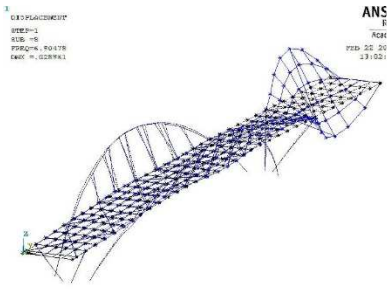	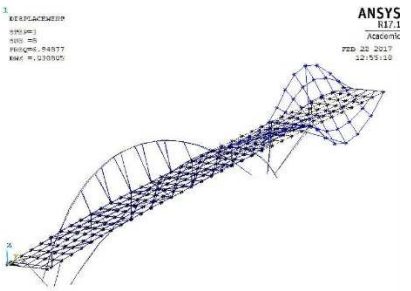
9	WO-P: 6.908 W-P: 7.055	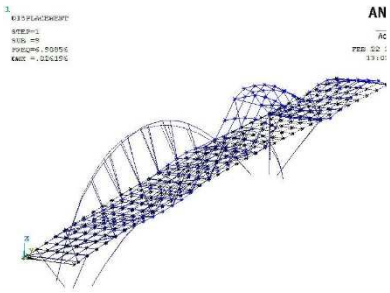	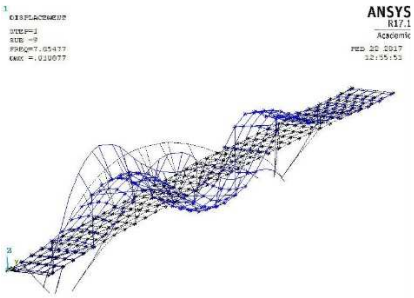
10	WO-P: 7.062 W-P: 8.850	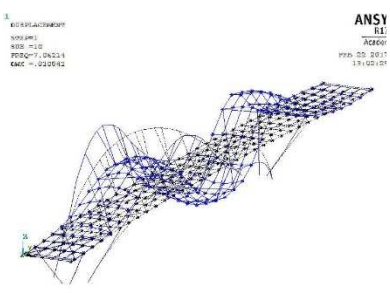	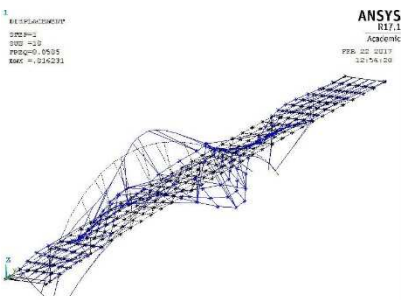

Table D. 3 Eigenfrequencies and modal shapes for the Model3.

Mode	Frequency [Hz]	Modal shape w/o pretension	Modal shape with pretension
1	WO-P:1.103 W-P: 1.132	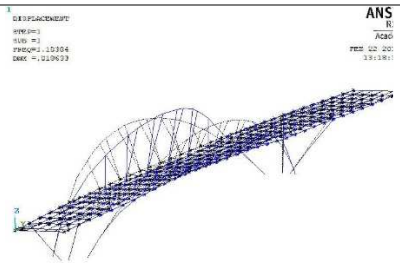	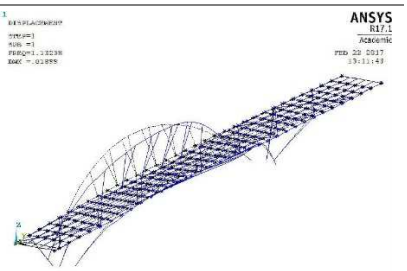
2	WO-P:1.561 W-P: 1.566	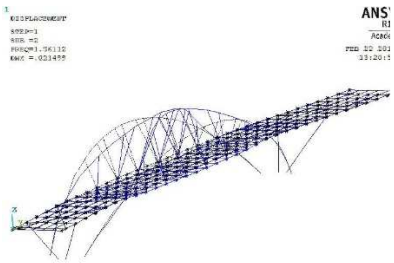	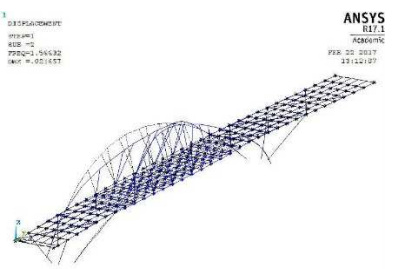
3	WO-P:2.737 W-P: 2.843	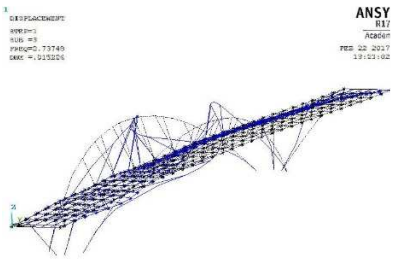	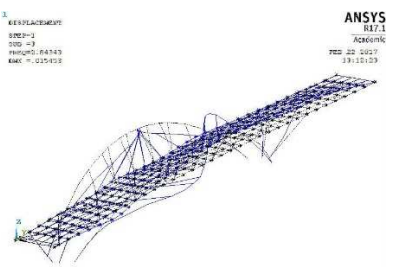
4	WO-P:3.237 W-P: 3.387	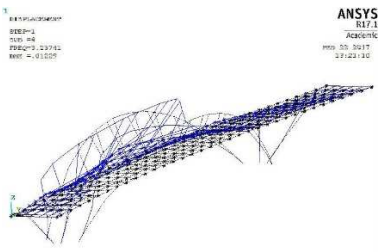	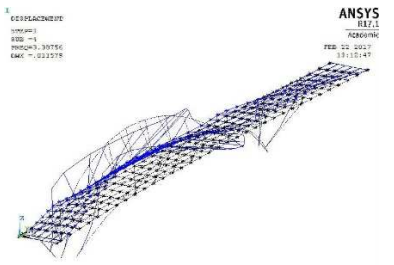
5	WO-P:3.605 W-P: 3.593	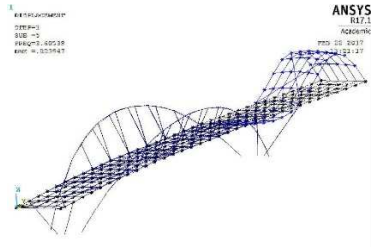	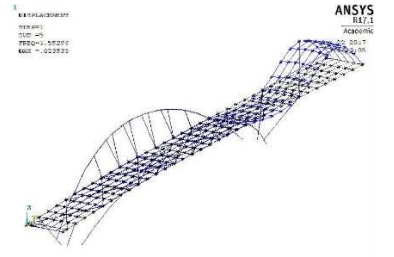

Mode	Frequency [Hz]	Modal shape w/o pretension	Modal shape with pretension
6	WO-P:4.279 W-P: 4.276	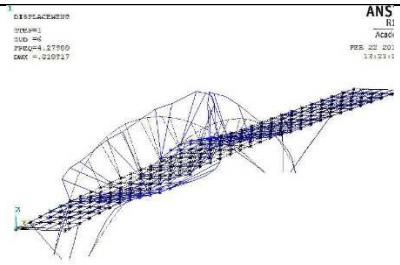	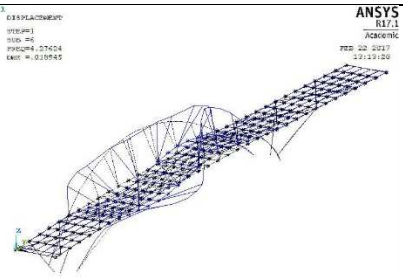
7	WO-P:4.639 W-P: 4.781	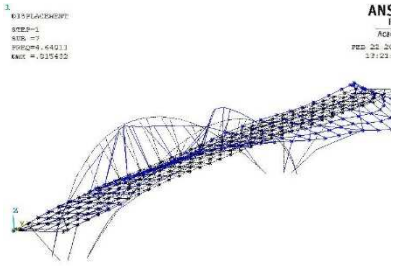	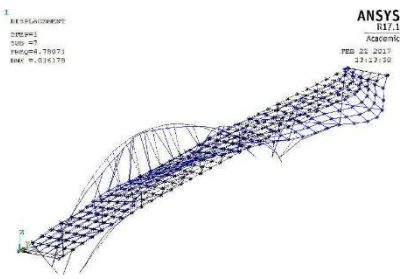
8	WO-P:6.075 W-P: 6.258	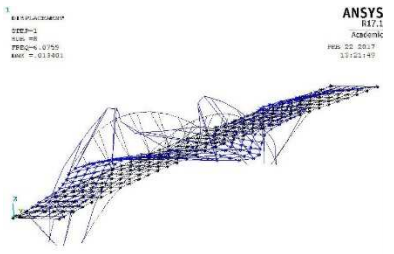	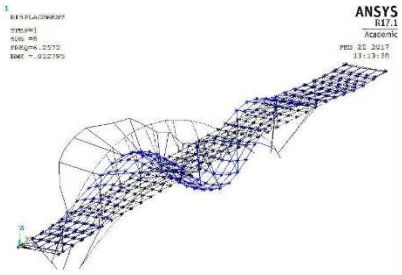
9	WO-P:6.259 W-P: 6.434	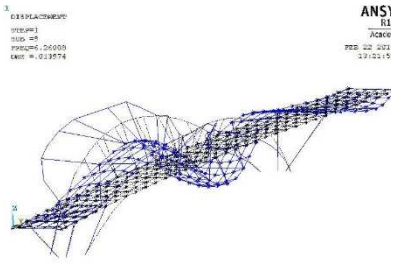	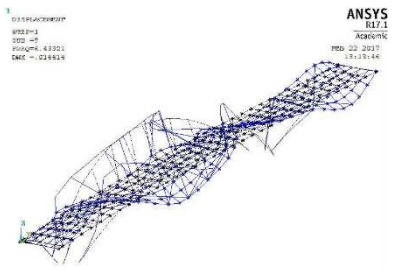
10	WO-P:6.357 W-P: 6.751	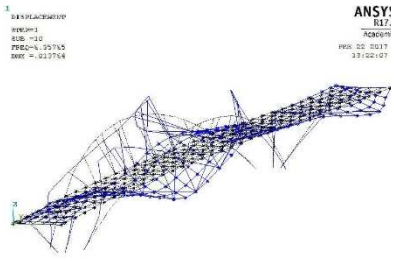	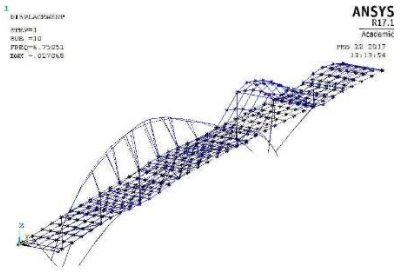

APPENDIX E
REALRUN1

The numerical code RealRun1, written in Matlab language, can generate a text file according to code rules of Ansys Mechanical APDL for the execution of a transient analysis. The program is adopted for the generation of force time histories induced by one running person, accounting for the fact that running is characterized by load cycles. Each load cycle is different from the others and during a given load cycle, the value of force applied on the structure-is not constant. Finally, moving from a load cycle to the next means also the change of position.

The starting point of RealRun1 was a .mat file, where the load time history was stored inside an array for a period of 100 *s* with sampling frequency of 200 *Hz* (Figure 5.5.1).

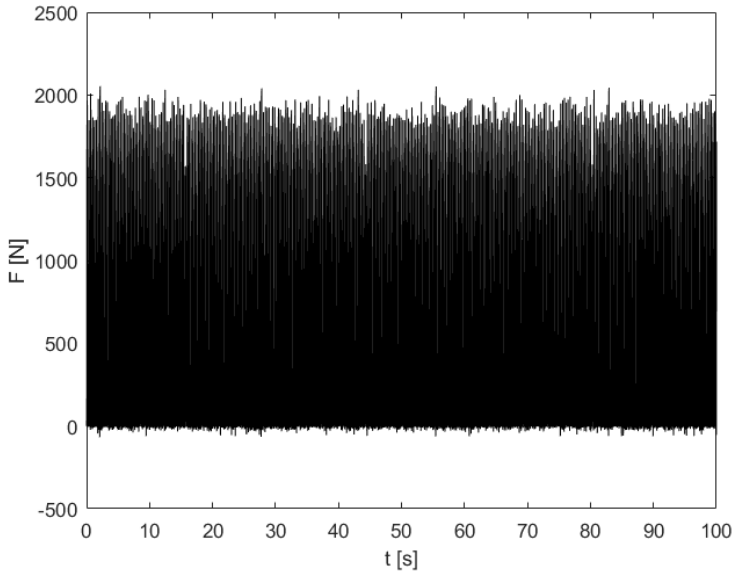

Figure 5.5.1 Force time history produced by a running pedestrian during an interval of 100*s* [47].

In the following paragraphs, the functions contained in RealRun1 will be presented, while some sample of the generated text file is reported in in APPENDIX C.2. A scheme of the code architecture is given in Figure 5.5.2.

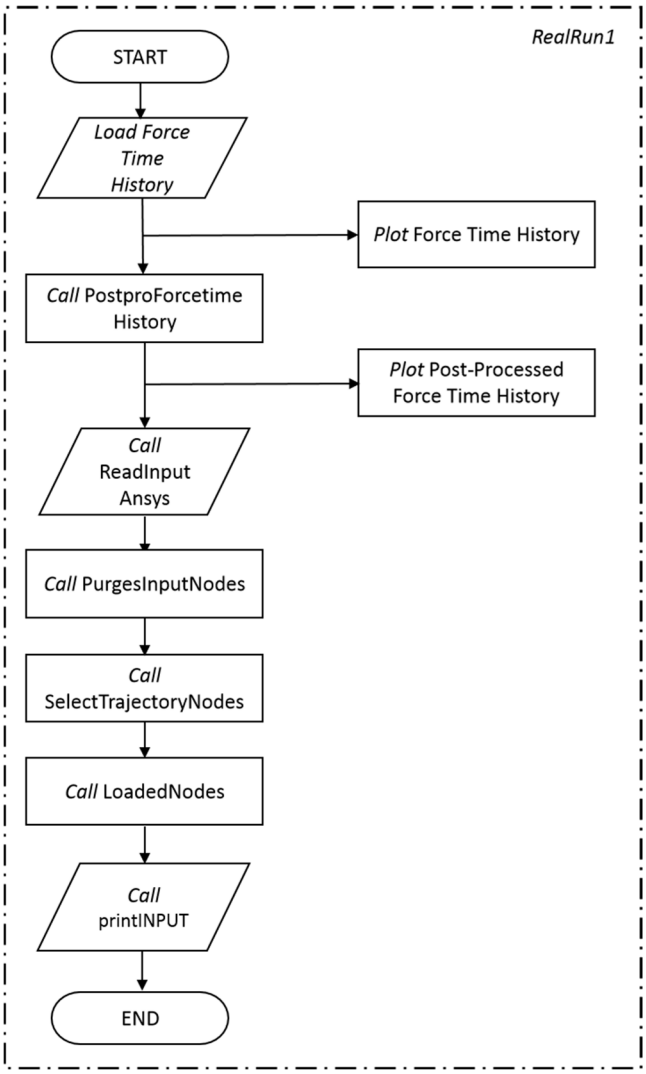

Figure 5.5.2 Flow chart of the Matlab code RealRun1.

The flow chart of the code can be described schematically through the following list:

1. "START": definition of some fundamental variables in the first lines of the code:
    a. Time duration to cross the footbridge;
    b. Coefficients α e β of the Rayleigh damping;
    c. Coordinates of the first contact point;
    d. The array of nodes to be neglected in the determination of nodes potentially influenced by the trajectory. They are nodes that are not part of the regular mesh grid The reason of this choice is related to the fact that shape functions used in point 10 are adapted for use on regular mesh grids only.

2. "*Load Force Time* History", is the phase in which the .mat file is loaded into RealRun1. The file contains the array of the force time history and its duration, the sampling frequency, the pedestrian weight and speed and the contact frequency between the structure and the pedestrian;
3. "*Plot* Force Time History" produces a plot of the load time history as it is;
4. "*Call* PostproForcetimeHistory" extracts the number of load cycles needed to cross the footbridge considering the pedestrian speed;
5. "Plot Post-Processed Force Time History" produces a plot of the load time history of the run done to cross the footbridge;
6. "*Read deck nodes*" reads deck nodes from the input text file where the FE model was written in Ansys Parametric Design Language;
7. "*Call* PurgeInputNodes", to get rid of undesired nodes from the read ones;
8. "*Call* SelectTrajectoryNodes", to select nodes that can be potentially loaded during the run;
9. "*Call* LoadedNodes", to determine nodes loaded during each load cycle;
10. "*Call* PrintINPUT", to print the txt file readable by Ansys for doing the transient analysis. It calls two other functions: "ExtractLoadCycle" and "CreateNodalLoads".
11. "END".

E.1 PostproForceTimeHistory

The function “PostproForceTimeHistory” post-processes the vector of the force time history loaded from the .mat file produced by the *Racic and Morin* numerical generator.
The purpose of this function is to give as output the following data:

- the vector of the force time history for the time needed to cross the footbridge;
- a vector containing durations of each load cycle;
- number of load cycles to be realized during the crossing of the footbridge;
- the initial phase before the start of the first load cycle.

Other than being smaller in duration, the post-processed force time history has two more features: it has not negative values and each load cycle is clearly characterized by a phase in which the force is different from zero (contact phase) and another in which the force is always equal to zero (flying phase). Before the post-processing, some oscillations of the load were present during the flying phase.
Three main loops constitute this function. All negative values of the original force time-history array are set to zero during the first loop. Through an iterative procedure, which is based on a mathematical concept, all values of force of the flying phase are set to zero in the second loop.
Let us consider the single load cycle time history in Figure E. 1 before being post-processed.

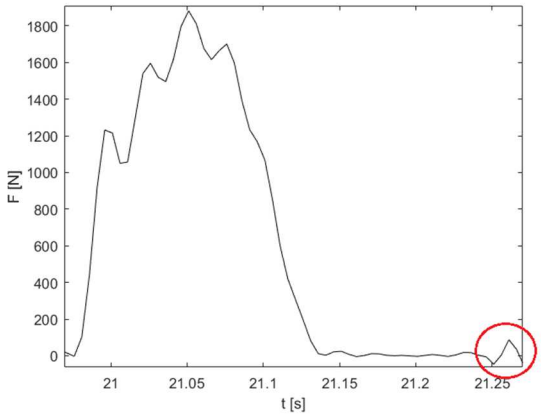

Figure E. 1 One example of a complete load cycle. Oscillations can be observed in the flying phase of the cycle. The rounded zone is zoomed in figures Figure E. 2 and Figure E. 3.

The code needs to recognize which value of time in the cycle indicates that the runner is in the flying phase. Given the nature of the curve, for a given time value t_i, if the first derivative between t_i and t_{i+1} is negative while the one between t_i and t_{i-1} is positive, when the image of t_i has a smaller value than the mean value of images of all time values of the load time

history, then, the t_i is one of the moments in which the runner is in the flying phase and its image can be set to zero (Figure E. 2).

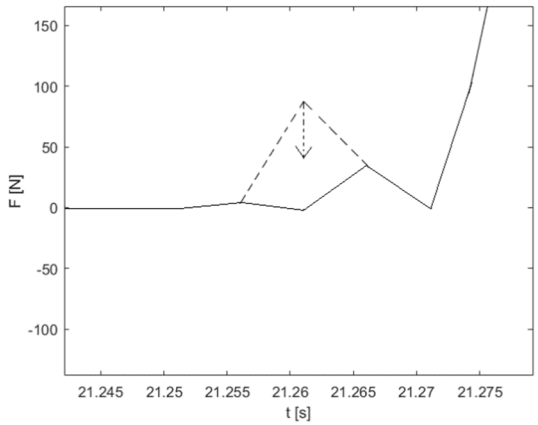

Figure E. 2 Zoom of rounded zone in Figure E. 1. Situation in which there are conditions to set the force value to zero: 1st iteration.

The problem is that, as it can be seen from Figure E. 2, two branches of the curve with negative derivative could be one after the other. For this reason, iterations are necessary until all peaks are reduced to zero (Figure E. 3).

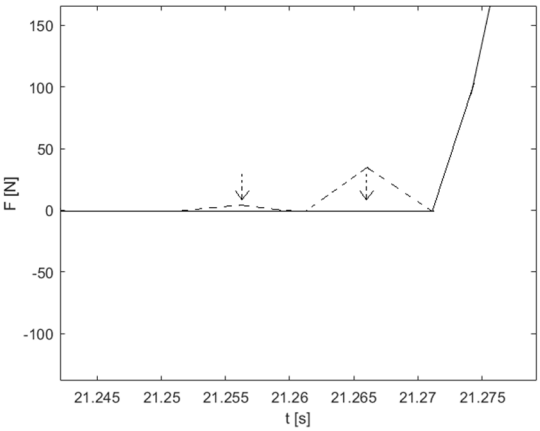

Figure E. 3 Zoom of rounded zone in Figure E. 1. Situation in which there are conditions to set the force value to zero: 2nd iteration.

Then, using some conditional instructions and some variables as flags, the third loop recovers values of time durations τ_k of each load cycle of the considered load time history, making a distinction between contact and flying phases and determining when an entire load cycle is done.

E.2 ReadInputAnsys

The function “ReadInputAnsys” allows to read the input text file used for the generation of the FE model in Ansys and stores number and coordinates of nodes of the problem. To use this function two important assumptions must be done. First, the input file that has to be read must be in the same folder of the Matlab project and, second, since we are interested only in deck nodes, they must be the first nodes defined in the Ansys input file. Even if this last constraint can be modified and the function adapted to more general situations, at the moment, the function stores numbers and coordinates of the read nodes until the line “!*End of deck nodes!*” is read.

E.3 PurgeInputNodes

The function “PurgeInputNodes” makes a comparison between the stored nodes read from the Ansys input file with the nodes to be neglected chosen by the user in the START phase. The output vector will contain nodes that can be potentially loaded during the run over the bridge.

E.4 SelectTrajectoryNodes

The function “SelectTrajectoryNodes” finds nodes to the left and to the right of the trajectory from the nodes vector that takes as input variable. Since the trajectory is assumed to be rectilinear, the function exploits the abscissa value of the first contact point defined in the START phase to identify these nodes.

Being the footbridge deck modeled by a regular mesh grid, the first step is the determination of the number of nodes that constitute the bridge for each line parallel to the y- and the x-axis.

Then, two loops are used for the determination of nodes to the left and to the right of the trajectory. Consider the first transversal line of the deck in Figure E. 4, where nodes number go from 1 to 6 and where node 1 is to the left of the trajectory in every case because of the position of the reference system. The maximum number of possible comparisons is established as the number of nodes along the x-direction. Through the comparison of the starting point abscissa with the one of each node laying on the same transversal line, the two loops give the possibility to store the first node to the left or to the right of the trajectory and all nodes with the identical abscissa laying on the same longitudinal grid line.

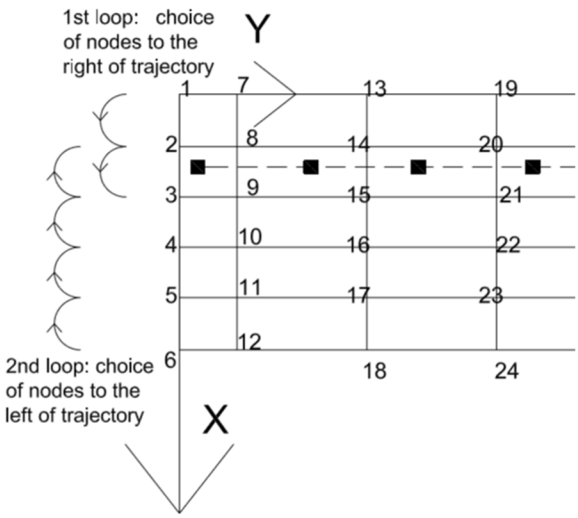

Figure E. 4 Schematic description of loops necessary to determine nodes to the left and to the right of the trajectory.

E.5 LoadedNodes

The function "LoadedNodes" defines nodes in front and behind each contact point on its influence area during the passage over the bridge (nodes 8 and 9 and nodes 2 and 3 in Figure E. 4 for the first contact point).

The function's purpose is to individuate number and coordinates of these nodes for each load cycle.

In order to select nodes, the first step is the computation of the vector of cumulative distances covered by the runner through the use of a mean value of the step length Then, the second operation was the creation of the vector containing ordinates of nodes laying on a line parallel to the trajectory. Finally, by comparison of each value of the former with each value of the latter vector, two matrices containing number and coordinates of nodes in front and behind the contact points were created.

The importance of this function is due to the fact that, in case the stride length is not so large, it is capable to handle the case in which the runner is located twice, or more times, on the same influence area for different load cycles.

E.6 PrintINPUT

The function "printINPUT" produces a text file with readable commands for a transient analysis in Ansys. In the order, the function prints:

a. First commands and options for a transient analysis;

b. Load steps (LSs) and related information to simulate variation of loads in time, for a given load step, and in space, changing point of application between different load steps;
c. LSs to simulate an unloaded transient phase after the passage of the runner over the footbridge;
d. Last commands for the execution of the transient analysis.

Architecture of the function is described in Figure E. 5.

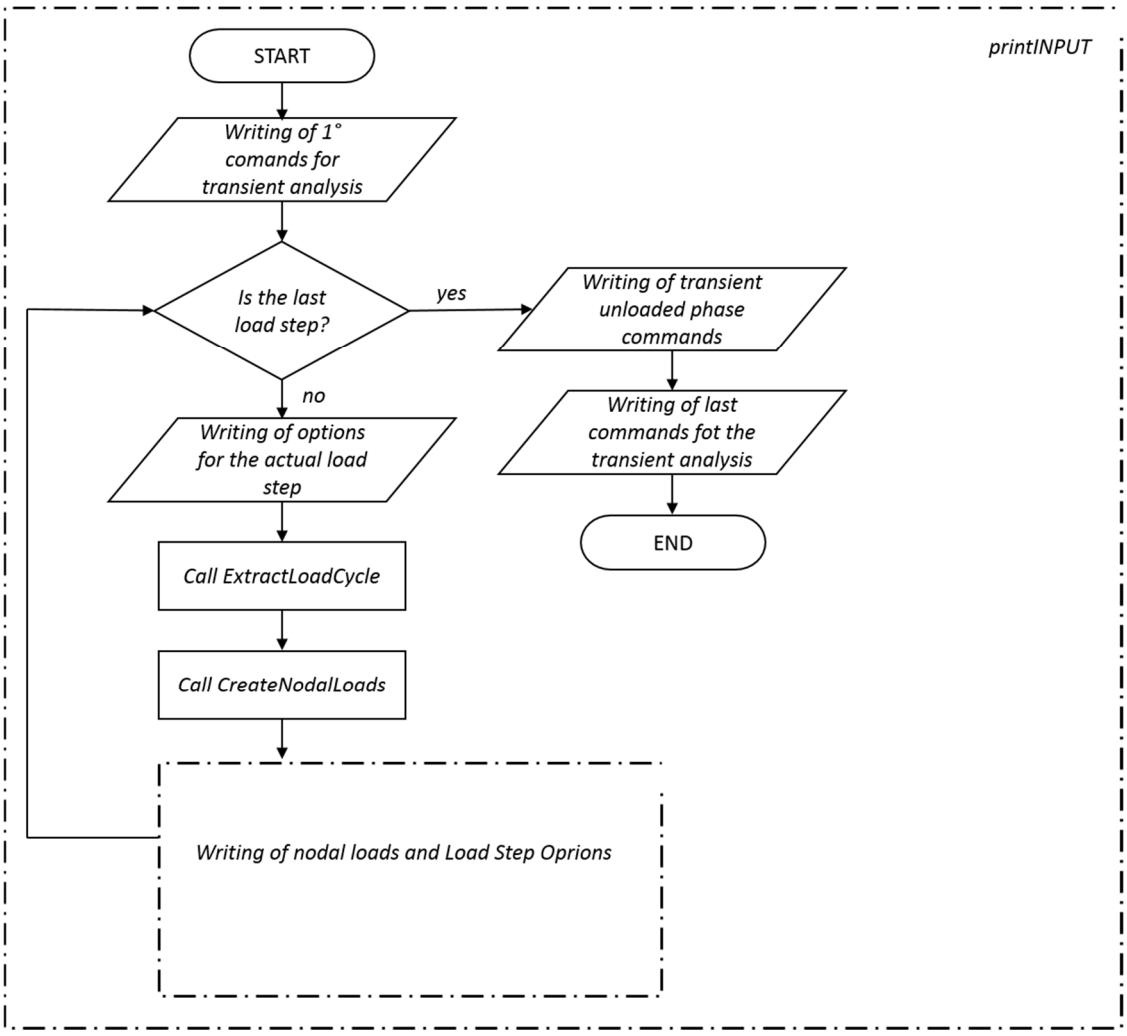

Figure E. 5 Flow chart of "printINPUT" function.

"PrintINPUT" is composed of three main blocks of instructions. The first concerns the writing of options and commands to execute a transient analysis in Ansys. This block is split in two parts, one at the begin and one at the end of the function.

The second block is the most important loop of the function, where loads and options of each LS are written. In each cycle of the loop, the call to two new functions is done to recover the

load time history of the current LS and transform it into proper nodal loads time histories using specific shape functions (ExtractLodCycle and CreateNodalLoads, described at sections E.7 and E.8). For each LS, nodes are renumbered from 1 to 4 as function of their position on corners of the contact point influence area. Then, since these nodes are stored in different vectors, a series of conditional instructions allows to choose the right node and apply to them the nodal loads (Figure E. 6).

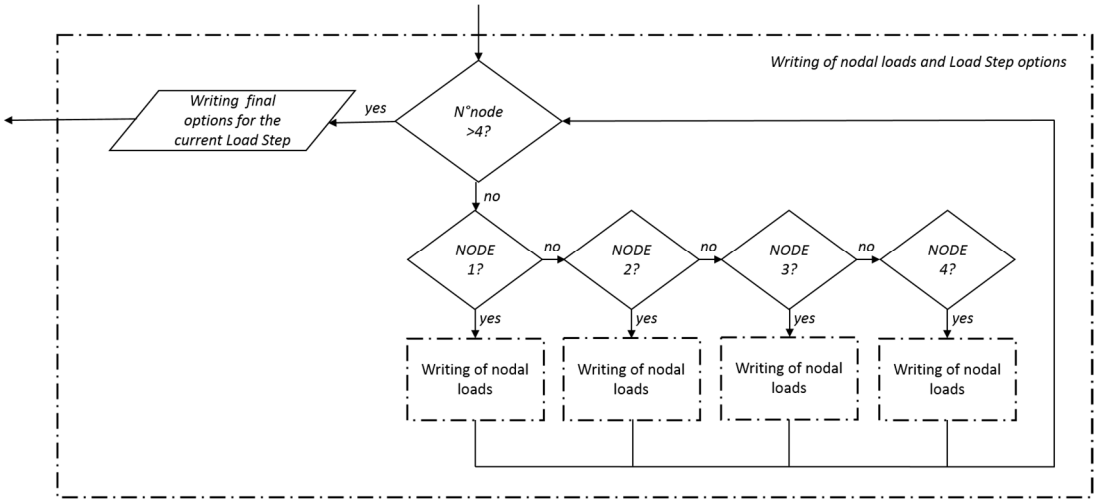

Figure E. 6 Flow chart of the 2nd loop of instructions in the "printINPUT" function.

The force produced by the runner generates vertical forces and two different moments on the corners of the influence area. Thus, to print the right command for Ansys, other conditional instructions have been created (Figure E. 7).

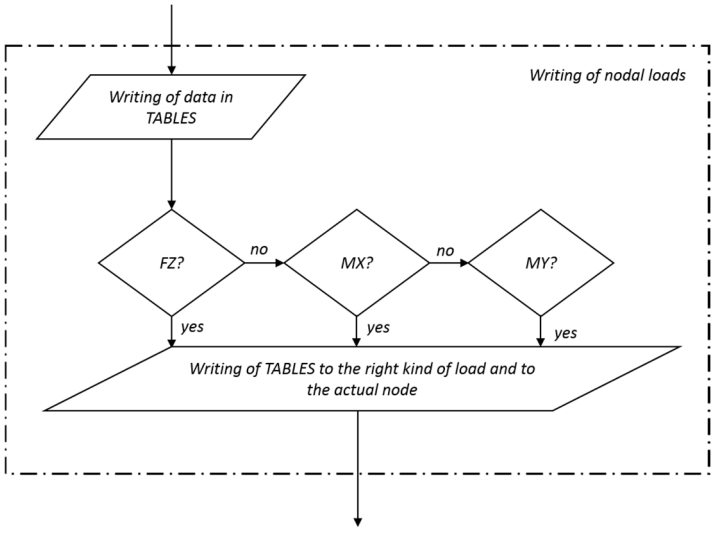

Figure E. 7 Choice of the right label for the considered nodal load.

Finally, the third block of instructions to complete the generation of the text file is represented by lines of code which purpose is to generate an extra number of LSs to

reproduce the free vibration phase of the footbridge after the completed passage of the runner.

E.7 ExtractLoadCycle

The function "ExtractLoadCycle" extracts the *i*th load cycle values from the postprocessed force time history array using the sampling frequency and the array containing durations of each load cycle. This function is used for each of the load cycles needed to cross the bridge in the loop inside "printINPUT".

E.8 CreateNodalLoads

Once the needed array of load cycle values is extracted from the postprocessed force time history array, the function "CreateNodalLoads" produces forces and moments to apply on each of the four nodes at the corner of the contact point influence area. It makes use of special shape functions to transform running forces into nodal vertical loads and x- and y-moments. Shape functions have been taken from *Lai* [10] and are reported in section E.8.1.

E.8.1 Shape functions for determination of nodal loads

The determination of the shape functions used to transform the vertical load into nodal loads is based on the assumption that the bridge deck can be modeled with bending plate elements and, according to the Kirchhoff's theory, each node of the plate has only three degrees of freedom (DOFs) (Figure E. 8).

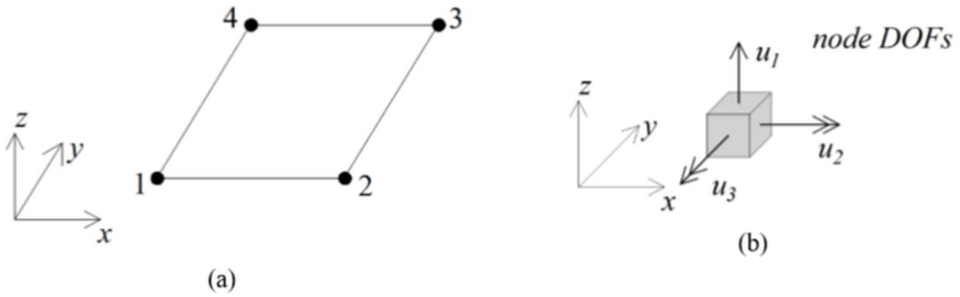

Figure E. 8 a) Node numbering of the shell element and b) DOFs of node 1 [10].

The computation of shape functions, made by *Lai* in [10], is based on the following formulation for the displacement field:

$$w(x,y) = \alpha_1 + \alpha_2 x + \alpha_3 y + \alpha_4 x^2 + \alpha_5 xy + \alpha_6 y^2 + \alpha_7 x^3 + \alpha_8 x^2 y + \alpha_9 xy^2 + \alpha_{10} y^3 + \alpha_{11} x^3 y + \alpha_{12} xy^3 \quad \text{Eq. E. 1}$$

We do not report here the analytical developments but, following the usual procedure that is done for all types of finite elements, the displacement field will be determined by the following expression:

$$\begin{aligned} w(x,y) = {} & N_1(x,y)u_1 + N_2(x,y)u_2 + N_3(x,y)u_3 + N_4(x,y)u_4 \\ & + N_5(x,y)u_5 + N_6(x,y)u_6 + N_7(x,y)u_7 + N_8(x,y)u_8 \\ & + N_9(x,y)u_9 + N_{10}(x,y)u_{10} + N_{11}(x,y)u_{11} + N_{12}(x,y)u_{12} \end{aligned} \quad \text{Eq. E. 2}$$

where $N_i(x,y)$ are the shape functions and u_i the degrees of freedom of the considered element.

Expressions of the shape functions are the following:

$$N_1 = \frac{(\Delta x - x_p)(\Delta y - y_p)\left(\Delta x^2(\Delta y^2 + \Delta y y_p - 2y_p^2) + \Delta x \Delta y^2 x_p - 2\Delta y^2 x_p^2\right)}{\Delta x^3 \Delta y^3} \quad \text{Eq. E. 3}$$

$$N_1 = \frac{(\Delta x - x_p)(\Delta y - y_p)\left(\Delta x^2(\Delta y^2 + \Delta y y_p - 2y_p^2) + \Delta x \Delta y^2 x_p - 2\Delta y^2 x_p^2\right)}{\Delta x^3 \Delta y^3} \quad \text{Eq. E. 4}$$

$$N_2 = \frac{x_p(\Delta x - x_p)^2(y_p - \Delta y)}{\Delta x^2 \Delta y} \quad \text{Eq. E. 5}$$

$$N_3 = \frac{y_p(\Delta y - y_p)^2(\Delta x - x_p)}{\Delta y^2 \Delta x} \quad \text{Eq. E. 6}$$

$$N_4 = \frac{x_p(\Delta y - y_p)\left(\Delta x^2 y_p(\Delta y - 2y_p) + 3\Delta x \Delta y^2 x_p - 2\Delta y^2 x_p^2\right)}{\Delta x^3 \Delta y^3} \quad \text{Eq. E. 7}$$

$$N_5 = \frac{x_p^2(\Delta x - x_p)(\Delta y - y_p)}{\Delta x^2 \Delta y} \quad \text{Eq. E. 8}$$

$$N_6 = \frac{y_p x_p(\Delta y - y_p)^2}{\Delta y^2 \Delta x} \quad \text{Eq. E. 9}$$

$$N_7 = \frac{y_p x_p\left(\Delta x^2(\Delta y^2 - 3\Delta y y_p + 2y_p^2)\right)}{\Delta x^3 \Delta y^3} \quad \text{Eq. E. 10}$$

$$N_8 = \frac{x_p^2 y_p(\Delta x - x_p)}{\Delta x^2 \Delta y} \quad \text{Eq. E. 11}$$

$$N_9 = \frac{y_p^2 x_p(y_p - \Delta y)}{\Delta y^2 \Delta x} \quad \text{Eq. E. 12}$$

$$N_{10} = \frac{y_p(\Delta x - x_p)\left(\Delta x^2 y_p(3\Delta y - 2y_p) + \Delta x \Delta y^2 x_p - 2\Delta y^2 x_p^2\right)}{\Delta x^3 \Delta y^3} \quad \text{Eq. E. 13}$$

$$N_{11} = \frac{-y_p x_p(\Delta x - x_p)^2}{\Delta x^2 \Delta y} \quad \text{Eq. E. 14}$$

$$N_{12} = \frac{y_p^2(\Delta x - x_p)(\Delta y - y_p)}{\Delta y^2 \Delta x}$$ Eq. E. 15

The terms of the shape functions are:

- Δx, length of the element;
- Δy, width of the element;
- x_p and y_p, coordinates of the pedestrian's position with respect to a local reference system located on node 2 of the element.

These parameters are showed in Figure E. 9.

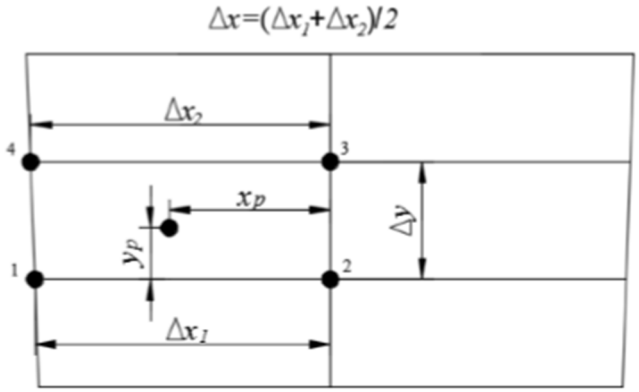

Figure E. 9 Bending plate element [10].

The vector **Q** of nodal forces is computed as the product of the shape functions, evaluated in the point $P(x_p, y_p)$, by the amplitude of the concentrated load F:

$$\boldsymbol{Q} = [\boldsymbol{Q}_1 \quad \boldsymbol{Q}_2 \quad \boldsymbol{Q}_3 \quad \boldsymbol{Q}_4]^T = \boldsymbol{N}(x_p, y_p)|F|$$ Eq. E. 16

where vector $\boldsymbol{Q}_i$ contains nodal forces of node i in the following order:

$$\boldsymbol{Q}_i = \begin{bmatrix} F_{z,i} \\ M_{x,i} \\ M_{y,i} \end{bmatrix}$$ Eq. E. 17

Considering that shape functions have been computed in a local reference system, it was assumed that the load F was perpendicular to the deck mesh. However, since the footbridge presents slopes different from zero, the human induced load must be rotated.

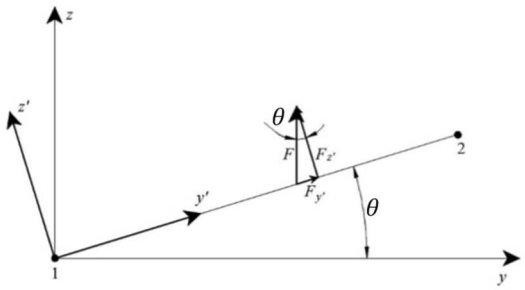

Figure E. 10 Projection of force F on the local reference system [10].

In Figure E. 10, a 2-D view of the plate, where the reference system zy is the same used in the finite element model and where y is oriented as the longitudinal axis of the footbridge. $z'y'$ is the local reference system. Then, F is the applied load and $F_{z'} = Fcos(\theta)$ is the nodal load that will be used by the shape functions to obtain the nodal loads $F_{z',i}$. The projection $F_{y'}$ has been neglected given the small values of slopes.

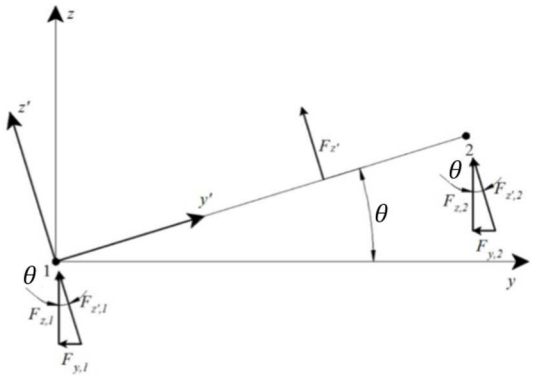

Figure E. 11 Projection of nodal forces on the global reference system [10].

Finally, to have nodal loads expressed in the global reference system, produced by RealRun and used by Ansys, one more rotation was done (Figure E. 11)

$$F_{z,i} = F_{z',i}cos(\theta) \qquad \text{Eq. E. 18}$$

Rue Archimède, 1 bte L6.11.01, 1348 Louvain-la-Neuve, Belgium www.uclouvain.be/epl